Understanding the role of NO-GC/cGMP in human, murine, and HIV-positive patient´s platelets and the effect of biochemical confinement in platelet morphology and mechanics

Dissertation

der Mathematisch-Naturwissenschaftlichen Fakultät
der Eberhard Karls Universität Tübingen
zur Erlangung des Grades eines
Doktors der Naturwissenschaften
(Dr. rer. nat.)

vorgelegt von
Johanna Rodríguez
aus Quito, Ecuador

Tübingen
2023

Gedruckt mit Genehmigung der Mathematisch-Naturwissenschaftlichen Fakultät der Eberhard Karls Universität Tübingen.

Tag der mündlichen Qualifikation:	10.07.2023
Dekan:	Prof. Dr. Thilo Stehle
1. Berichterstatter/-in:	Prof. Dr. Tilman Schäffer
2. Berichterstatter/-in:	Prof. Dr. Robert Feil
3. Berichterstatter/-in:	Prof. Dr. Robert Lukowski

“Sólo es posible avanzar cuando se mira lejos. Sólo cabe progresar cuando se piensa en grande“

José Ortega y Gasset

Zusammenfassung

Der NO-GC/cGMP-Signalweg ist an zahlreichen physiologischen Prozessen beteiligt, einschließlich der Thrombozytenhämostase. Die Dysregulation dieses Weges wurde mit der Entwicklung von kardiovaskulären Pathologien, einschließlich Thrombose, in Verbindung gebracht. Die Hemmung der Thrombozytenaktivierung wurde zuvor mit dem NO-GC/cGMP-Signalweg in Verbindung gebracht; die molekularen Mechanismen, die Modulation des Zytoskeletts und der Form von Blutplättchen beinhalten, wurden jedoch noch nicht untersucht. Wie sich die Thrombozytenbiomechanik auf die Thrombozytenfunktion auswirkt, ist noch eine Nische, die es zu erforschen gilt, daher liegt der Schwerpunkt dieser Dissertation auf dem Verständnis der zellulären Steifheit und Morphologie des Zytoskeletts in Thrombozyten.

Die Zellsteifigkeit wurde in humanen, Wildtyp- und Megakaryozyten-/Blutplättchen-spezifischen NO-GC KO-Mausplättchen gemessen, die mit NO-GC-Stimulator (Riociguat) und NO-GC-Aktivator (Cinaciguat) unter Verwendung von Rasterionenleitfähigkeitsmikroskopie (SICM) inkubiert wurden. . Die Zirkularität und Fläche der Blutplättchen wurden mithilfe von Deep-Learning-basierter Blutplättchen-Morphometrie quantifiziert. F-Actin- und P-Selectin-Co-Immunfärbung wurden in menschlichen und murinen Blutplättchen unter Verwendung von Immunfluoreszenzmikroskopie gemessen. Die Freisetzung von P-Selectin (CD62P) aus α-Granula wird erhöht, wenn Blutplättchen aktiviert werden. Die relative Menge an p-VASP-Phosphorylierung und NO-GC in menschlichen und murinen Blutplättchen, die mit cGMP-modulierenden Arzneimitteln inkubiert wurden, wurde ebenfalls mit Western Blot quantifiziert.

Die P-Selectin-Freisetzung, die F-Actin-Polymerisation und die Zellsteifigkeit wurden um ≈50 % in mit Riociguat oder Cinaciguat stimulierten humanen und Wildtyp-Mausplättchen verringert. Die relative Menge an p-VASP in humanen und Wildtyp-Mausplättchen, die mit NO-GC-Stimulator oder -Aktivator inkubiert wurden, war im Vergleich zur Vehikelkontrolle erhöht. Die Hochregulierung von p-VASP ist mit einer Herunterregulierung von F-Aktin und zellulärer Steifheit verbunden. Die Zirkularität der

Blutplättchen erhöhte sich um ≈50 % im Vergleich zur Vehikelkontrolle; jedoch wurden die Blutplättchenfläche und die relative Menge an NO-GC in menschlichen und Wildtyp-Mausblutplättchen, die mit cGMP-modulierenden Arzneimitteln stimuliert wurden, nicht verändert. Diese Ergebnisse legten nahe, dass der NO-GC-Signalweg die Zellsteifigkeit und -morphologie des Zytoskeletts in Blutplättchen moduliert, und ein pharmakologisches Targeting dieses Weges könnte als neuartige antithrombotische Therapie in Betracht gezogen werden.

Die klinische Anwendbarkeit von NO-GC-Stimulatoren (Riociguat oder Vericiguat) wurde auch bei HIV-positiven Patienten, die TFV- oder ABC-haltige Therapien einnahmen, im Vergleich zu HIV-negativen Patienten untersucht. Blutplättchenaggregation, endotheliale Mikropartikel (EMP)-Blutplättchenaktivierung, Crosstalk, Zirkularität, Fläche und F-Aktin-Polymerisation wurden untersucht. Riociguat und Vericiguat verringerten die Thrombozytenaggregation, Zirkularität und F-Aktin-Polymerisation bei HIV-negativen und HIV-positiven Patienten, die TFV-haltige Therapien einnahmen, was darauf hindeutet, dass die Aktivierung des NO-GC/cGMP-Signalwegs die Thrombogenität bei Thrombozyten einschließlich HIV-positiver Patienten verringert Patienten, die TFV-haltige Regime einnehmen. Die bei HIV-positiven Patienten, die ABC-haltige Regime einnahmen, beobachtete fehlende Wirkung auf die Thrombozytenaggregation, Zirkularität und F-Aktin-Polymerisation wurde mit der Hemmung des NO-GC/cGMP-Signalwegs durch CBV-TP (aktiver Anabolit von ABC) in Verbindung gebracht. Diese Ergebnisse bestätigen das klinische Potenzial von NO-GC-Stimulatoren bei HIV-positiven Patienten durch Verringerung der Thrombozytenhyperaktivität.

Übermäßige Thrombozytenaktivierung löst verschiedene Herz-Kreislauf-Erkrankungen aus, indem sie Thrombosen verstärkt. ADP und Thrombin sind die wichtigsten Blutplättchenagonisten, die an der Blutplättchenaktivierung beteiligt sind. In physiologischer Umgebung befinden sich Blutplättchen in Blutkapillaren mit einer Größe zwischen 5 µm und 10 µm. Um physiologische Bedingungen nachzuahmen, wurden Blutplättchen biochemisch in fluoreszierende Fibrinogen-beschichtete Linien mit einer Breite von 5 µm und einer Periodizität von 15 µm eingeschlossen, die mittels

Mikrokontaktdruck (μCP) in Zellkulturschalen gestempelt wurden. Die Auswirkungen des Einschlusses wurden in der Blutplättchenmorphologie und -mechanik untersucht. Die biochemische Begrenzung erhöhte die Blutplättchenfläche, das Seitenverhältnis, die Höhe und das Volumen in mit ADP aktivierten Blutplättchen, was darauf hindeutet, dass die Art des Blutplättchenagonisten die Blutplättchen-Fibrinogen-Überlappung beeinflusst. Die Steifheit der Blutplättchen verringerte sich im Einschluss im Vergleich zu nicht eingeschlossenen Blutplättchen. Die biochemische Begrenzung beeinflusst die Morphologie und Mechanik von Blutplättchen, folglich liefert diese Studie ein weiteres Verständnis der Blutplättchenaktivierung in einer relevanten physiologischen Umgebung.

Summary

NO-GC/cGMP signaling pathway is involved in numerous physiological processes including platelet haemostasis. The dysregulation of this pathway has been linked to the development of cardiovascular pathologies including thrombosis. Inhibition of platelet activation has previously been linked to NO-GC/cGMP pathway; however, the molecular mechanisms involving the modulation of platelet cytoskeleton and shape has not yet been investigated. How platelet biomechanics affects platelet function is still a niche to explore hence the focus of this dissertation is to understand cytoskeletal cellular stiffness and morphology in platelets.

Cellular stiffness was measured in human, wild-type, and megakaryocyte/platelet-specific NO-GC KO murine platelets, incubated with NO-GC stimulator (riociguat) and NO-GC activator (cinaciguat), using scanning ion conductance microscopy (SICM). Platelet circularity and area were quantified using deep learning-based platelet morphometry. F-actin and P-selectin co-immunostaining were measured in human and murine platelets using immunofluorescence microscopy. P-selectin (CD62P) release from α-granules is increased when platelets are activated. Relative amount of p-VASP phosphorylation and NO-GC in human and murine platelets incubated with cGMP-modulating drugs were also quantified with western blot.

P-selectin release, F-actin polymerization, and cellular stiffness were decreased by ≈50% in human and wild-type murine platelets stimulated with riociguat or cinaciguat. Relative amount of p-VASP in human and wild-type murine platelets incubated with NO-GC stimulator or activator were increased in comparison with vehicle control. Upregulation of p-VASP is linked to a downregulation in F-actin and cellular stiffness. Platelet circularity increased by ≈50% in comparison to vehicle control; however, platelet area and relative amount of NO-GC were not altered in human and wild-type murine platelets stimulated with cGMP-modulating drugs. These results suggested that NO-GC signaling pathway modulates cytoskeletal cellular stiffness and morphology in platelets, and a pharmacological targeting of this pathway may be considered as a novel anti-thrombotic therapy.

Clinical applicability of NO-GC stimulators (riociguat or vericiguat) were also investigated in HIV-positive patients taking TFV- or ABC-containing regimens compared to HIV-negative patients. Platelet aggregation, endothelial microparticle (EMP)-platelet activation crosstalk, circularity, area, and F-actin polymerization were investigated. Riociguat and vericiguat decreased platelet aggregation, circularity, and F-actin polymerization in HIV-negative patients and HIV-positive patients taking TFV-containing regimens, suggesting that activation of the NO-GC/cGMP signaling pathway decreases thrombogenicity in platelets including HIV-positive patients taking TFV-containing regimens. The lack of effect in platelet aggregation, circularity, and F-actin polymerization observed in HIV-positive patients taking ABC-containing regimens were linked to the inhibition of NO-GC/cGMP signaling pathway by CBV-TP (active anabolite of ABC). These results confirm the clinical potential of NO-GC stimulators in HIV-positive patients by reducing platelet hyperactivity.

Excessive platelet activation triggers different cardiovascular diseases by increasing thrombosis. ADP and thrombin are the main platelet agonists involved in platelet activation. In physiological environment, platelets are inside blood capillaries of sizes between 5 µm to 10 µm. To mimic physiological conditions, platelets were biochemically confined in fluorescent fibrinogen-coated lines with a 5 µm width and a 15 µm periodicity stamped in cell culture dishes using micro-contact printing (µCP). The effects of confinement were investigated in platelet morphology and mechanics. Biochemical confinement increased platelet area, aspect ratio, height, and volume in platelets activated with ADP, suggesting that the type of platelet agonist influences the platelet-fibrinogen overlap. Platelet stiffness decreased in confinement in comparison with unconfined platelets. Biochemical confinement affects morphology and mechanics in platelets, consequently this study provides further understanding of platelet activation in a relevant physiological environment.

Table of contents

List of figures

List of tables

Abbreviations

ABC	Abacavir suphate
AB	Antibody
ACD	Acid-citrate-dextrose
ADP	Adenosine diphosphate
AFM	Atomic force microscopy
ARRIVE	Animal research: reporting of in vivo experiments
Arp2/3	Actin related protein 2/3 complex
ART	Antiretroviral therapy
ATP	Adenosine tri-phosphate
BSA	Bovine serum albumin
BNP	B-Type natriuretic peptide
cAMP	Cyclic 3',5'-adenosine monophosphate
CBV-TP	Carbovir tri-phosphate
CD62P	Alpha granule binding (P-selectin)
CD63	Dense granule binding
CINA	Cinaciguat
cGKI	cGMP-dependent protein kinase I
cGMP	Cyclic guanosine monophosphate
CNN	Convolutional neural network
CNP	C-natriuretic peptide
Cre	Cyclisation/recombination SS
cGKs	cGMP-dependent protein kinases
CTCF	Corrected total cell fluorescence
CVD	Cardiovascular disease
DMSO	Dimethyl sulfoxide
D:A:D	Data Collection on Adverse Effects of Anti-HIV Drugs
ECM	Extracellular matrix
EMP	Endothelial-derived microparticles
eNOS	Endothelial-derived NO synthase
F-actin	Filamentous actin
FCS	Foetal calf serum
Fl/Fl	Flox/flox
FACS	Fluorescence activated cell sorting
GAPDH	Glyceraldehyde 3-phosphate dehydrogenase
GPVI	Glycoprotein VI
GC	Guanylyl cyclase
GP	Glycoprotein
GPCRs	G-protein coupled seven transmembrane domain receptors
GTP	Guanosine triphosphate
HCl	Hydrochloric acid
HEPES	4-(2-hydroxyethyl)-1-piperazineethanesulphonic acid
HIV	Human deficiency virus
HIV+	Human deficiency virus positive
HUVEC	Primary human umbilical vein endothelial cells
iNOS	Inducible NO synthase
INSTI	Integrase strand transfer inhibitor
IP_3	Inositol triphosphate
IPDs	Inherited platelet disorders
IRAG	Inositol 1,4,5-triphosphate-associated cGMP kinase substrate

KO	Knock-out
KCl	Potassium chloride
K_2HPO_4	Dipotassium phosphate
LAMP-3	Lysosome-associated membrane protein-3
MI	Myocardial infarction
MFI	Mean fluorescence intensity
$MgCl_2$	Magnesium chloride
MLCP	Myosin-light-chain phosphate
MPs	Microparticles
NaCl	Sodium chloride
$NaHCO_3$	Sodium bicarbonate
NaH_2PO_4	Monosodium phosphate
NO	Nitric oxide
NO-GC	Nitric oxide-sensitive gualyyl cyclase
NOS	Nitric oxide synthase
nNOS	Neuronal nitric oxide synthase
NRTI	Nucleotide reverse-transcriptase inhibitor
ODQ	1H-[1,2,4]oxadiazolo[4,3-a]quinoxalin-1-one
PAC-1	Platelet $\alpha_{IIb}\beta_3$ integrin activation
PARs	Protease-activated receptors
PBS	Phosphate-buffered saline
PDE	Phosphodiesterase
PDMS	Polydimethylsiloxane
PECAM-1	Platelet-endothelial cell adhesion molecule-1
PEG	Polyethylene glycol
PF4	Platelet factor-4
pGC	Particulate gualylyl cyclase
PGE_1	Prostaglandin E1
PGI_2	Prostacyclin
PI	Protease inhibitors
PLL-g-PEG	Poly-l-lysine grafted to PEG
PLHIV	People living with HIV
PPP	Platelet poor plasma
PRP	Platelet-rich plasma
PrEP	Pre-exposure prophylaxis
PKG	cGMP-dependent protein kinase
PWB	Platelet wash buffer
RBCs	Red blood cells
RIO	Riociguat
ROI	Region of interest
ROCK	Rho-associated coiled-coil kinase
ROS	Reactive oxygen species
RT	Room temperature
RT-DC	Real-time deformability cytometry
RT-FDC	Real-time fluorescence and deformability
SDS	Sodium dodecyl sulfate
SDS-PAGE	Sodium dodecyl sulfate-polyacrylamide gel electrophoresis
SICM	Scanning ion conductance microscopy
SOP	Standard operating procedure
TAF	Tenofovir alafenamide
TDF	Tenofovir disoproxil fumarate
TFV	Tenofovir

TNF- α	Tumor necrosis factor alpha
TG	Transgenic
TRAP-6	Thrombin receptor activator peptide-6
TXA_2	Tromboxane A2
µCP	Micro-contact printing
VASP	Vasodilator-stimulated phosphoprotein
VERI	Vericiguat
vWF	von Wilebrand factor
WBCs	White blood cells
WT	Wild-type

1 Introduction

1.1 Platelets and NO-GC/cGMP signaling pathway

1.1.1 Role of platelets in health and disease

Platelets are multipurpose cells with influence in cardiovascular pathologies, inflammation, and cancer biology (1). Platelets are small anucleate discoid cells with 2 – 5 µm in diameter, which circulate in the blood (2). Platelets circulate in a resting state, prevent blood loss where there is a vessel damage, and are involved in the process of hemostasis (3). Activated platelets have a protective and a pathological role mediated by the release of soluble agonists and further activation of multiple pathways (4). Activated platelets adhere to the site of injury, spread on the surface and release intracellular contents inducing the formation of platelet aggregation (3). During platelet activation, a reorganization of the actin cytoskeleton, cell contraction, increased release of growth factors, and development of filopodia and lamellipodia are observed (4). Platelets also plays an important role in innate immunity (5). P-selectin exposure on the platelet surface during activation recruits leukocytes inducing a local inflammatory reaction and a normal immune process (2).

Platelets are immediately recruited where there is an endothelial injury, an inflammatory signal, or a pathological alteration (2). Blood clot formation can be described by the following steps: 1) first, platelets accumulate at the site of injury to form a monolayer (initiation phase); 2) second, the release of platelet agonists, such as ADP and thrombin, induces platelet activation, adhesion, and spreading (extension phase); 3) lastly, a platelet plug (or thrombus) is formed (stabilization phase) (2). Platelet aggregation occurs in a fibrinogen-dependent manner supported by glycoprotein Ib-IX-V and integrin $\alpha_{IIb}\beta_3$ binding (2). Upon platelet activation a conformational change of $\alpha_{IIb}\beta_3$ occurs (6). $\alpha_{IIb}\beta_3$ stabilizes platelet aggregates and support platelet-platelet binding via fibrinogen, von Willebrand factor (VWF), and fibronectin (6).

Disrupting the balance between bleeding and clotting cause serious medical conditions such as thrombocytopenia, among others (2). In addition, atherosclerosis is linked to a decreased production of nitric oxide (NO) (7), which contributes to dysfunctional platelet NO-GC/cGMP signaling pathway (8) and persistent platelet activation (9). In addition to cardiovascular pathologies, platelets are involved in inflammatory processes and cancer biology (1).

1.1.2 Platelet activation signaling pathways

During platelet adhesion and aggregation, platelet recruitment is mediated by the interaction between the platelet receptor glycoprotein (GP) Ib and collagen bound to von Willebrand factor (vWF), which then activates the immunoglobulin-like GPVI and leads to further release of two platelet agonists (ADP and TXA_2) (10) and cytosolic calcium release (11). αIIbβ3 is the main integrin responsible for platelet aggregation and adhesion to the ECM through binding to plasma fibrinogen (12).

During platelet activation, α-granules and dense granules secrete numerous prothrombotic and inflammatory mediators (6). P-selectin is stored inside the α-granules, while serotonin, calcium, magnesium, adenosine triphosphate (ATP), and adenosine diphosphate (ADP) are inside the dense granules (13).

ADP-induced platelet activation (Figure 1) is mediated by two G-protein coupled seven transmembrane domain receptors (GPCR) $P2Y_1$ and $P2Y_{12}$ (14) located on the cell surface and responsible for platelet aggregation, shape change, TXA_2 release, and calcium mobilization (15). $P2Y_1$ and $P2Y_{12}$ are involved in platelet aggregation (16). ADP is also a positive-feedback mediator of platelet activation and aggregation (17).

Thrombin is the most effective platelet agonist and is also involved in the coagulation process (18). Thrombin polymerizes soluble fibrinogen to fibrin (19). This polymerization is the initial step to form hemostatic plugs at sites of injury (19). Thrombin-induced platelet activation in platelets (Figure 1) is mediated by protease-activated receptors (PARs) coupled to the GPCRs (PAR1 and PAR4) (20). Platelet

shape change is an important aspect of platelet activation, and this extremely rapid process involves the formation of lamellipodia and filopodia, actin polymerization, and stimulation of actomyosin-based contractile processes (18).

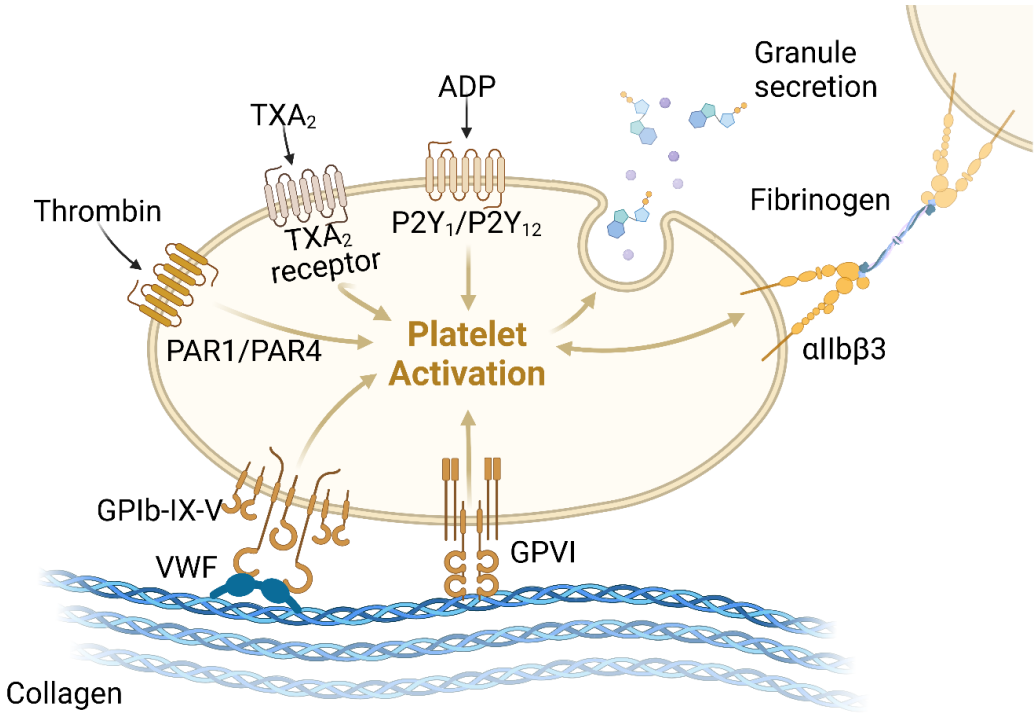

Figure 1. Mechanisms of platelet activation. This figure was partially modified from a template and designed in Biorender.com (2023).

1.1.3 NO-GC/cGMP signaling pathway, NO-GC stimulators and activators

NO is a small gaseous molecule which regulates many physiological processes in the human body (21). The release and synthesis of NO from endothelial cells increases in response to acetylcholine and mechanical shear stress caused by blood flow (21). Drugs for angina pectoris like NO-releasing organic nitrates (22), phosphodiesterase (PDE) inhibitors, and stimulators or activators of nitric oxide (NO)-guanylyl cyclase (NO-GC) have demonstrated to be a successful pharmacological approach to target the cyclic guanosine monophosphate (cGMP) signaling pathway (23).

There are two cGMP generators, soluble and particulate NO-GC (22). Platelets only express the soluble NO-GC (8). The binding of NO to GC converts guanosine triphosphate (GTP) to cGMP (Figure 2) (8). cGMP-dependent protein kinases (cGKs),

cGMP-regulated phosphodiesterases, and cGMP-gated ion channels are the main effector molecules downstream of cGMP (24). The NO-GC/cGMP signaling pathway has physiological relevance in the inhibition of platelet aggregation (25), vascular smooth muscle relaxation (26) and nervous system function (24) (Figure 2).

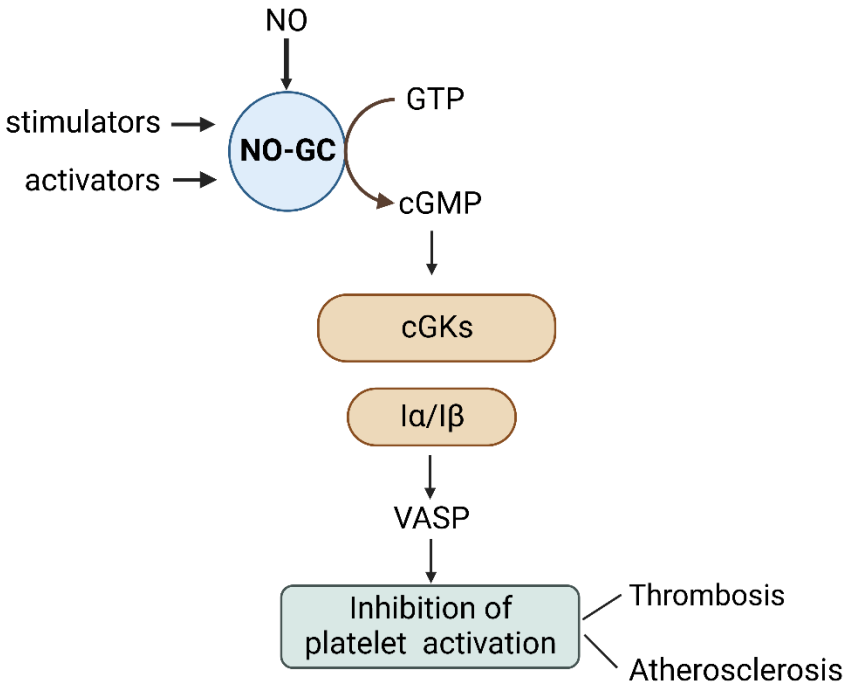

Figure 2. cGMP signaling pathway in platelets. This figure was partially modified from (22), and designed in Biorender.com (2023).

NO-GC stimulators and activators activate NO-GC in a NO-independent manner stimulating cGMP formation (27), albeit through a different mechanism of action. NO-GC stimulators stimulate GC in an NO-independent manner, but also stabilize the binding of NO to GC through the sensitization of GC when there are low levels of NO (27). During the development of these drugs, the hypothesis that NO-GC could be redox regulated was formulated, and this may be a key pathological mechanism for several cardiovascular pathologies, which are characterized by redox stress (28). Therefore, NO-GC activators were developed to activate the haem-free oxidized form of NO-GC (28) and to mimic NO-bound haem binding (27).

Riociguat is a NO-GC stimulator which has a dual mode of action (29). It is the most successful NO-GC stimulator used for the treatment of pulmonary hypertension (28).

Vericiguat is also a NO-GC stimulator, but its improved formulation has a better oral bioavailability than riociguat allowing a daily dosage intake (28). Cinaciguat is a potent NO-GC activator which is currently discontinued, and runcaciguat (a new NO-GC activator) is being investigated for the treatment of cardiovascular diseases (CVDs) (30,31). NO-GC activators have a strong pharmacological potential in diseases with high level of nitro-oxidative stress where the haem of the NO-GC becomes oxidized (32). NO-GC activators could activate GC even when NO bioavailability is low, activating the NO-GC/cGMP signaling pathway (32).

Abnormalities in the NO-GC/cGMP signaling pathway contributes to platelet hyperreactivity in thrombosis and ischemic heart disease (8). Riociguat has recently been shown to reduce thrombosis in a shear-dependent manner in mice expressing the cGMP sensor cGi500 globally (33). Shear stress increases NO sensitivity of NO-GC resulting in inhibition of platelet activation in later stages of thrombus formation (33). Increased levels of cGMP in platelets can block platelet activation by the inhibition of calcium release from the dense granules (8).

The focus of this thesis is the modulation of NO-GC signaling pathway in platelets through the above explained NO-GC stimulators and activators, specifically riociguat, vericiguat, and cinaciguat. Since the specificity of 1H-[1,2,4]oxadiazolo[4,3-a]quinoxalin-1-one (ODQ), a potent NO-GC antagonist, remains not well understood, I used platelets from mice with genetically deleted NO-GC (platelet-specific NO-GC KO) to corroborate the effect of NO-GC in platelet biomechanics and shape.

1.1.4 Platelet biomechanics

Cell stiffness has been suggested as a potential biomarker to identify disease states, including pathologies involving platelets (34). Loosely speaking, stiffness is defined as the resistance of a material to deform under applied external force. Micro-pipette aspiration, atomic force microscopy (AFM), scanning ion conductance microscopy (SICM), and real-time deformability cytometry (RT-DC) are some techniques used to investigate platelet cytoskeleton mechanics (35).

Micropipette aspiration quantifies the membrane deformation and the viscoelastic properties of an immobilized single platelet, by applying a continuous pressure with a borosilicate glass micropipette (36). RT-DC and real-time fluorescence and deformability cytometry (RT-FDC) combines cell mechano-phenotyping labelling with flow cytometry (37), which allows high-throughput study of platelet deformability, stiffness, size, and other morphological parameters in whole blood suspension (34). RT-DC allows to understand the derivation of stiffness from deformability (34).

AFM is capable of measuring samples which quantifies force interactions at the nanometer (nm) scale (38). It uses a cantilever which scans the surface topography of the sample based on cantilever deflection (38). SICM is a technique for non-contact, low-force imaging of living cells (39), which prevents cell deformation (40). In SICM, an ionic current is passed through a nanopipette that scans the surface of the sample allowing the investigation of the mechanical properties of living cells, at high spatial resolution (41,42). The nanopipette inner radius limits the resolution of the obtained images (42). Biomechanical properties of platelets during platelet activation and migration (41) have been elucidated with SICM (43).

SICM was the technique of choice to investigate the biomechanical properties of living platelets in this study. It allowed me to quantify stiffness and height profiles of platelets under the stimulation of cGMP drugs. My work suggests that stiffness could be a potential biomarker to identify different stages of platelet activation and spreading.

1.1.5 Role of NO-GC/cGMP signaling pathway in the platelet cytoskeleton

The extracellular matrix (ECM)-integrin-cytoskeleton connections are mediated by actomyosin activity which impacts the platelet mechanical stability (44). Filamentous actin (F-actin), microtubules, intermediate filaments and binding proteins are the main components of platelet cytoskeleton (45). F-actin extends to the platelet filopodia and lamellipodia, microtubules disperse inside the platelet, and the intermediate filaments extend to the plasma membrane (45). Actin is a highly conserved globular protein, and upon platelet activation, the total amount of F-actin increases (45). The dynamic motion of filopodia and lamellipodia in platelets is driven also by actin polymerization.

Vasoactive-stimulated phosphoprotein (VASP) is the major substrate of cyclic adenosine monophosphate (cAMP) and cGMP-dependent protein kinases in human platelets, and it also plays a role in the inhibition of platelet activation (4,46). Deletion of VASP has been shown to enhance platelet aggregation and increase expression of P-selectin (platelet activation marker) (47,48). VASP is localized along the platelet filopodia and lamellipodia (4), and it affects the Asp2/3 complex (49). Arp2/3 is a complex required for lamellipodia extension and actin filament formation (49), so a branched actin network is generated (50). Phosphorylation of VASP (pVASP) is mediated by cAMP and cGMP-dependent protein kinases at three serine/threonine residues (51). A serine 1 and 2-containing sites (LRKV**S**KQQEEA) and (HIERRV**S**NAG), and a threonine-containing site (MNAVLARRRKA**T**QVGE) (51). The main phosphorylation sites of VASP are serine-157, serine-239, and threonince-278 (52). pVASP upregulation in platelets inhibits platelet activation suggesting that actin filaments and nucleating activity may be inhibited (53). Additionally, a decrease in calcium and granule release in platelets may be also related to a VASP-independent mechanism (47). Therefore, VASP could serve as a switch between inhibiting or stimulating actin polymerization (4).

However, nothing is known about the role of the platelet cytoskeleton in the regulation of platelet activation and F-actin polymerization by the NO-GC/cGMP signaling pathway. It is known that an enhanced production of cGMP can reduce platelet aggregation (54,55), but how this occurs at a single-platelet level has not been elucidated yet. The modulation of the platelet cytoskeleton not only allows us to understand its biomechanical properties, but also the link to platelet activation via changes in circularity, area, aspect ratio, and number of filopodia. Actin polymerization triggers the release of platelet agonists from α-granules which enhance platelet activation (45,56). Targeting the NO-GC/cGMP signaling pathway with NO-GC stimulators (riociguat or vericiguat) and activators (cinaciguat) could give a hint on the role of NO-GC in platelet biomechanics, and potentially become pharmacological tools to decrease the thrombogenic risk of platelet hyperactivation in cardiovascular pathologies.

1.1.6 Role of NO-GC/cGMP signaling pathway in the inhibition of platelet activation and platelet shape

Increased levels of cGMP, NO, and endothelial cell-derived prostacyclin inhibit platelet activation (57). Previous studies suggested that the NO-GC/cGMP signaling pathway in platelets can be both inhibitory or stimulatory for platelet function (57). cGMP/PKG pathway may have a biphasic role in platelets, consisting of an initial stage of platelet activation (stimulatory response), followed by inhibition of platelet activation (delayed inhibitory phase) (58). The speculative stimulatory role of PKG may be related to a cGMP-independent effect (57). This suggests that that longer drug incubation times may be required to reach high levels of cGMP concentrations and have an inhibitory cGMP/PKG-dependent effect in platelet activation (57).

Shape changes in platelets are dependent on actin rearrangements in the cytoskeleton (59). ADP induces platelet shape changes through the activation of P2Y1 receptor, which increases calcium release (60). Protein kinase A (PKA) and PKG have overlapping effects (61) and are responsible for the phosphorylation of different substrates which play a role in the inhibition of platelet activation (57) and platelet shape (61). Activation of the downstream signaling cascade RhoA/ROCK/MLCP is involved in the regulation of platelet shape (62). NO blocks RhoA activation, and consequently RhoA/ROCK/MLCP pathway inhibiting platelet shape changes (63).

Considering the role of NO in platelet shape from the literature, we hypothesized that an upregulation of the NO-GC/cGMP signaling pathway may have an influence on platelet shape and platelet cytoskeleton mechanics. High throughput platelet morphology studies were established with a deep learning, neural network approach to study platelet shape parameters such as circularity, aspect ratio, number of filopodia and area during migration and spreading (64). Shape parameters (morphometry) can provide unique information about platelet shape, which then could be correlated with spreading or activation stages (64).

1.1.7 Role of the NO-GC/cGMP pathway in people living with HIV (PLHIV)

1.1.7.1. Current drug treatments in PLHIV

Around 36 million people are living with human immunodeficiency virus (HIV), although current treatment has improved their life expectancy and quality considerably (65). HIV can be managed with two nucleoside reverse transcriptase inhibitors (NRTIs) plus a third agent of a different class (66). The preferred backbone treatments for PLHIV are tenofovir alafenamide (TAF), tenofovir disoproxil fumarate (TDF), or abacavir sulphate (ABC) (66). The third agent usually is a non-nucleoside reverse inhibitor, a protease inhibitor (PI), or an integrase strand transfer inhibitor (INSTI) (66). The goal of an ART regimen is to maximize the quality of life of PLHIV and to reduce the viral load in plasma (66). However, evidence from the Data collection on Adverse Effects of Anti-HIV Drugs Study (DAD) have determined that ART can increase the risk of cardiovascular diseases (67,68), and metabolic disorders such as dislipidaemia or diabetes (69).

TDF showed more off-target effects in comparison with TAF. TDF is a highly effective regimen; however, it might lead to a deterioration of the renal and bone function (reduced glomerular filtration and bone density) (70). Tenofovir (TFV) is formulated as a prodrug because of its low oral availability (71). TDF and TAF are the two prodrugs from TFV which are metabolized to tenofovir-diphosphate in plasma (70). TDF produce four times more tenofovir-diphosphate in plasma than TAF, consequently the side effects are more likely to occur when HIV-positive patients take TDF (70). Additionally, TFV is also formulated as a pre-exposure prophylaxis (PrEP) in the prevention of HIV infection (71).

ABC is a guanosine analogue reverse transcriptase inhibitor (72) which has been associated with the development of cardiovascular diseases; consequently, it has been removed from the clinical guidelines in HIV-positive patients with cardiac dysfunction (73). The active metabolite of ABC is carbovir triphosphate (CBV-TP) which could interact with major signaling pathways and enhance thrombus formation and platelet activation (74). The mechanism of action is not yet elucidated; however, it seems to be

related to the inhibition of NO-GC/cGMP signaling pathway (65,72) or any other major paracrine signals (74).

1.1.7.2 Disruption of the NO-GC/cGMP pathway in platelets from HIV-positive patients taking abacavir sulphate (ABC)-containing regimens

The major health complications of long-time exposure to some ARTs in PLHIV are an increased platelet reactivity which can lead to myocardial infarction, thrombosis, and endothelial dysfunction (75). Endogenous NO derived from endothelial nitric oxide synthase (eNOS) modulates platelet aggregation and activation, and the other two isoforms (inducible NOS and neuronal NOS) are negligible in platelet function *in vivo* (76). Lack of eNOS in platelets negatively impact platelet function and impairs the endogenous NO-GC/cGMP signaling pathway (77).

There is clinical evidence of an increased risk of myocardial infarction (MI) in HIV-positive patients currently taking ABC-regimens, and a reduction of the cardiovascular risk after drug withdrawal confirming the link between ABC and cardiovascular toxicity. (78). ABC increases oxidative stress and downregulates eNOS in human endothelial cells impairing endothelial function (79), increasing arterial stiffness and aggregability (80). Long TFV exposure is also associated with renal toxicity, disturbances in vitamin D absorption, and heart failure (73). However, tenofovir mechanism of action has not been linked in literature to a NO-GC/cGMP impairment like in the case of ABC-containing regimens (73).

ABC disrupts NO-mediated platelet inhibition and enhances platelet aggregation and platelet granule release, while TFV did not affect platelet function *in vitro* and *in vivo* (65). CBV-TP is a guanosine analogue and a competitive inhibitor of guanoine triphosphate (GTP), which inhibits the downstream NO-GC/cGMP signaling pathway (65,72). However, other mechanisms related to ABC cardiovascular toxicity have been investigated such as the activation of the purinergic ATP-$P2X_7$ receptors and endogenous ATP which led to platelet activation and adhesion to endothelial cells (74,81).

Based on this prior research, we postulate a possible mechanism of action of CVB-TP in platelets, which involves NO-GC/cGMP signaling pathway in platelet biomechanics (Figure 3).

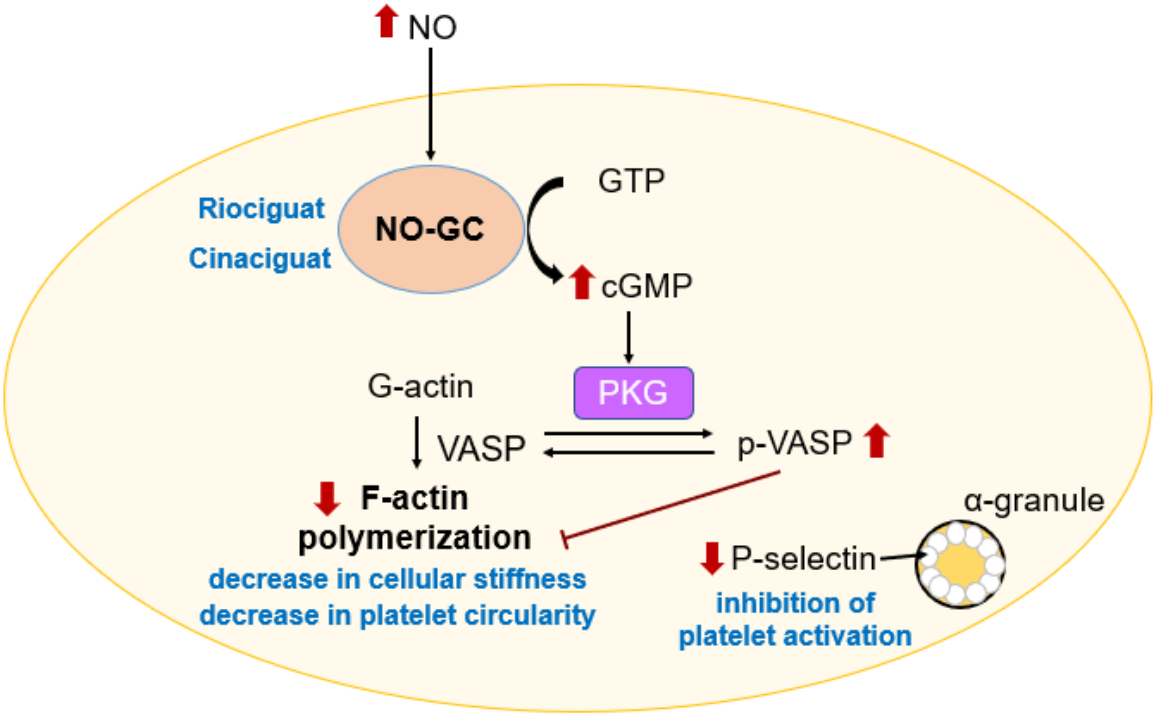

Figure 3. Role of the NO-GC/cGMP pathway in the inhibition of platelet activation, decrease in cellular stiffness, and loss of thrombo-protection.

1.2 Aims

The aims of this dissertation are divided in three different parts:

1. To investigate the functional role of the NO-GC enzyme in platelet biomechanics (cellular stiffness) in correlation with the inhibition of platelet activation and platelet shape. A NO-GC stimulator (riociguat) and a NO-GC activator (cinaciguat) were tested in human, murine wild-type, and megakaryocyte/platelet-specific NO-GC knockout platelets. Stiffness was investigated with SICM and platelet shape with a deep learning neural network approach. The NO-GC/cGMP signaling pathway was investigated in the context of platelet cytoskeleton modulation. This study suggests that activation of NO-GC decreases the thrombogenic risk of platelets by targeting platelet cellular stiffness.

2. To study the effect of NO-GC stimulators in a clinical setting. Platelets from HIV-positive patients currently taking TFV- or ABC-containing regimens were treated with riociguat or vericiguat to test whether NO-GC stimulators reduce platelet hyperreactivity in these patients depending on their ART treatment. Maximum ADP and collagen-induced aggregation, F-actin quantification, and morphological studies were done with platelets from HIV-positive patients taking TFV- or ABC-containing regimens. It is postulated that HIV-positive patients currently taking ABC-containing regimens have an impaired NO-GC/cGMP pathway. CBV-TP is a competitive antagonist of cGMP, which consequently induces a loss of thromboprotection.

3. To determine the effect of biochemical confinement on platelet morphology and mechanics, optical microscopy combined with a deep learning morphometric analysis and AFM were used. Platelet-fibrinogen overlap, area, aspect ratio, height, volume, stiffness, and F-actin mean fluorescence (MIF) were investigated. Untreated, ADP or thrombin-activated platelets were confined onto micro-contact printed lines with a width of 5 µm coated with human fluorescent fibrinogen and a periodicity of 10 µm. These micro-patterns were used to resemble blood vessels and to study platelet activation in a physiological environment. How micro-environmental geometry spaces affect platelet mechanics and morphology is still a niche to explore.

2 Materials and Methods

2.1 Materials

2.1.1 Common reagents and chemicals

Compound	Company & Cat. No
ACD	Sigma Aldrich (C3821)
BSA fraction V	PanReac AppliChem (A1391)
Ca_2Cl	Sigma Aldrich (449709)
Citric acid	Carl Roth (77-92-9)
Ethanol	VWR (JT8006-89)
D-glucose monohydrate	Sigma Aldrich (14431-43-7)
Fibrinogen from human plasma	Sigma Aldrich (9001-32-5)
Fluorescent fibrinogen 594	ThermoFischer (F13193)
Formaldehyde	Sigma-Aldrich (462-95-3)
HEPES	Sigma-Aldrich (7365-49-9)
HPLC water	Sigma Aldrich (7732-18-5)
KCl	Sigma Aldrich (7477-40-70)
KH_2PO_4	Merk (7447-40-7)
$MgCl_2$ (Tübingen)	MERCK (7778-77-EC)
$MgCl_2$ (London)	Sigma Aldrich (7789-30-3)
NaCl	MERCK (7647-14-5)
$NHCO_3$	Sigma Aldrich (144-55-8)
Na_2HPO_4	Sigma Aldrich (10028-24-7)
NaH_2PO_4	Carl Roth (10049-21-5)
PBS (Tübingen)	Sigma Aldrich (P3813)
PBS (London)	Cytiva (SH3025601)
PDMS Sylgard 184	Avantor
PLL-g-PEG	Surface Solutions
PMSF	Sigma-Aldrich (329-98-9)
SDS	Carl Roth (151-21-3)
Sodium citrate	Sigma Aldrich (6132-04-3)
tri-Sodium Citrate 2-hydrate	Carl Roth (68-04-2)
TRIS	Carl Roth (77-86-1)
Triton X-100	Sigma-Aldrich (9036-19-5)

2.1.2 Drugs and compounds

Compound	Company & Cat. No
ADP	Sigma Aldrich (01905)
CBV-TP	Toronto Research Chemical (C177757)
Cinaciguat hydrochloride	Sigma Aldrich (646995-35-9)
Horm Collagen	Takeda
ODQ	Cayman Chemicals (41443-28-1)
Riociguat	Cayman Chemicals (625115-55-1)
Tenofovir	Selleckchem (GS-1278)
Thrombin	Sigma Aldrich (520222)
Vericiguat	Cambridge Bioscience (CAY35253-5)
8-Br-cGMP	Sigma Aldrich (51116-01-09)

2.1.3 Antibodies for immunostainings and western blot

Compound	Company & Cat No	Cat.No
ActinGreen™ 488	Invitrogen™, ThermoFisher	R37110
Annexin V	Biolegend	640937
P-selectin (CD62P)	Bioscience™, ThermoFischer	Psel.K02.PE
CD31 (PECAM-1)	Biolegend	303121
CD105 (Endoglin)	Biolegend	800509
CD62P	BD Biosciences	550888
CD63	BD Biosciences	556020
PAC-1	Fisher Scientific	340507
p-VASP Ser239	Cell Signaling	3114S
GAPDH	Cell Signaling	2118S
NO-GC β1	Abcam	24824

2.1.4 Platelet isolation buffers

ACD buffer, pH 4.69

Compounds	Concentration
Tri-Sodium Citrate-2-hydrate	85 mM
Citric acid (anhydrous)	72.9 mM
D-glucose	110 mM

Platelet Wash Buffer (PWB), pH 6.5 (murine platelets)

Compounds	Concentration
K_2HPO_4	4.3 mM
Na_2HPO_4	4.3 mM
NaH_2PO_4	24.3 mM
D-glucose	5.5 mM
NaCl	113 mM

Tyrode Buffer, pH 6.5 (human platelets)

Compounds	Concentration
NaCl	136.8 mM
NaH_2PO_4	8.4 mM
KCl	2.6 mM
D-glucose	5.5 mM

Tyrode-HEPES buffer, pH 7.4 (healthy human volunteers)

Compounds	Concentration
HEPES	6 mM
NaCl	136.8 mM
NaH_2PO_4	8.4 mM
KCl	2.6 mM
D-glucose	5.5 mM

Tyrode-HEPES buffer, pH 7.4 (platelets from HIV-positive patients)

Compounds	Concentration
HEPES	10 mM
NaCl	140 mM
KCl	5 mM
$MgCl_2$	1 mM
D-glucose	5 mM
NaH_2PO_4	0.42 mM
$NaHCO_3$	12 mM

Tyrode-HEPES buffer, pH 7.4 (murine platelets)

Compounds	Concentration
HEPES	10 mM
NaCl	137 mM
$NaHCO_3$	12 mM
KCl	2.7 mM
D-glucose	5.5 mM
BSA	1 %

2.1.5 SDS-PAGE and western blot buffers

Lysis buffer

Compounds	Concentration
Tris pH 8.3	21 mM
SDS	0.67 %
PMSF	0.2 mM
H_2O	1 mL

10 × SDS loading buffer

Compounds	Concentration
Tris	15.1 g
Glycine	72.0 g
SDS	5.0 g
H_2O	to 500 mL

Anode blotting buffer I (pH 10.4)

Compounds	Concentration
Tris	300 mM
Methanol	20% (v/v)

Anode blotting buffer II (pH 10.4)

Compounds	Concentration
Tris	300 mM
Methanol	20% (v/v)

Cathode blotting buffer II (pH 7.6)

Compounds	Concentration
Tris	30 mM
Methanol	20% (v/v)
6-Aminocapronic acid	40 mM

10x TBS (pH 8.0)

Compounds	Concentration
Tris/Cl	100 mM
NaCl	1.5 M

TBS-T

Compounds	Concentration
TBS	1x
Tween-20	0.1%

ECL reagent

Compounds	Concentration
ECL reagent	1:1 to 1:10 in TBS-T

10% separating gel (1 gel with 1.5 mm)

Compounds	Concentration
Rotiphorese® Roth (30% acrylamide/0.8% bisacrylamide)	15.1 g
4x Tris-Cl/SDS (pH 8.8)	2.5 mL
H_2O	4.1 mL
20% Ammonium persulphate (APS)	50 µL
TEMED	10 µL

4% stacking gel (1 gel with 1.5 mm)

Compounds	Concentration
Rotiphorese® Roth (30% acrylamide/0.8% bisacrylamide)	0.65 mL
4x Tris-Cl/SDS (pH 8.8)	1.25 mL
H_2O	3.05 mL
20% Ammonium persulphate (APS)	25 µL
TEMED	10 µL

The following methods are partially modified from the manuscripts presented below in the results section.

2.2 Mouse lines

All experiments were reported according to ARRIVE guidelines (82), and approved by the local authority (Regierungspräsidium Tübingen, IB 02/20M). Platelets from mice of 3 to 12 months of age were used in these experiments. CD57Bl6/J (wild-type mice) and megakaryocyte/platelet specific NO-GC KO mice with a Pf4-Cre (wt/Cre); NO-GC (flox/flox) genotype were used (83). Pf4-Cre line (B6-Tg(Cxcl4-cre)Q3Rsko/J) (84) were

crossed with NO-GC (flox/flox) line (B6.129-Gucy1b3tm1.2Frb) (85) to generate megakaryocyte/platelet specific NO-GC KO mice.

2.3 Blood sampling

Platelets were isolated from healthy human volunteers and HIV-positive patients currently taking TFV- or ABC-containing regimens. Informed consent was obtained from all the volunteers in Tübingen and London.

2.3.1 Human blood

All procedures were in accordance with the declaration of Helsinski and approved by the institutional ethics committees (Medical Faculty and University Clinics at the University of Tübingen, 273/2018B02 and 064/2022).

1. Add 1.25 mL of sterile ACD buffer in each 4.9 mL monovettes (1:4 ratio ACD:blood) before blood collection.
2. Collect venous blood in ACD anticoagulant (RT). Gently mix ACD and whole blood after collection.
3. Transport the samples to the lab while keeping them at 37^0C.
4. Pre-heat all buffers to 37^0C before isolation.
5. The content of one 4.9 ml monovettes is transferred into the one 15mL falcon, by positioning the monovette at an angle against the inner wall of the falcon and pouring slowly.
6. Centrifuge falcons at 200 x g, 20 min, RT, no acceleration, or break.
7. Meanwhile: prepare Tyrode-HEPES buffer, pH 7.4 and Tyrode buffer, pH 6.5.
8. Three specific layers in whole blood are visible after centrifugation (Figure 4):
9. Bottom layer: red blood cells
10. Middle layer: very thin white layer of white blood cells (“buffy coat”)
11. Top layer: straw-colored platelet rich plasma (PRP)
12. Fill one 15mL falcon with 1mL of Tyrode buffer, pH 6.5. Collect upper 2/3 of the PRP and transfer it into the 15mL falcon (max. 2.5 mL PRP per falcon).
13. Fill up the falcons in a 1:3 ratio with Tyrode buffer, pH 6.5.
14. Centrifuge falcons at 800 x g, 10 min, RT, no acceleration, or break.

15. Discard the supernatant and resuspend the pellet in 1mL of Tyrode-HEPES buffer, pH 7.4.
16. To verify the density and viability of the platelets, add 50 µL of the washed platelet suspension and 1mL of Tyrode-HEPES buffer, pH 7.4 in a CellStar plastic cell culture dish and observe platelets under the microscope. Wash the platelets after 15 min to get rid of the unadhered platelets.

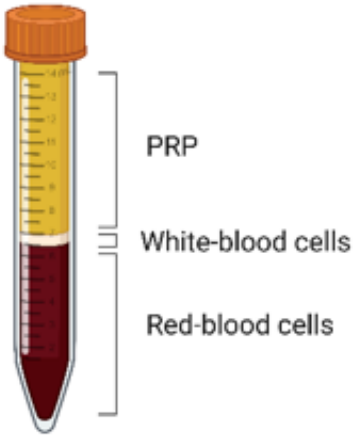

Figure 4. Layers found in whole blood after centrifugation. This figure was designed in Biorender.com (2023).

2.3.2. HIV-positive patient's blood

Platelets from HIV-positive patients taking TFV- or ABC-containing regimens, registered at Chelsea and Westminster Hospital NHS Trust, were obtained in accordance with research ethics permits 294707 21/NW/0148 approved by the NHS Health Research Authority and Chelsea and Westminster Hospital NHS Trust. This standard operating protocol (SOP) was partially modified from an existing protocol in the laboratory from Dr. Michael Emerson at Imperial College London.

Blood collection

1. Blood collection must be conducted by a competent individual in the phlebotomy room. Alternatively, blood will be transported from external clinical sites in capped vials within double bags inside an unlabeled screw top plastic container.
2. Wear appropriate PPE (nitrile gloves, confirm that donor does not have an allergy).
3. Apply tourniquet to the arm.

4. Identify vein and wipe area with cotton and alcohol.
5. Allow alcohol to dry.
6. Connect butterfly to vacutainer adaptor and insert needle into the vein (if successful, there will be a backflush of blood into the tubing and syringe).
7. Draw blood into the required number of vacutainers.
8. Loosen tourniquet.
9. Remove needle.
10. Apply pressure with fresh cotton wool.
11. Dispose of needle in appropriate sharps bin.
12. Wait for bleeding to stop and apply plaster to puncture site.
13. Transport blood to bench using secondary container.

Platelet preparation

1. *Platelet-rich plasma (PRP)*
2. Place vacutainers into centrifuge (ICTEM 508).
3. Centrifuge at 175 *x g*, 15 min (no break applied for the end of spinning program).
4. Transfer PRP to a fresh 50 mL centrifuge tube inside the MSC hood.
5. ** for PRP experiments prepare platelet-poor plasma (PPP) by centrifugation in a microfuge at 15,700 *x g*, 3 min.

Washed platelets (WP)

1. Add 150 µL ACD and 5 µL PGE_1 to the PRP and mix by inversion.
2. Centrifuge PRP at 1400 *x g*, 10 min, brake level 2.
3. Remove PPP using a 3 mL Pasteur pipette.
4. Re-suspend platelets in 1 mL Tyrode-HEPES buffer, pH 7.4 using P1000.
5. Top-up to 20 mL with Tyrode-HEPES buffer, pH 7.4, add 3mL ACD, and 5µL PGE_1.
6. Centrifuge platelet suspension at 1400 *x g*, 10 min, brake level 2.
7. Remove supernatant.
8. Resuspend platelets in 1mL Tyrode-HEPES buffer, pH 7.4.

2.3.3 Murine blood

This SOP was partially modified from an existing protocol in the laboratory from Prof. Dr. Robert Feil.

1. Preload an Eppendorf with 100 µL of ACD buffer and withdraw blood from the retro-orbital sinus of wild-type and megakaryocyte/platelet-specific NO-GC KO mice under isoflurane anesthesia.
2. Add 300 µL of PWB, pH 6.5 and blood into a FACS tube.
3. Centrifuge at 250 *x g*, 2 min, no brake.
4. Collect PRP (upper layer) in another extra tube A. Use cut-off pipette tip when pipetting platelets.
5. Add 600 µL PWB to remaining tube and centrifuge again at same settings.
6. Transfer supernatant to extra tube A.
7. Centrifuge at 2000 *x g*, 1 min, brake 5.
8. Re-suspend pellet in 100 µL – 1 mL Tyrode-HEPES buffer depending on pellet size.

2.4 Drug treatments for human and murine platelets

The following sample preparation was performed for human and murine platelets for immunofluorescence, deep learning platelet morphometry, and SICM measurements.

1. Coat thirty-five mm glass-bottom cell culture dishes (81218, ibidi, Gräfelfing, Germany) with 0.1 mg/mL human plasma fibrinogen and incubate for 30 min at 37 ^{0}C.
2. Supplement Tyrode-HEPES buffer with 1mM of $CaCl_2$ and $MgCl_2$.
3. Incubate human or murine platelets for 10 min with the different drug treatments. ADP (3µM), DMSO (1:1000), 8-Br-cGMP (1 mM), riociguat (10 µM), cinaciguat (10 µM), vericiguat (10 µM), ODQ (20 µM), CBV-TP (50 µM), TFV (50 µM)
4. Add 50 µL of human or murine treated-platelets to the fibrinogen-coated cell culture dishes containing 1mL of supplemented Tyrode-HEPES buffer for 15 min.

5. Remove unattached platelets with three washing steps with human or murine supplemented Tyrode-HEPES buffer before imaging.

2.5 Immunofluorescence microscopy

Immunofluorescence microscopy aids in the characterization, localization, and expression of proteins in biological systems using well-characterized fluorescent antibodies (86). Epifluorescence images were recorded with an optical microscope (TiE, Nikon, Tokio, Japan) with a 100x/1.45 NA oil immersion objective and a monochrome digital camera (DS-Qi2, Nikon) with 300 ms exposure time. Platelets from human healthy volunteers, wild-type, and platelet-specific NO-GC KO mice were treated as described above, and then co-stained with F-actin and P-selectin. F-actin stains the platelet cytoskeleton, while P-selectin is a marker for platelet activation. P-selectin staining aids in the identification of α-granules distribution inside the human or murine platelets previously treated with DMSO (1:1000), 8-Br-cGMP (1mM), riociguat (10 µM) and cinaciguat (10 µM).

F-actin and P-selectin co-immunostaining

1. Take the cell culture dishes with the human or murine platelets. Sample was prepared according to the description presented in section 2.4.
2. Fix previously treated platelets in PBS containing 2% formaldehyde for 10 min.
3. Wash the sample three times with PBS.
4. Incubate fixed platelets with 1% BSA in PBS for 10 min.
5. Wash the sample three times with PBS.
6. Stain P-selectin (CD62P) on human or murine platelets with an anti-CD26P antibody at a 1:200 dilution for 45 min, in a dark humidified chamber.
7. Wash the sample three times with PBS.
8. Stain human or murine F-actin with ActinGreen^{TM} 488 at a 1:2000 dilution for 20 min in a dark humidified chamber.
9. Wash the sample three times with PBS.
10. Record immunofluorescent images.

Platelets from HIV-positive patients currently taking TFV- or ABC-containing regimens, and biochemically confined platelets were only stained with F-actin. Sample preparation of the confined platelets will be further explained below.

F-actin immunostaining

1. Fix platelets in PBS containing 2% formaldehyde for 10 min.
2. Wash the sample three times with PBS.
3. Incubate with 0.1% Triton X-100 for 10 min.
4. Wash again three times with PBS.
5. Stain human platelet F-actin with ActinGreenTM 488 at 1:2000 dilution in PBS for 20 min in a dark humidified chamber.
6. Record the immunofluorescence images.

Image analysis

ImageJ software (https://imagej.nih.gov-7ij) was used to analyze immunofluorescence platelet images from human healthy volunteers, wild-type, and platelet-specific NO-GC KO mice. Corrected total cell fluorescence (CTCF) was obtained with the following formula: CTCF = fluorescence intensity integrated over the cell area – (mean fluorescence intensity of the background × cell area). Individual actin content for confined and unconfined platelets was quantified as the mean fluorescence intensity (MFI).

2.6 Scanning ion conductance microscopy

Live imaging of platelets from humans and wild-type and platelet-specific NO-GC KO mice were performed with SICM (87). Platelets, previously treated were placed on fibrinogen-coated cell culture dishes. Figure 5 shows a classical SICM set-up which consists of an electric voltage applied by two electrodes (one inside the bath solution, and another inside the upper part of the nanopipette), which generates an ionic current through the nanopipette filled with an electrolyte solution (88).

The slope of the ion current *I* vs. *z*-position distance curve (IZ-curve) between 99% and 98% of the saturation current for each pixel gives the platelet cellular stiffness, which is calculated based on a finite element model (89). The ion current is strongly dependent on the pipette-sample distance, which allows non-contact imaging of platelets (87).

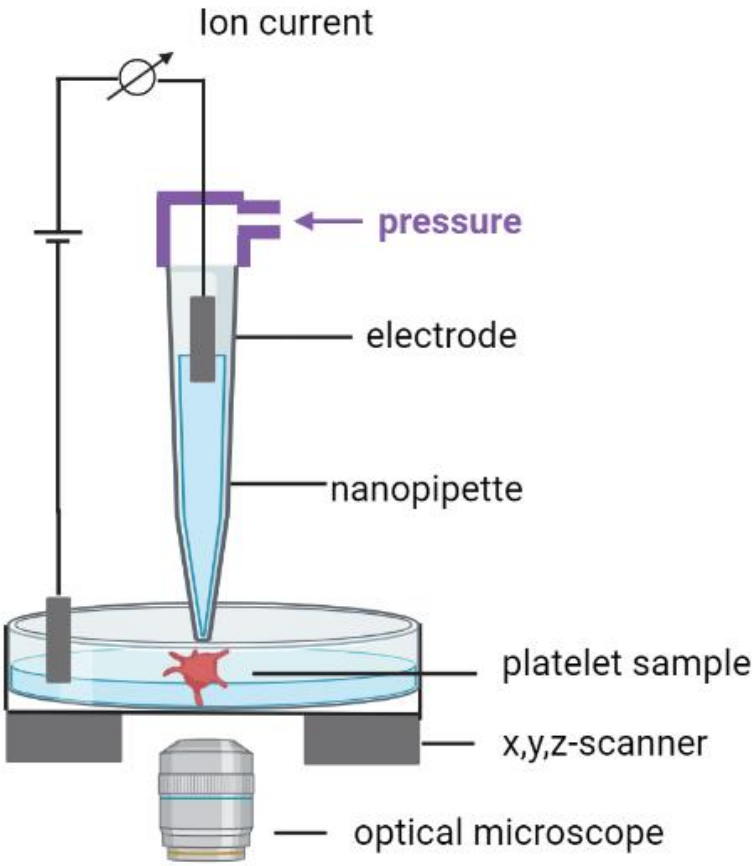

Figure 5. SICM set-up. This figure was designed in Biorender.com (2023).

SICM imaging

1. Fabricate borosilicate nanopipettes (1B100F-4, World Precision Instruments Inc., Sarasota, FL) with an inner radius of 90 nm using a CO_2-laser-based micropipette puller (P-2000; Sutter Instrument, Novato, CA, USA).
2. Place the sample in a custom-build SICM set-up. Live-imaging measurement of platelets must be completed within 1 h because of the platelet short life span after isolation.
3. Record platelet cellular stiffness and topography with a constant pressure of 10 kPa applied at the upper end of the pipette.

4. For each sample, record a zero-pressure map, and a pressure map of the first platelet imaged to confirm that the pressure is working properly.
5. Image single platelets with the following parameters: pixel rate 25 Hz; 30 × 30 or 65 × 65 pixels size (for high resolution images); scan size: 30 × 30 μm^2.
6. Average the median value of each cellular stiffness map within the area of the platelet to obtain the cellular stiffness value of a single platelet.

2.7 Atomic force microscopy

Live imaging of confined and unconfined platelets, previously activated with two platelet agonists ADP or thrombin, were performed with a commercial AFM setup (MFP3D-BIO, Asylum Research, Santa Barbara, CA) mounted on an inverted optical microscope (Ti-S, Nikon). Figure 6 shows an AFM setup which consists of a cantilever, a laser, and a photodiode (90). The laser beam is reflected on the back surface of the cantilever, and then reflected onto the photodiode (90). The position of the laser beam only changes when the cantilever deflects, which is usually upon tip-sample contact (90). Hooke´s law (equation 1) describes the force calculation in a force-curve in AFM (91).

$$F = -kd \tag{1}$$

where F is the force, k the cantilever spring constant, and d the cantilever deflection (91). Force volume maps are a two-dimensional matrix of the force curves collected from the sample (91). Height maps, stiffness maps, and volume values were obtained from living platelets. The stiffness of single platelets was calculated as the median of the values in the stiffness map, and the volume as the mean height of the platelets multiplied with the platelet area excluding areas of the substrate and the lowest 20% of the platelet data.

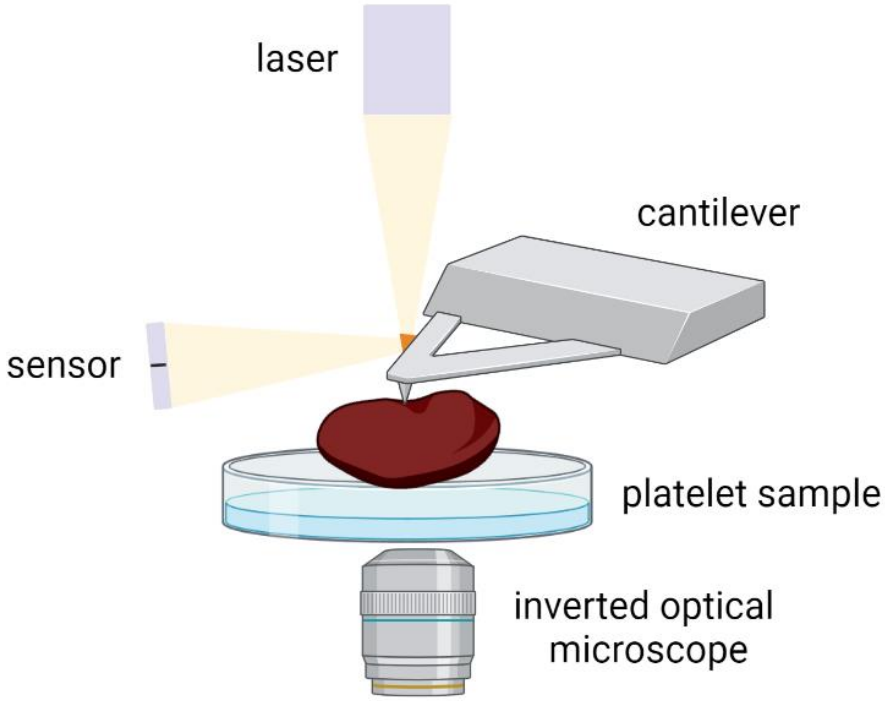

Figure 6. AFM set-up. This figure was designed in Biorender.com (2023).

AFM imaging

1. Switch on the microscope and place the sample. Measurement was recorded within one hour after blood isolation because of the short platelet life-span.
2. Use MLCT-Bio DC B cantilevers (Bruker, Camarillo, USA) with a pyramidal tip shape (35° face angle, 20 pN/nm nominal spring constant). Calibrate the cantilever spring constant with the thermal noise method (92)
3. Record force indentation curves at many positions of the platelets in the force mapping mode with the following parameters:
    - Force curve rate: 4.8 Hz
    - Retract distance: 1 µm
    - Trigger force: 200 pN
    - Number of pixels: 35 × 35 pixels
    - Scan size: 20 × 20 μm^2 to 25 × 25 μm^2
4. Fit the Hertz model (93) for pyramidal indenters to each force-indentation curve in the force maps using Igor Pro.

5. Remove the influence of the stiff substrate by implementing the height correction method and limiting the maximum force to 20pN during the analysis. Height correction method was applied because the median heights of the corresponding platelets were lower leading to higher stiffness values.

2.8 Deep learning convolutional neural network

Different shape parameters were obtained with a deep learning CNN analysis, including platelet area, aspect ratio, circularity, and number of filopodia (64). Circularity and number of filopodia are unitless parameters (64). Platelet aspect ratio is defined as the length to the width ratio, while circularity measures platelet roundness (circularity =1 for a perfect circle) (64). Shape parameters can be correlated to platelet activation and spreading stages.

Consequently, phase contrast images of fixed platelets from human healthy volunteers, and wild-type and platelet-specific NO-GC KO mice were recorded with an optical microscope (TiE, Nikon, Tokio, Japan) with a 100x/1.45 NA oil immersion objective and a monochrome digital camera (DS-Qi2, Nikon) with 300 ms exposure time. Phase

contrast images of fixed platelets from HIV-positive patients taking TFV- or ABC-containing images were taken at the FILM (Facility for Imaging by Light Microscopy) at Imperial College London with a WF3 Zeiss Axio Observer microscope, a Zen Blue software with a 100x/1.4 Oil Ph3 Plan Apochromat, a phase illumination for the transmitter light channel, and a Hamamatsu Flash 4.0 camera with a pixel size of 65 nm.

Record of phase contrast images for neural network analysis (fixation protocol)

1. Fix platelets in PBS containing 2% formaldehyde for 10 min.
2. Wash the sample three times with PBS.
3. Incubate with 0.1% Triton X-100 for 10 min.
4. Wash again three times with PBS.
5. Record phase contrast images.

2.9 SDS-PAGE and Western Blot

This SOP was partially modified from an existing protocol in the laboratory from Prof. Dr. Robert Feil. SDS-PAGE separates denatured negatively charged proteins in a polyacrylamide gel according to their size (94).

Human, wild-type, and platelet-specific NO-GC KO murine platelets were incubated for 10 min at 37 ^{0}C with control (PBS), DMSO (1:1000), ADP (3 µM), 8-Br-cGMP (1mM), riociguat (10 µM) and cinaciguat (10 µM). Platelet lysates were extracted from all the pre-treated platelets by centrifuging at 2000 × g for 1 min and re-suspending in a lysis buffer. Each sample was frozen in liquid nitrogen for 2 min, and then thawed at room temperature. Protein lysates were separated by SDS-PAGE and detected with the following antibodies: phosphorylated (p-VASP) Ser239 (rabbit, 1:1000, Cell Signaling #3114S), glyceraldehyde-3-phosphate dehydrogenase (GAPDH) (rabbit, 1:1000, 14C10, Cell Signaling #2118S) and NO-GC (sGC β1, rabbit, 1:100, abcam 24824)

SDS-PAGE

1. Assemble the gel casting system (BioRad Laboratories, Inc, Hercules, USA).
2. Prepare separating and stacking gel solutions and then store at 4 ^{0}C.
3. Add TEMED and APS to the separating gel solution and pour the gel between the glass plates. The gel needs 45 min to polymerize.
4. Add TEMED and APS to the stacking gel solution and pour the gel between the glass plates. Insert the comb (1.5 mm, 15 wells). The gel needs 30 min to polymerize.
5. Remove the gel cassette assemblies from the casting strand.
6. Fill the inner chamber of the gel with 140 mL of 1 × SDS running buffer.
7. Fill the outer chamber of the gel with 250 mL of 1 × SDS running buffer.
8. Remove the comb and rinse the wells with 1 × SDS running buffer.
9. Load 3 µL of standard protein and maximum 20 µL of the corresponding sample.
10. Apply 100 V for 15 min through the stacking gel, and then 150 V for 1h to 2h. Stop the voltage when the lowest standard band is about 0.5 cm from the bottom of the gel.

Western blot

1. Cut approximately 16 Whatman filter papers (Hartenstein, Würzburg, Germany) per gel, and Immobilon P PVDF membrane.
2. Immerse the immobilon P membrane in methanol, and then submerge in the anode blotting buffer II.
3. Immerse the whatman papers in the order shown below starting from the anode of the transfer chamber. Then assemble a blotting sandwich on the semi-dry blotting device.

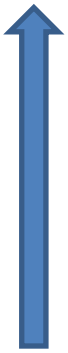

- Cathode of the transfer chamber
- 8 Whatman papers in cathode blotting buffer
- Gel
- PVDF membrane
- Whatman papers in anode blotting buffer II
- Whatman papers in anode blotting buffer I
- Anode of the transfer chamber

4. Blot the gel for 1h at 60 mA.
5. Mark the protein bands properly.
6. Block membrane with 5% milk powder in TBS-T for 1h.
7. Wash the membrane with TBS-T and transfer it inside a falcon tube with the diluted primary antibody.
8. Incubate at 4 ^{0}C overnight or for 2h at room temperature.
9. Wash three times for 5 min with 1 × TBS-T.
10. Incubate 1 h at room temperature in the secondary antibody.
11. Wash three times for 5 min with 1 × TBS-T.
12. Prepare ECL reagent at appropriate dilution in TBS-T. Place membranes in a plastic container and apply ECL reagent with a pipette. Record the images with the protein standard bands using the Alphamager device at different exposure times.

Western blot quantification

1. Upload the western blot images on the Image J software.
2. Go to Edit > Invert.
3. In case the western blot bands are not well aligned. Align the images using Image J software. Go to Image > Transforms > Rotate > Choose the degree angle you would like to rotate (e.g., 5 degrees).
4. Get rid of the image background, so the western blot bands are clear. Go to Image > Adjust > Brightness/Contrast > modify accordingly.
5. Make a rectangle around the first band's lines. Go to Analyze > Gels > Select First Lane.
6. Repeat the same procedure for all the remaining band´s lines.
7. Go to Analyze > Gels > Plot Lanes
8. Click on each parabola to get the area under the curve. This corresponds to each band of the western blot.
9. Copy the data to an Excel file.
10. Determine the ratio for NO-GC and p-VASP and analyze each drug treatment respectively. Identify your protein control group (GAPDH). Equation 2 shows an example of how to calculate the ratio of p-VASP in DMSO-treated platelets.

$$\text{Ratio DMSO (p} - \text{VASP)} = \frac{\text{DMSO treated platelets (p}-\text{VASP)}}{\text{DMSO treated platelets (GAPDH)}} \quad (2)$$

11. Normalize the ratio values obtained against 8-Br-cGMP.
12. Plot the quantification graphs for p-VASP and NO-GC using Igor Pro (Wavemetrics, Lake Oswego, Oregon, USA)

2.10 Endothelial-derived microparticles

Endothelial dysfunction has been correlated with cardiovascular diseases (95). Platelet aggregation, leukocyte recruitment and blood coagulation are regulated by the vascular endothelium (95). Disruption in the endothelium by ARTs administration may potentially lead to the development of thrombosis and other CVDs (95). Endothelial micro-particles (EMPs) have been isolated from human umbilical cord vein endothelial cells (HUVEC)

to understand how EMPs incubated with vericiguat and riociguat influence platelet activation in HIV-positive patients taking TFV- or ABC-containing regimens. Endothelial-platelet crosstalk was evaluated in platelets isolated from HIV-positive patients taking TFV- or ABC-containing regimens.

Endothelial Cell Culture (Figure 7 – part 1)

1. Thaw and culture HUVEC cells (PromoCell GmbH, Germany) in 80 cm^2 Nunclon Delta-treated tissue culture flasks (Thermo Scientific, United Kingdom) filled with endothelial cell growth media-2 (PromoCell GmbH) supplemented with 10% fetal calf serum.
2. Change the media the next day with the endothelial cell growth media-2 supplemented with 10% fetal calf serum.
3. On day 4, split the cells at around 50,000 cells/mL into 6-well Nunclon Delta-treated tissue culture plates (Thermo Scientific, United Kingdom).
4. On day 5, treat cells with the desired drugs for 48h. HUVECs cells were treated with control (PBS), DMSO (1:1000), ADP (3 µM), riociguat (10 µM), vericiguat (10 µM), and ODQ (20 µM).
5. On day 7, treat cells with 10 ng/mL tissue necrotic factor (TNF)-α (R&D systems, United Kingdom) for 6 hours before the endothelial microparticle isolation for each drug treatment (Figure 7, step 1).

Endothelial microparticle isolation and characterization (Figure 7 – steps 1 to 5)

1. Transfer cell medium to micro-centrifugation tube.
2. Spin at 3,000 × *g* for 5 min to remove dead cells/ cell debris.
3. Transfer supernatant to fresh tube.
4. Spin at 17,000 × *g* for 60 min at 4 ^{0}C to isolate EMPs. (Figure 7, step 2).
5. Re-suspend EMP pellet in filter sterilized AnnexinV (AnV) binding buffer (refer to Table 1) (Figure 7, step 3).
6. Prepare AnV binding buffer (Table 1) with FACS antibodies in a 1:50 dilution.
    - Annexin V
    - CD31 (PECAM-1)
    - CD105 (Endoglin)
7. Add 5 µL of EMP to wells with AnV and FACS antibodies (stain in 50 µL).

8. Incubate for 30 min in the dark, at RT, with gentle shaking (Figure 7, step 4).
9. Add 150 µL filter sterilized AnV buffer.
10. Add $2x10^5$ 3 µm latex beads.
11. Run on flow cytometer within an hour (Figure 7, step 5).
12. Gating tube should contain 0.3 µm and 1 µm latex beads (Fortessa can go as low as 0.2 µm). Apply gate between the two beads and carry forward to following tubes.
13. The total number of EMP per mL was calculated using Equation 3 (95).

$$\frac{\text{EMP}}{\text{mL}} = \frac{\text{Beads added}}{\text{Beads counted}} \times \text{AnV positive events} \times \frac{\text{EMP resuspension volume}}{\text{Volume of EMP stained}} \times \frac{1000}{\text{Initial supernatant volume (mL)}} \quad (3)$$

14. Keep the isolated EMPs in the fridge at 4 ^{0}C and use the next day for the endothelial-platelet crosstalk experiment.

Annexin V binding buffer (pH 7.4)

Compounds	Concentration
HEPES	10 mM
NaCl	140 mM
$CaCl_2$	2.5 mM

Table 1. Annexin buffer

2.11 Flow cytometry

This SOP was partially modified from an existing protocol in the laboratory from Dr. Michael Emerson at Imperial College London. During activation, platelets undergo morphological changes, and they release activation molecules. Flow cytometry is a standard technique used to assess the changes in the expression of platelet activation markers. Flow cytometers evaluate single events (cells) and record their forward (FSc) and side scatter (SSc) profiles based on their size and granularity, respectively. The fluorescence of each antibody is detected and recorded using specific fluorescence detectors and wavelength. The instrument used in this experiment is Accuri C6 plus which has four fluorescent channels (FL1-FL4), allowing four different wavelengths to

be recorded. Accuri C6 plus flow cytometer is equipped with a 488 nm (blue) and 640 nm (red), four fluorescent detectors and two scatter detectors.

Instrument start-up procedure

1. Check that fluid bottles are topped-up (excluding waste bottle) before turning machine on.
2. Press the power button on the front of the Accuri and turn on acquisition PC.
3. Wait for Accuri to start-up (approx. 13 min) and leave to allow laser to warm up (approx. 30 – 40 mins total).
4. Log-on to PC
5. Run fresh distilled H_2O (10 min, fast), and check number of events s^{-1} (clean fluidics 0-4 events s^{-1}).

Agonist-evoked expression of activation markers by platelets (Figure 7 – steps 6 to 8)

1. Set-up plot area to monitor activation markers:
2. Plot all the FSc/SSc density for the main platelet activation markers:
    - FITC: PAC-1 (active integrin $\alpha_{IIb}\beta3$
    - PE: CD63 (lysosome-associated membrane protein-3, LAMP-3)
    - APC: CD62P (P-selectin – α granule marker)
3. Set threshold to 20,000 events.
4. Save the template file for further experiments.
5. Dilute PRP into Tyrode-buffer pH 7.4 in (1:10) ratio.
6. Mix isolated EMPs with platelet PRP, and incubate for 30 min (Figure 7, step 6).
7. Prepare a FACS master mix for the final volume of 120 µL for each drug treatment (Table 2).
8. ADP and collagen were used to evoke platelet activation.
9. Mix 5 µL platelets with 103 µL master mix (Table 2) and register on the software (Figure 7, step 7).
10. Press ´run´ to start acquisition (Figure 7, step 7).
11. Run sample for 30 sec (shown in sample stats – lower left of screen) (Figure 7, step 7).
12. Bend a gel loading tip 45^0 and add 12 µL agonist into the sample (Figure 7, step 7).

13. Mix the sample with the pipette for 30 s and acquire events for 4 min 30 sec (Figure 7, step 8).
14. Discard in autoclave waste and repeat for each sample.
15. At the end of day perform ´SIP clean´, follow on-screen instructions and place tube with 2 mL FACS clean and press ´start´, when prompted replace tube with 2 mL distilled H_2O and press ´start´.
16. Check number of events, if above 0 – 4 then see troubleshooting for extra cleaning steps.
17. Export data for analysis in FlowJo/Excel/CFlow

Master mix for FACS

Compounds	**Volume (µL) for 1 sample**
PAC-1	2
CD62P	2
CD63	2
Platelet Tyrode Buffer, pH 7.4	97
Platelets	5
10x Agonist (3µM ADP or 3µM collagen)	12
Total volumes	120

Table 2. Master mix for FACS

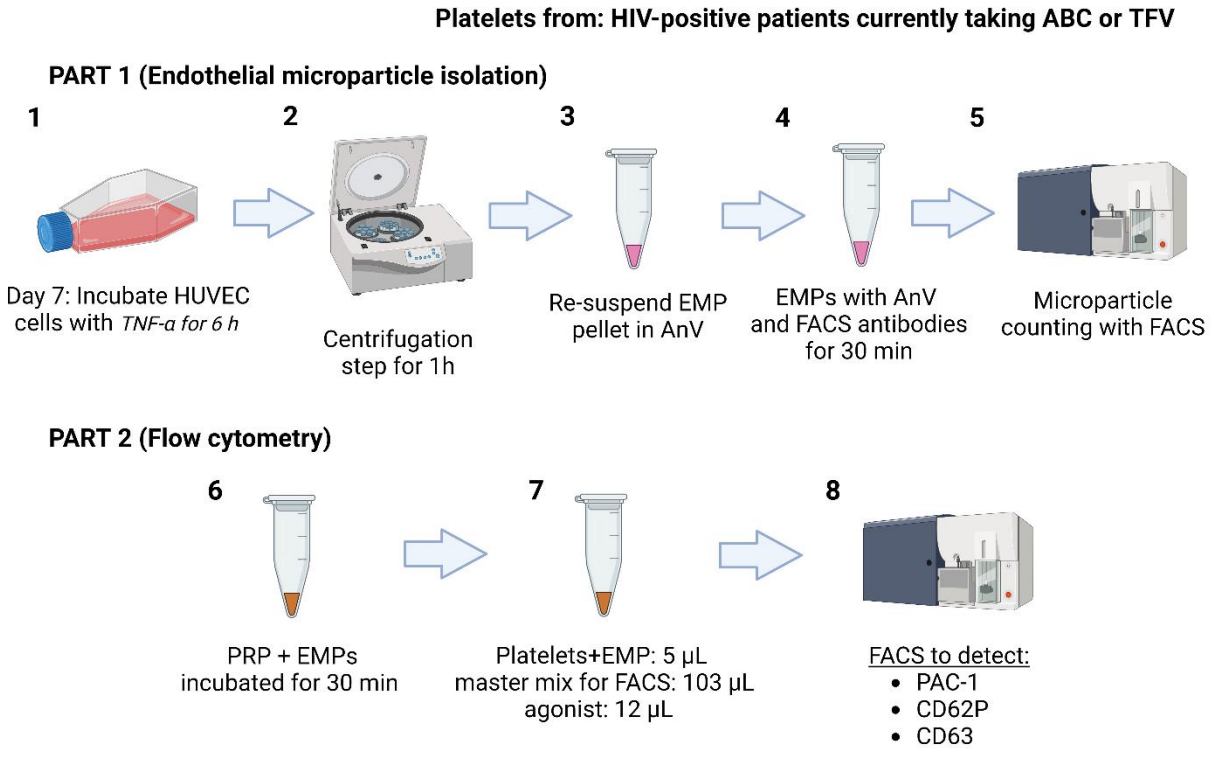

Figure 7. Endothelial microparticle isolation and flow cytometry to identify platelet activation markers in platelets isolated from HIV-positive patients currently taking ABC or TFV. This figure was designed in Biorender.com (2023).

2.12 Light transmission aggregometry

Platelet aggregation occurs when platelets adhere to each other (96). This phenomenon can be replicated in vitro by adding different agonists such as ADP, collagen, or TRAP-6 to PRP (96). Platelet aggregation is the gold-standard test to characterize platelet function and to test potential therapeutical agents (96). The aggregometer is constantly stirring at 37^0C to emulate the shear stress of a vessel, with a fixed wavelength (96). The beam of infrared light passes through the cuvette containing the samples PRP or PPP (96). PPP is the sample reference, and it is considered as 100% aggregation (96). The difference in light transmission between PPP and PRP gives the percentage of aggregation (96).

In vitro platelet aggregation in a 96 well plate format was studied in human platelets from HIV-positive patients taking ABC or TFV and healthy volunteers. This standard operating procedure (SOP) was partially modified from an existing protocol in the laboratory from Dr. Michael Emerson at Imperial College London.

Platelet aggregation

1. Turn on plate reader (Tecan SUNRISE).
2. Open Magellen 7.2 SP1 Software and select “Aggregation” protocol file (N.B. Aggregation protocol shortcut saved onto desktop).
3. *Settings*
    - Mode: kinetic
    - Time: 16 min (00:16:00)
    - Wavelength: 595 nm
    - Read mode: sweep
    - Plate: 96 well
    - Temp control: yes
    - Pre-heating: yes
    - Temperature: 37^0C

4. Before each reading: Shaking = yes; Intensity = 3; Duration = 7 sec.
5. Select “New Plate”, “Read”, “Read Plate”.
6. Close the door and leave plate reader to reach desired temperature. The door of the plate reader should be closed during the procedure to maintain the temperature at 37^0C.
7. Pre-incubate the platelet PRP with the different drugs in a 1:1 ratio at 37^0C (refer to Table 3).
8. Label 96-well plate according to your experimental design (Figure 8).
9. Prepare agonist (10 µL/concentration/well) (Table 4)
10. Pipette agonists to respective wells (inverse pipetting, multichannel)
11. Add PPP, PRP, and PBS to reference wells.
12. Pour RP into reagent reservoir and add 90 µL to respective wells.
13. Place plate into plate reader and start recording.
14. Remove plate, apply plate seal, and dispose in the autoclave waste.
15. To export entire timepoint data:
    - Select “Edit method”.
    - Under the “Data handling” section, select “Data export”.
    - Move “Well positions” and “Raw data” into the right-hand column.
    - Click on “File” in the top menu bar and select “Excel Export”.
    - Export data on a USB stick or email spreadsheet to yourself.
16. Analyze in excel the data exported.
17. At the end of experiment, close reader door, close software and turn off plate reader.

Drugs combination	**Time**
DMSO	20 min
ODQ	20 min
Carbovir	20 min
ODQ-Carbovir	10 min (ODQ) + 10 min (CBV-TP)
Tenofovir	20 min
ODQ-Tenofovir	10 min (ODQ) + 10 min (TFV)
Riociguat	20 min
ODQ-Riociguat	10 min (ODQ) + 10 min (Riociguat)
Vericiguat	20 min
ODQ-Vericiguat	10 min (ODQ) + 10 min (Vericiguat)

Table 3. Incubation times and drugs used in platelet aggregation experiments.

Agonist	Concentration
ADP	10 µM
Collagen	10 µM

Table 4. Agonist concentrations used in platelet aggregation experiments.

		1	2	3	4	5	6	7	8	9	10
	A	**PPP**				**PRP**				**PBS**	
ADP	**B**	DMSO	ODQ	CBV	ODQ CBV	TFV	ODQ CBV	RIO	ODQ RIO	VERI	ODQ VERI
ADP	**C**	DMSO	ODQ	CBV	ODQ CBV	TFV	ODQ CBV	RIO	ODQ RIO	VERI	ODQ VERI
Collagen	**D**	DMSO	ODQ	CBV	ODQ CBV	TFV	ODQ CBV	RIO	ODQ RIO	VERI	ODQ VERI
Collagen	**E**	DMSO	ODQ	CBV	ODQ CBV	TFV	ODQ CBV	RIO	ODQ RIO	VERI	ODQ VERI

Figure 8. Scheme of a 96-well plate labelled for a healthy volunteer aggregation experiment.

2.13 Micro-contact printing and biochemical confinement

Platelet morphology and mechanics are affected by physical confinement. The development of micro-contact printed fibrinogen lines in cell culture dishes, with a width of 5 µm and a periodicity of 15 µm, providing the necessary physiological conditions, which mimics a blood capillary, allowed us to understand the effects of biochemical confinement on platelet morphology and mechanics. This study is the first to compare different platelet agonists (ADP or thrombin) in biochemical confinement.

µCP sample preparation

1. Fabricate a PDMS silicon master using replica-molding as previously described (97). The stamp is divided into a flat and µCP line patterned regions.
2. Make a wafer pattern consisting of parallel and rectangular channels with a periodicity of 15 µm, depth of 5 µm, and width of 5 µm using PDMS Sylgard 184 (Avantor, Radnor, Pennsylvania, USA) in a 10:1 ratio for monomer and crosslinker.
3. Centrifuge the PDMS mixture for 3 min at 1200 × g and pour over the silicon wafer.

4. Cure the sample for 2 hours at 80 ^{0}C and place the sample in the desiccator for 30 min to remove air bubbles.
5. Remove the PDMS layer from the silicone master and cut into smaller parts providing stamps for µCP (Figure 9, step 1).
6. Wash PDMS stamps with 70% ethanol, dry with pressurizer air, and plasma clean with oxygen (Zepto-QRS 200, Diener electronic GmbH) for 30 s.
7. Coat the pattern for 30 min at 37 ^{0}C with fluorescent fibrinogen (66 µg/mL, Alexa FluorTM 594 Conjugate, F1391, ThemoFischer Chemical, Waltham, MA, USA) (Figure 9, step 2).
8. Wash the samples with sterile water and dry with Nitrogen gas.
9. Plasma clean the glass bottom cell culture dishes with oxygen for 30 sec (81218, ibidi, Grafeling, Germany) with oxygen plasma for 30 s using the same procedure described above.
10. Face-down the fibrinogen-coated PDMS stamps on the center of the cell culture dishes and incubate them for 15 min at 37 ^{0}C (Figure 9, step 3).
11. Remove the fibrinogen-coated PDMS stamps from the cell culture dishes.
12. Incubate the cell culture dishes for 1 h with PEG-grafted poly-L-lysine (PLL-g-PEG, 10 µg/mL in 10 mM HEPES) to prevent the adhesion of platelets to the regions without fibrinogen (Figure 9, step 4).
13. Wash three times with PBS to remove the excess of PEG from the cell culture dishes.
14. Isolate platelets (procedure explained above) (Figure 9, step 5)
15. Incubate freshly isolated platelets with ADP (10 µM) or thrombin (0.13 U/mL) for 2 min at 37 ^{0}C (Figure 9, step 6)
16. Add platelets pre-incubated with ADP or thrombin, or untreated, to the cell culture dishes filled with Tyrode-HEPES buffer, pH 7.4. Allow platelets to spread for 25 min at 37 ^{0}C and wash the sample three times to remove non-adherent platelets. Prepare each sample for live-imaging or F-actin immunostaining (Figure 9, step 7).
17. Record AFM images of living platelets (Figure 9, step 9) and epifluorescence images of the flat and the µCP line patterned region in the same cell culture dish (Figure 9, step 8).

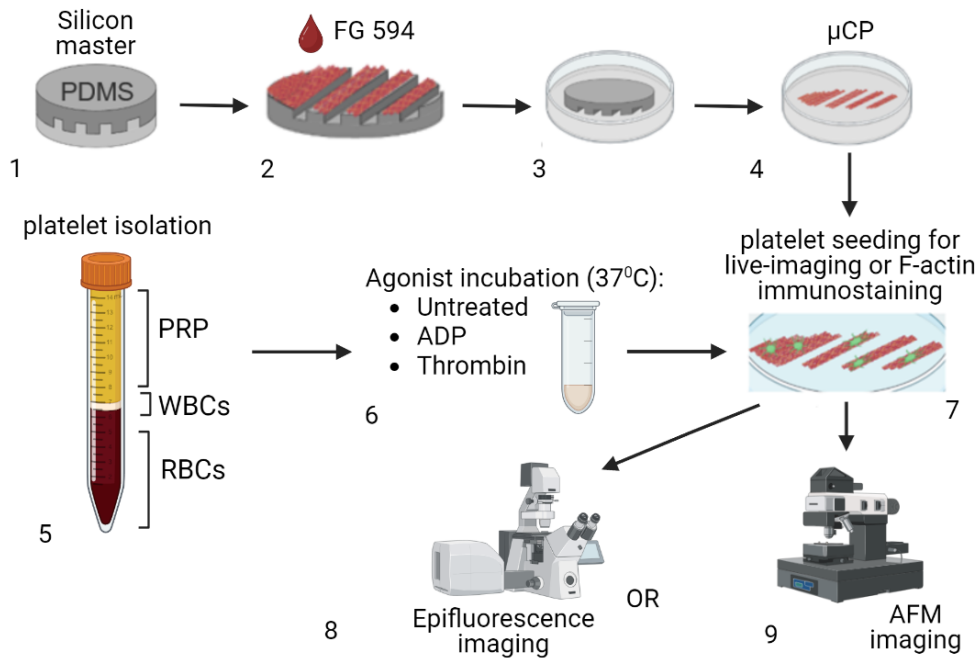

Figure 9. Micro-contact printing and sample procedure. This figure was designed in Biorender.com (2023).

2.14 Statistics

Igor Pro (Wavemetrics, Lake Oswego, Oregon, USA) was used to do all the statistical analysis and to process the data obtained. Significant differences were tested with parametric or non-parametric multiple group comparisons with Tukey´s or Dunn´s post-hoc tests. Statistically significant differences were defined according to the following $^{*}P < 0.05$; ** $P < 0.01$; $^{***}P < 0.001$; ns, not significant.

3 Results and Discussion

3.1 Role of NO-GC/cGMP pathway in human and murine platelets

Authors of the related publication: Johanna G. Rodríguez, Aylin Balmes, Jan Seifert, Daniel Pinto-Quintero, Akif A. Khawaja, Marta Boffito, Maike Frye, Andreas Friebe, Michael Emerson, Francesca Seta, Robert Feil, Susanne Feil, Tilman E. Schäffer

Author position: 1

Title of paper: Role of NO-GC/cGMP signaling pathway in platelet biomechanics

Status in publication process: Manuscript in revision

Pre-print in bioRxiv with this DOI: https://doi.org/10.1101/2023.04.28.538670

Detailed contribution to the manuscript as part of this chapter

- Scientific ideas (50%)
  - Experimental design and detailed analysis was carried out.
  - Understanding the effect of NO-GC/cGMP signaling pathway in human and murine platelets morphology and biomechanics, including platelets from HIV-positive patients.
- Data generation (75%)
  - Performance of all the sample preparation including isolation of human and murine platelets. Mice were obtained from AG Feil.
  - Optimization of all sample preparation protocols including SICM and immunofluorescence imaging.
  - Performance of all experiments including phase contrast images for CNN deep-learning analysis.
  - Performance of all experiments in Imperial College London.
  - SICM imaging was performed in collaboration with Aylin Balmes (Fig. 11).
  - Western Blot was performed in collaboration with Daniel Pinto-Quintero (Fig. 11c, f, i).
- Analysis & interpretation (50%)
  - Analysis of the data, composition, and interpretation in all figures.
  - CNN deep-learning morphology data was performed in collaboration with Dr. Jan Seifert (Fig. 12 and Fig. 13 a, b). Further data morphological analysis and interpretation was performed by Johanna Rodríguez.
- Paper writing (40%)

3.1.1 Role of NO-GC/cGMP in platelet biomechanics and morphology

The methods section of this manuscript has been removed to avoid repetition and placed in the materials and methods section above. Everything else was kept the same.

Role of the NO-GC/cGMP signaling pathway in platelet biomechanics

Johanna G. Rodríguez[1,3], Aylin Balmes[1], Jan Seifert[1], Daniel Pinto-Quintero[2], Akif A. Khawaja[3], Marta Boffito[4,5], Maike Frye[6], Andreas Friebe[7], Michael Emerson[3], Francesca Seta[8], Robert Feil[2], Susanne Feil[2], Tilman E. *Schäffer*[1]

[1] *Institute of Applied Physics, University of Tübingen, Tübingen, Germany*

[2] *Interfaculty Institute of Biochemistry (IFIB), University of Tübingen, Tübingen, Germany*

[3] *National Heart and Lung Institute, Imperial College London, London, UK*

[4] *Department of Infectious Disease, Imperial College London, London, UK*

[5] *Chelsea and Westminster NHS Foundation Trust, London, UK*

[6] *Institute for Clinical Chemistry and Laboratory Medicine, University Medical Center Hamburg-Eppendorf, Hamburg, Germany*

[7] *Physiological Institute, Julius Maximilian University of Würzburg, Würzburg, Germany*

[8] *Vascular Biology Section, Chobanian & Avedisian School of Medicine, Boston University, Boston, MA, USA*

ABSTRACT

Introduction

Cyclic guanosine monophosphate (cGMP) is a second messenger produced by the NO-sensitive guanylyl cyclase (NO-GC) enzyme. In platelets, the NO-GC/cGMP pathway inhibits aggregation. One aspect of the inhibitory mechanism involves changes in the cytoskeleton; however, the molecular mechanisms underlying platelet inhibition and its correlation with cytoskeletal cellular stiffness are poorly understood.

Methods

We measured the cellular stiffness of individual platelets after treatment with the NO-GC stimulator riociguat or the NO-GC activator cinaciguat, using scanning ion conductance microscopy (SICM). We quantified changes in platelet shape using deep learning-based platelet morphometry. Cytoskeletal actin polymerization and platelet activation were measured by co-immunostaining F-actin and P-selectin, respectively. To test for clinical applicability of NO-GC stimulators in the context of increased thrombogenicity risk, we investigated the effect of riociguat on platelets from human immunodeficiency virus (HIV)-positive patients taking abacavir sulphate (ABC)-containing regimens, compared with HIV-negative volunteers.

Results

Stimulation of human and murine platelets with the NO-GC stimulator riociguat or with the NO-GC activator cinaciguat downregulated P-selectin expression, decreased F-actin polymerization, and decreased cellular stiffness by ≈50%, compared to vehicle control. In addition, platelets became more circular, indicating decreased activation. Riociguat did not cause any change in platelet aggregation or circularity in HIV-positive patients taking ABC-containing regimens.

Conclusions

These results corroborate a functional role of the NO-GC enzyme in platelet biomechanics (cellular stiffness) in correlation with the inhibition of platelet activation and morphological changes. The observed changes in stiffness and platelet shape therefore demonstrate the possibility of pharmacologically targeting the NO-GC/cGMP pathway.

Introduction

Platelets are small anucleate blood cells responsible with critical roles in hemostasis and thrombosis (3). Novel approaches to target inhibition of platelet activation, and hence thrombus formation, are currently being studied to reduce mortality in individuals affected by atherosclerosis, increased arterial stiffness (98), thromboembolism (99), or bleeding disorders such as thrombocytopenia (2). Upon activation, platelets release inflammatory cytokines and become highly adhesive with a drastic change in shape (98). The platelet cytoskeleton supports platelet shape in the resting state, and it changes dynamically during platelet activation in response to vascular damage (3). Studies have shown that abnormalities in the biomechanical properties of platelets are related to inherited platelet cytoskeletal diseases (100). Therefore, measuring platelet shape or cellular stiffness (amount of resistance of an object against deformation in response to an applied force), could help in the assessment of the bleeding risk in patients with cytoskeletal disorders (101).

Nitric oxide (NO) is an endogenous platelet inhibitor that binds to NO-sensitive guanylyl cyclase (NO-GC) (102). In platelets, NO-GC has been shown to be the only NO receptor (103). NO-GC catalyzes the conversion of guanosine 5'-triphosphate (GTP) to cyclic guanosine 3',5'- monophosphate (cGMP) (104). An increase in cGMP activates the cGMP-dependent protein kinase (PKG), which phosphorylates, among other proteins, vasodilator-stimulated phosphoprotein (VASP) in platelets and other cell types (33). NO is involved in signaling cascades that support a healthy cardiovascular system including inhibition of platelet aggregation *in vitro* (104) and *in vivo* (105), making NO-GC an attractive target for cardiovascular pathologies including thrombosis (13); however, continuous nitrate administration can lead to drug resistance because of the desensitization of NO-GC (102).

In a cardiovascular pathology such as ischemia, heme, the essential NO-GC co-factor, becomes oxidized, preventing NO from binding NO-GC and impairing cGMP generation (106). Riociguat is a NO-GC stimulator, which has been approved for the treatment of pulmonary arterial hypertension and chronic thromboembolic pulmonary hypertension (107). Riociguat has a dual effect on NO-GC: it stimulates the enzyme itself and decreases the dissociation of NO from NO-GC (108). On the other hand,

cinaciguat is a NO-GC activator that can activate NO-GC independently of its heme redox status (heme-oxidized or heme-free NO-GC) and irrespective of impaired NO signaling (32).

In the present study, we examined the effects of riociguat and cinaciguat on platelet biomechanics using scanning ion conductance microscopy (SICM), a non-invasive imaging technique that allows simultaneous measurement of morphological and mechanical properties in living cells (39,88) with high resolution. SICM has already been used to investigate the Young's modulus (stiffness) of living migrating and non-migrating platelets (43) and to show that reduced platelet stiffness is related to increased bleeding in *MYH9*-related disease (109). We correlated SICM measurements with F-actin and P-selectin (CD62P) immunostaining in human and wild-type (C57Bl6/J) or platelet-specific NO-GC knockout (KO) murine platelets. Additionally, platelet morphology was investigated with deep learning platelet morphometry (64).

Lastly, we studied the effect of riociguat on platelet morphology (circularity) in HIV-positive patients taking the anti-viral drug abacavir-sulphate (ABC) as part of their daily antiretroviral regimen, compared with platelets from HIV-negative volunteers. Currently, the first line of antiretroviral therapy for HIV-positive patients involves a combination of nucleotide reverse transcriptase inhibitors such as ABC (110). Carbovir tri-phosphate (CBV-TP), the active ABC anabolite (110) is a guanosine derivative shown to compete and antagonize cGMP in the NO-GC/cGMP signaling pathway in platelets (110). Therefore, the potential blockage of NO-GC/cGMP pathway by CBV-TP could increase the risk of thrombogenic events and lead to an increased development of cardiovascular pathologies in HIV patients taking the drug (110). Our study is the first to analyze the effect on morphology (circularity) of the NO-GC stimulator riociguat in the setting of HIV.

Results

Platelet activation, stiffness, and shape changes were investigated in platelets isolated from human, wild-type, and platelet-specific NO-GC KO mice.

Platelet activation is dampened by riociguat and cinaciguat. We first examined the effect of the NO-GC stimulator riociguat and the NO-GC activator cinaciguat on the cytoskeleton and activation for human platelets as well as platelets isolated from wild-type (C57Bl6/J) and platelet-specific NO-GC KO mice (Figure 10). We found that the cGMP-modulating drugs 8-Br-cGMP, riociguat, or cinaciguat decreased F-actin (Figure 10b, e) and P-selectin (Figure 10c, f) in isolated human platelets and wild-type murine platelets by ≈50%, compared to vehicle control (DMSO).

The P-selectin CTCF values ranged 2 – 225 [a.u.] in human platelets, 2 – 80 [a.u.] in wild-type murine platelets, and 2 – 25 [a.u.] in NO-GC KO murine platelets. Thus, these values indicate a lower basal protein expression of F-actin (Figure 10i) and P-selectin (Figure 10h) in the KO mice. Moreover, no further decreases in F-actin and P-selectin were observed in NO-GC KO platelets treated with riociguat or cinaciguat, whereas 8-Br-cGMP decreased F-actin and P-selectin by an additional ≈50% (Figure 10g, h, i). Downregulation of P-selectin suggests an inhibitory role of the NO-GC pathway in platelet activation (Figure 10c, f, i).

Interestingly, P-selectin was observed mostly in the form of nodule-like local spots that might be individual granules distributed throughout the platelet in the treated wild-type murine platelets (Figure 10d), while a more homogenous distribution was observed in the case of NO-GC KO murine platelets (Figure 10g). For human platelets, nodule-like spots were only observed after treatment with riociguat or cinaciguat (Figure 10a). Overall, these results indicate that F-actin and P-selectin are modulated by the NO-GC enzyme and that an increase in cGMP decreases the downregulation of F-actin and P-selectin. The NO-GC KO animals were used to show that the drug effect from riociguat or cinaciguat is indeed mediated by NO-GC.

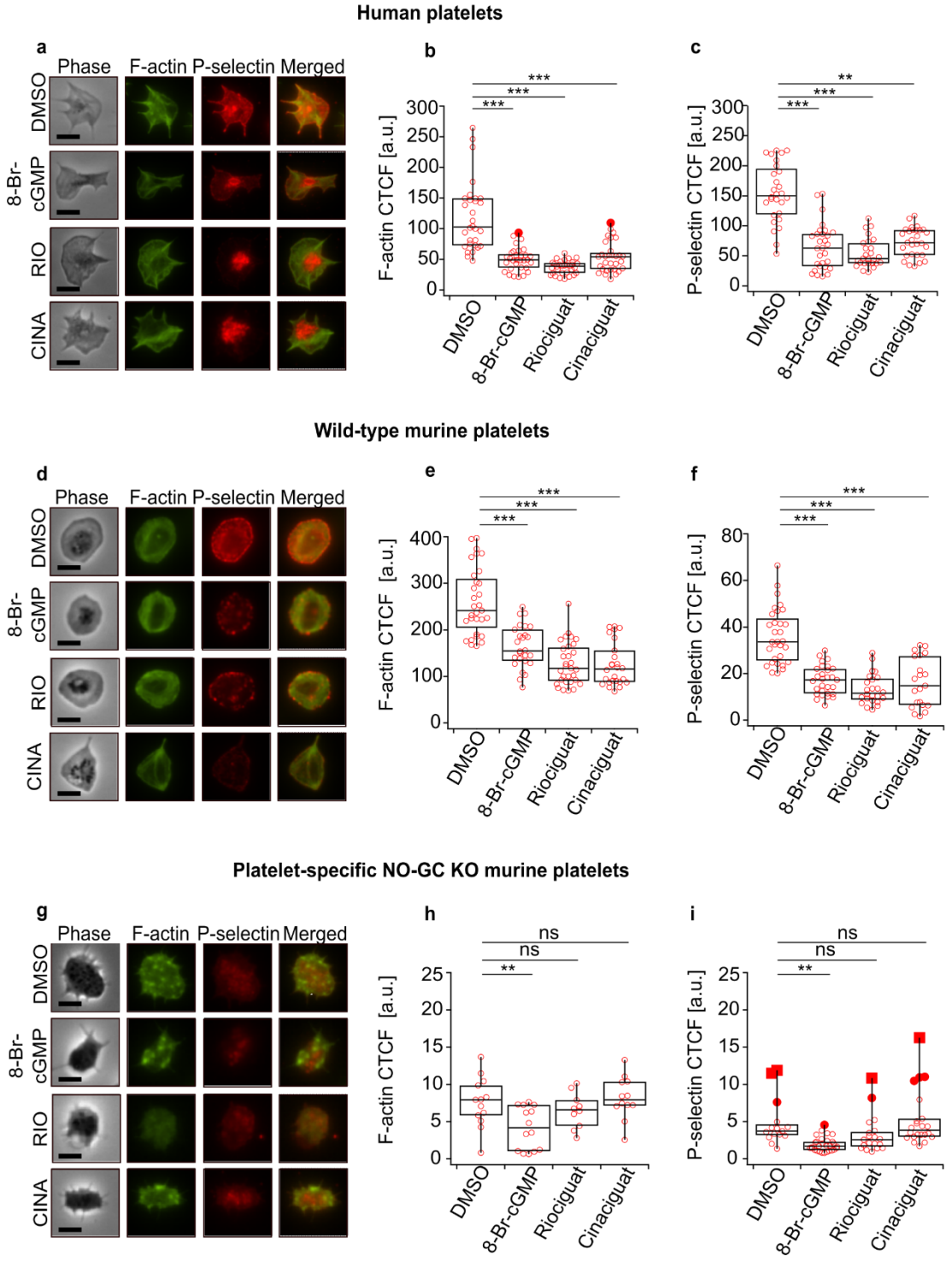

Figure 10. F-actin and P-selectin are decreased in human platelets and wild-type (C57Bl6/J) murine platelets when treated with 8-Br-cGMP, riociguat, or cinaciguat. **(a, d, g)** Co-staining of F-actin and P-selectin in washed human, wild-type murine, and platelet-specific NO-GC murine KO platelets. **(b, e, h)** F-actin and **(c, f, i)** P-selectin fluorescence quantification. DMSO (1:1000), 8-Br-cGMP (1 mM), riociguat (10 µM), cinaciguat (10 µM). The significance level of P values is indicated by asterisks (* P < 0.05; ** P < 0.01; *** P < 0.001; ns, not significant; Tukey's test). Scale bars: 5 µm. Experiments were performed with ≈15 platelets per donor from n=2 (human), n=2 (wild type mice), n=2 (NO-GC KO mice) donors.

Platelet stiffness is decreased by riociguat and cinaciguat. SICM was used to investigate the role of NO-GC in the biomechanical properties (stiffness) of wild-type murine, platelet-specific NO-GC KO murine, and human platelets. Topography and stiffness images of platelets were recorded with high spatial resolution (Figure 11). Human (Figure 11b) and wild-type murine platelets (Figure 11e) treated with cGMP-modulating drugs had a significantly decreased average cellular stiffness (≈2 kilopascal, kPa) in comparison to DMSO-treated platelets (≈5 kPa), indicating a decrease of ≈50% in cellular stiffness.

In contrast, NO-GC KO platelets (Figure 11h) showed no decrease in cellular stiffness after the treatment with riociguat or cinaciguat (≈5 kPa) in comparison with DMSO (≈5 kPa). A change in cellular stiffness by ≈60% was only observed when NO-GC KO platelets were treated with 8Br-cGMP (≈2 kPa) (Figure 11b, c, d). Furthermore, we found increased levels of phosphorylated VASP (p-VASP), a downstream effector of cGMP and regulator of F-actin polymerization (111), in wild-type and human platelets for all the treatments (Figure 11c, f). In contrast, VASP phosphorylation was almost undetectable in NO-GC KO platelets treated with riociguat or cinaciguat, but still detectable when NO-GC KO platelets were stimulated with 8-Br-cGMP (Figure 11i).

Efficient NO-GC deletion in platelets of megakaryocyte/platelet-specific NO-GC KO mice was confirmed via Western blot (Figure 11i). Taken together, these results suggest that NO-GC-mediated VASP phosphorylation and actin cytoskeletal rearrangements (Figure 10) may be linked to the regulation of cellular stiffness in platelets (Figure 11). Specific deletion of NO-GC in platelets corroborated the role of NO-GC in platelet stiffness treated with riociguat or cinaciguat, suggesting that stiffness can be modulated through the NO-GC/cGMP pathway.

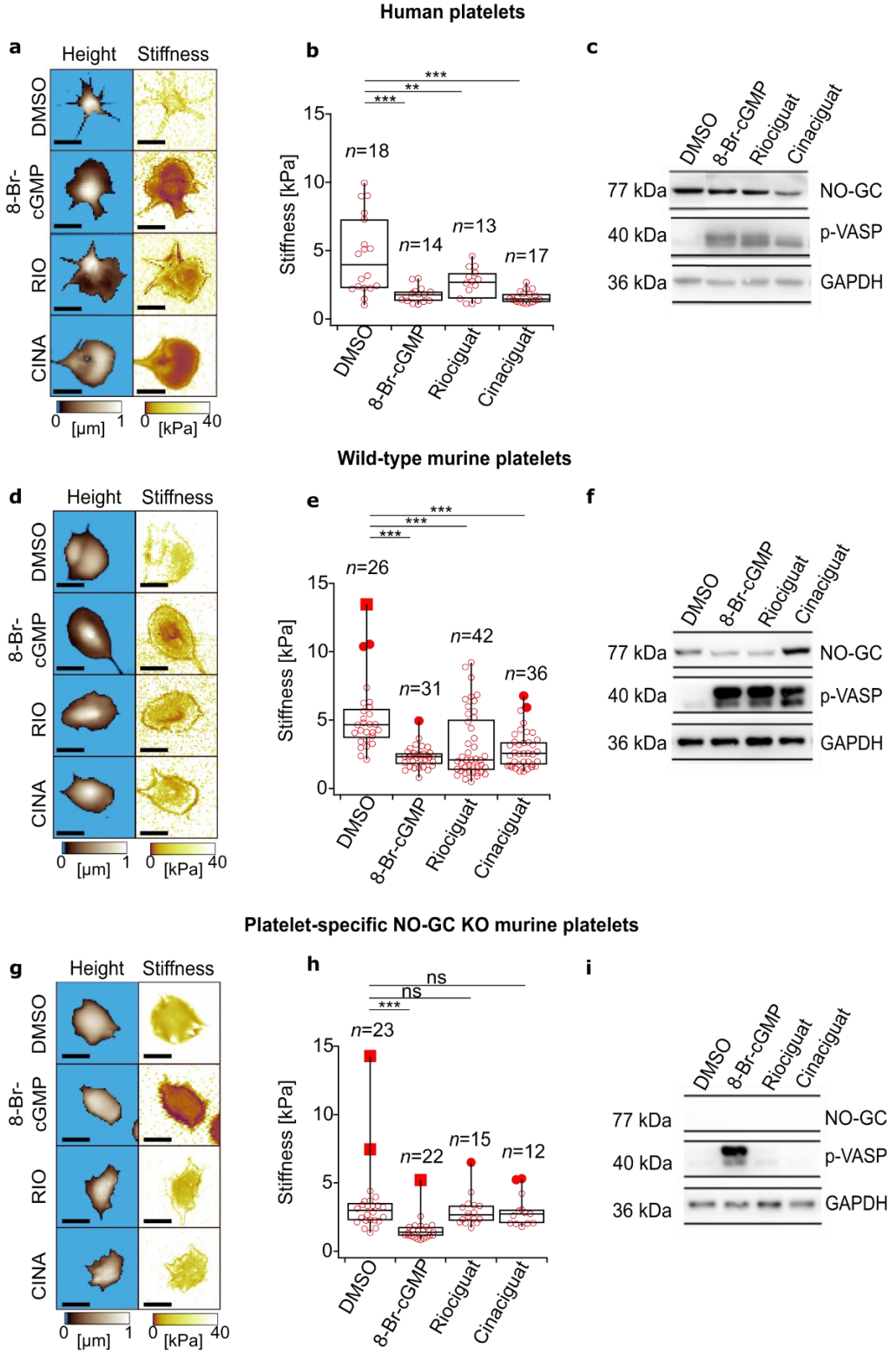

Figure 11. Cellular stiffness is decreased in human platelets and wild-type (C5BI6/J) murine platelets when treated with 8-Br-cGMP, riociguat or cinaciguat **(a, d, g).** Topography and cellular stiffness images of washed human platelets, wild-type murine, and platelet-specific NO-GC murine KO platelets. **(b, e, h)** Cellular stiffness quantification. **(c, f, i)** Western blot analysis of VASP phosphorylation (p-VASP) and NO-GC. GAPDH was used as loading control. DMSO (1:1000), 8-Br-cGMP (1 mM), riociguat (10 µM),

cinaciguat (10 µM). The significance level of P-values is indicated by asterisks (* P < 0.05; ** P < 0.01; *** P < 0.001; ns., not significant; Tukey's test). Scale bars: 5 µm. Experiments were performed with 6-21 platelets per donor from n=2 (human), n=2 (wild type mice), n=2 (NO-GC KO mice) donors. Control blots were from the same sample, and performed from n=3 (human), n=3 (wild type mice), n=4 (NO-GC KO mice) donors. SICM images were obtained in collaboration with Aylin Balmes. Western blots were done in collaboration with Daniel Pinto-Quintero.

Platelet shape is influenced by riociguat and cinaciguat. Platelet shape changes were investigated with deep learning platelet morphometry (Figure 12). A convolutional neural network (CNN) was used to generate binary prediction images from optical phase contrast images for the analysis of the circularity of human, murine wild-type, and platelet-specific NO-GC KO platelets. Platelet circularity could be an indicator of platelet activation and spreading stages. When human platelets and wild-type murine platelets were treated with cGMP-modulating drugs, a significant increase in platelet circularity was observed (Figure 12a-d). However, the circularity (circ) of platelets from platelet-specific NO-GC KO mice did not change when treated with riociguat (circ = 0.5; $P = 0.98$) or with cinaciguat (circ = 0.5; $P = 0.94$), compared to DMSO (circ = 0.5) (Figure 12e, f). The absence of a change in the circularity of NO-GC KO platelets treated with riociguat or cinaciguat demonstrated that platelet shape is likely modulated via NO-GC-mediated signaling.

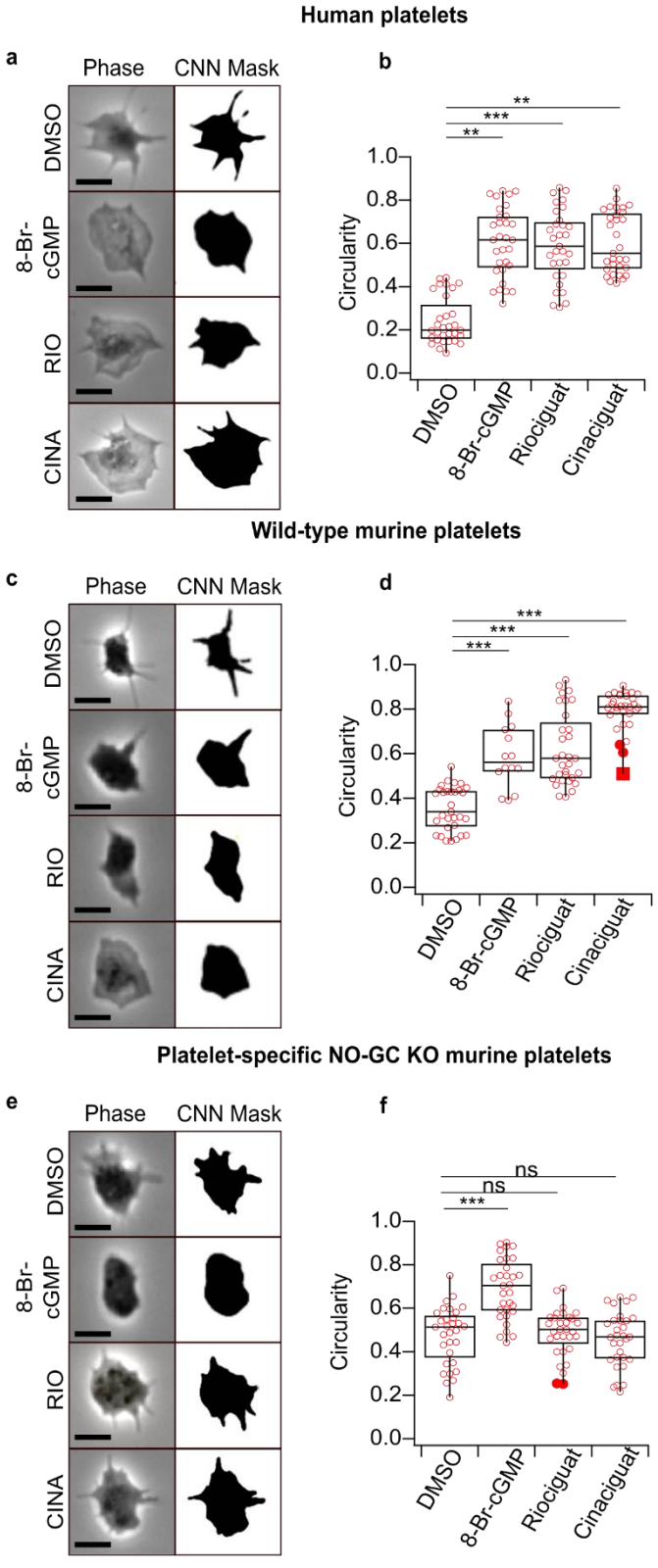

Figure 12. Platelet shape is altered in human platelets and wild-type (C57Bl6/J) murine platelets when treated with 8-Br-cGMP, riociguat, or cinaciguat. **(a, c, e)** Phase contrast and binary prediction images obtained via deep learning morphometry in washed human, wild-type murine, and platelet-specific NO-GC KO murine platelets. **(b, d, f).** Platelet circularity. DMSO (1:1000), 8-Br-cGMP (1 mM), riociguat (10 µM), cinaciguat (10 µM). The significance level of P-values is indicated by asterisks ($^{*}P < 0.05$; $^{**}P < 0.01$; $^{***}P < 0.001$; ns, not significant; Dunn's test). Scale bars: 5 µm. Experiments were performed with ≈15 platelets per donor from n=2 (human), n=2 (wild type mice), n=2 (NO-GC KO mice) donors.

Circularity and aggregation are decreased in riociguat-treated platelets from HIV-negative donors but not in platelets from HIV-positive patients treated with ABC. The circularity of platelets from HIV-negative platelet donors was significantly increased (P = 0.001) by ≈50% when treated with riociguat (circ = 0.60) compared to DMSO (circ = 0.31) (Figure 13a), consistent with our findings of riociguat-treated platelets from healthy human volunteers (Figure 13b). However, the circularity of platelets from HIV-negative platelet donors did not change (P = 0.71) when treated with the active ABC anabolite CBV-TP (circ = 0.29), which mimics CBV-TP present in HIV-positive patients taking ABC-containing regimens, compared to DMSO control (circ = 0.31) (Figure 13a). Interestingly, the circularity of riociguat-treated platelets from HIV-positive patients taking ABC-containing regimens (circ = 0.37) did not change compared to DMSO control (circ = 0.34) (Figure 13b). Additionally, ADP median circularity for HIV-negative volunteers (circ = 0.21) and HIV-positive patients taking ABC-containing regimens (circ = 0.25) was ≈30 % smaller than for DMSO, albeit not significantly different (Figure 13a, b). These findings could indicate a disruption of the thrombo/cardio-protective NO-GC/cGMP signaling pathway in HIV-positive patients treated with ABC-containing regimens.

Similarly, microplate reader-based analysis of platelet aggregation showed decreased aggregation of platelets isolated from HIV-negative donors when treated with riociguat (20% for riociguat, 58% for DMSO; P = 0.027) (Figure 13c), but not in platelets isolated from HIV-positive patients ABC-containing regimens (58% for both riociguat and DMSO; P = 0.58) (Figure 13d). Moreover, platelets isolated from HIV-negative volunteers treated with CBV-TP showed a similar percentage of aggregation as platelets from HIV-negative volunteers treated with the selective NO-GC antagonist ODQ (P = 0.99; percentage of aggregation= 42% to 40%) (Figure 13c). No pharmacological interaction of CBV-TP with ODQ was observed (Figure 4c). Likewise, ODQ showed no effect in platelet aggregation when pre-incubated together with riociguat in HIV-positive patients taking ABC-containing regimens (Figure 13d). Additionally, when comparing the different drug combinations (ODQ-CBV-TP for HIV-negative patients, ODQ-riociguat for both HIV-negative and HIV-positive patients taking ABC-containing regimens), the maximum ADP-induced aggregation was identical (≈42%), and no significant difference compared to aggregation values for DMSO (≈42%) was detected.

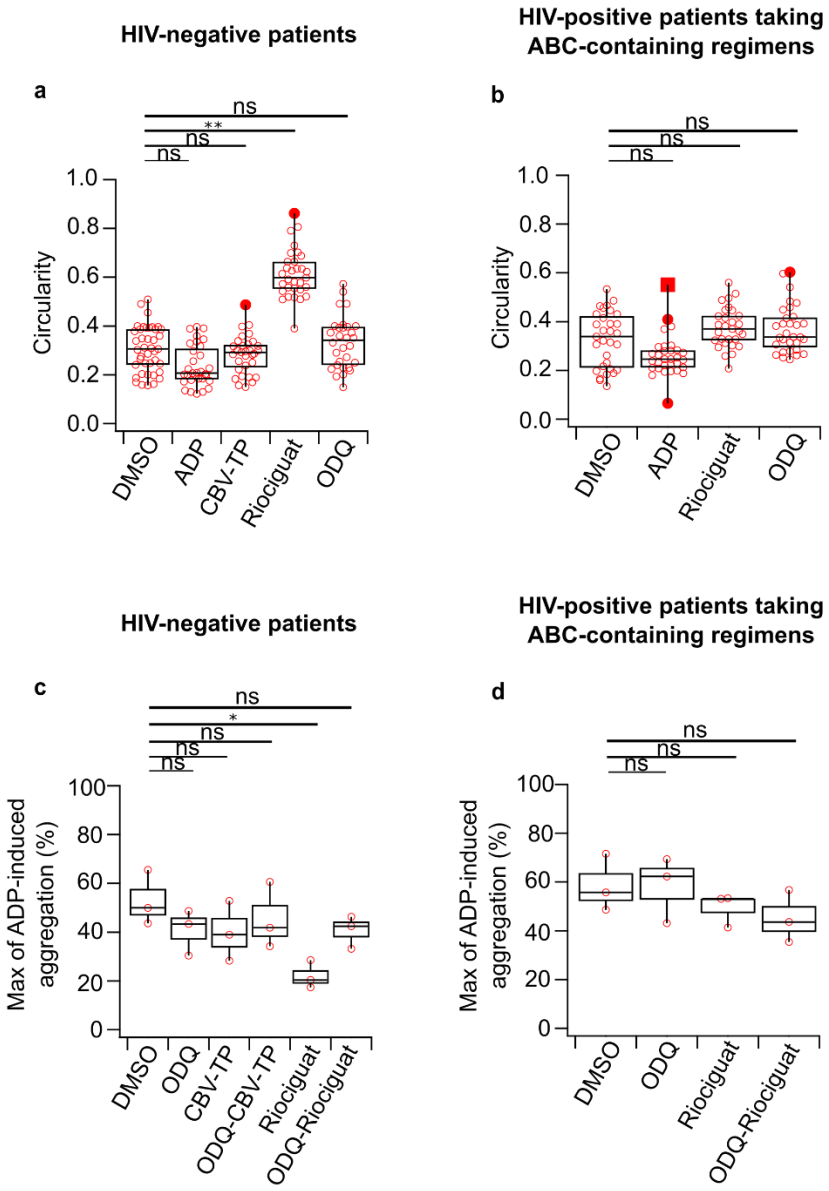

Figure 13. Riociguat increases platelet circularity and decreases platelet aggregation in HIV-negative volunteers, but not in HIV-positive patients taking ABC-containing regimens. **(a, b)** Platelet circularity. **(c, d)** Maximum of ADP-induced aggregation in response to indicated drug treatments. ADP (3 µM), DMSO (1:1000), CBV-TP (50 µM), riociguat (10 µM), ODQ (20 µM). Platelet numbers for circularity: n ≈ 15 per donor from n=2 donors. The significance level of P-values is indicated by asterisks (* P < 0.05; ** P < 0.01; *** P < 0.001; ns, not significant; Tukey's test). Donors for aggregation experiments: n=3.

Taken together, our findings show that activation of the NO-GC/cGMP pathway in platelets results in platelet de-activation (or maintenance of platelets in an inactive state) and interestingly correlates with a decrease in cellular stiffness, downregulation of F-actin, and decrease in platelet circularity (Figure 3). Platelet shape changes (circularity increase) observed in riociguat-treated platelets from healthy volunteers were not observed in riociguat-treated platelets from HIV-positive patients currently taking ABC (Figure 13b). Riociguat did not exert any changes in platelet shape in

platelets isolated from HIV-positive patients currently taking ABC, because the thrombo-protective effect of the NO-GC/cGMP pathway was abolished. Our data further suggests that CBV-TP could block the NO-GC/cGMP pathway and thereby the inhibition of platelet aggregation (Figure 3).

Discussion

The goal of this study was to investigate molecular mechanisms that mediate platelet biomechanics, which could become novel strategies for the treatment or diagnosis of thrombosis and related cardiovascular pathologies in a variety of clinical settings. Specifically, we sought to elucidate the role of the NO-GC/cGMP signaling pathway in human and murine platelets, with a focus on cytoskeleton biomechanics.

Platelets store P-selectin in their alpha granules and upon platelet activation, the external membrane of the platelet exposes P-selectin (112). We found that P-selectin expression and cytoskeletal F-actin polymerization were decreased in human and wild-type murine platelets after treatment with different cGMP-modulating drugs (Figure 10a and 10d) and these changes correlated with decreased platelet cellular stiffness (Figure 11a, 11d). The specificity of our findings was confirmed with platelets from platelet-specific NO-GC KO mice, where cGMP-modulating drugs did not have any effect on cytoskeletal F-actin (Figure 10h), P-selectin (Figure 10i), platelet cellular stiffness (Figure 11g), or platelet circularity (Figure 12f).

At the molecular level, we also observed an increase in phosphorylated VASP (Figure 11c, 11f). Phosphorylation of VASP at serine239 (p-VASP) is a marker for PKG activity and NO-mediated effects in platelets (113) and is involved in the downregulation of F-actin polymerization (114), which leads to a decrease in platelet cellular stiffness. The phosphorylation of VASP in platelets is also associated with inhibition of fibrinogen receptor (integrin GPIIb/IIIa) (115). Fibrinogen binding to GPIIb/IIIa has been linked to thrombus stabilization (116), suggesting that the activation of NO-GC/cGMP signaling and subsequent VASP phosphorylation decreases thrombus formation (33).

Platelet shape (circularity) is mediated by actin-binding proteins (114), and upon platelet activation, filopodia and lamellipodia are formed. Platelet shape change is

essential for platelet adhesion (117) and spreading, which occur via four different stages (59): (1) platelet adhesion; (2) formation of filopodia; (3) development of filopodia and lamellipodia; and (4) presence of lamellipodia and of orthogonally arrayed short actin filaments inside the lamellipodia (59). Our results suggest that the circularity in platelets treated with 8-Br-cGMP, riociguat, or cinaciguat is significantly increased (Figure 12b, 12d), owing to a more circular platelet spreading state and shape with fewer filopodia and lamellipodia. This gives an indication that NO-GC plays a role in platelet shape change, because the circularity was not altered by the treatments in NO-GC KO platelets (Figure 12f). Platelet morphological features such as circularity could define morphological subtypes such as not-spread, partially, or fully spread (118). According to the circularity values obtained in this study, most of the platelets that were stimulated with cGMP stimulating drugs fit within a partially spread category. This suggests that when platelets increase cGMP upregulation through NO-GC stimulation (riociguat) or activation (cinaciguat), platelets do not reach a fully spread state or become fully activated. NO-GC has a basal, NO-independent activity, which would add to the NO-induced, endothelium-derived inhibition and probably influence platelet morphology (roundish shape).

Similarly, for platelets treated with riociguat, increased circularity values were observed in healthy volunteers but not in HIV-positive patients taking ABC (Figure 13), suggesting that the NO-GC/cGMP pathway may be downregulated or blocked by off-target effects of antiretrovirals such as ABC in these patients. This thinking is supported by the fact that platelet circularity was not altered by any GC-modulating treatment suggesting platelets are hyperactivated in these patients. Consistent with this finding, riociguat decreased platelet aggregation in HIV-negative volunteers but not in HIV-positive patients currently taking ABC regimens (Figure 13e, 13d), suggesting that CBV-TP, the active ABC anabolite, inhibits the NO-GC/cGMP pathway in platelets. However, further studies on the interaction between cGMP and ABC are warranted. Our studies suggest that treatment of HIV-positive patients with ABC-containing regimens blocks NO-GC/cGMP-mediated thrombo-protection (readout circularity), potentially putting these patients at higher risk of thrombotic events. This is supported by observational studies, indicating an increased risk of myocardial infarction in patients taking ABC (68).

Platelets have high concentrations of PKG (above 0.1 µmol/mL), mainly the PKG-Iβ isoform (119). Platelets can also be regulated by phosphodiesterases (PDEs) (120) through the hydrolysis of cyclic adenosine 3', 5'-monophosphate (cAMP) and cGMP (121). Dipyridamole is an unspecific PDE inhibitor that decreases cGMP hydrolysis, and it is occasionally used in combination with acetylsalicylic acid in therapy to inhibit platelet activation; however, its efficacy is questioned (119). Platelet inhibition occurs via cGMP/PKG activation, which is consistent with our finding that in platelets lacking NO-GC, treatments with NO-GC stimulator or activator did not have any effect on the platelet activation marker P-selectin (CD62P), suggesting that cGMP/PKG is essential for platelet inhibition.

In summary, our study indicates that the NO-GC/cGMP signaling pathway is involved in the inhibition of P-selectin expression and downregulation of cytoskeletal F-actin polymerization. Moreover, when cGMP/PKG is stimulated via a NO-GC stimulator (riociguat) or a NO-GC activator (cinaciguat), a decrease in platelet cellular stiffness and platelet circularity occurs via NO-GC. Furthermore, we conclude that NO-GC/cGMP signaling regulates the cellular stiffness and shape changes of platelets. As cellular stiffness indicates the mechanical state of the platelet cytoskeleton, measuring cellular stiffness could become a novel biomarker to evaluate patients' cardiovascular risk, considering that platelet hyperactivation is associated with multiple cardiovascular conditions such as increased arterial stiffness (122), detrimental blood flow (123), or atherosclerosis. Also, platelet circularity could give a hint of platelet activation state suggesting that circularity could also become a biomarker in clinical research (Figure 13), which allows to identify patients with a tendency of developing a cardiovascular pathology. In conclusion, both platelet stiffness and shape changes are biological parameters that could be exploited as biomarkers in clinical research. Future studies should include patients with a broad range of diseases since platelet activation responses and pharmacological responses are likely to vary according to disease setting.

Acknowledgments

This work was funded by the Deutsche Forschungsgemeinschaft (DFG, German Research Foundation) – Projektnummer 335549539/GRK2381 and Projektnummer 374031971 - TRR 240. The Facility for Imaging by Light Microscopy (FILM) at Imperial College London is partly supported by the Wellcome Trust (grant 104931/Z/14/Z) and BBSRC (grant BB/L015129/19). A.B. is supported by the Add-on Fellowship of the Joachim Herz Foundation.

Informed Consent Statement

Informed consent was obtained from all the subjects involved in the study in Tübingen and London.

Author Contribution

Conceptualization: J.R., A.B., J.S., D.P.Q., M.E., F.S., R.F., S.F., and T.E.S; Investigation: J.R., A.B., J.S., D.P.Q., and A.K.; Resources: A.F., M.E., M.B., S.F., R.F., and T.E.S.; Writing - original draft preparation: J.R; Writing - review and editing: J.R., A.B., J.S., D.P.Q., A.K., M.B., M.F., A.F., M.E., F.S., R.F., S.F., T.E.S.; Visualization: J.R., A.B., J.S., D.P.Q., A.K., M.B., M.F., A.F., M.E., F.S., R.F., S.F., T.E.S.; Supervision: M.E., F.S., R.F., S.F., T.E.S.; Project administration: J.R., T.E.S.; Funding acquisition: T.E.S. All authors have read and agreed to the published version of the manuscript.

Conflict of Interest

The authors declare no conflict of interest.

3.1.1.2 Effect of NO-GC stimulators and activators on human and murine platelet morphology, p-VASP and NO-GC

The following part of the chapter is not part of a manuscript, and it is not necessary to declare and disclose the detailed contributions.

3.1.1.2.1 Platelet morphology

The manuscript presented above is part of the chapter “Role of NO-GC/cGMP pathway in platelet biomechanics” and explains in detail the role of NO-GC in the modulation of the platelet cytoskeleton and shape in human and murine platelets (WT and platelet-specific NO-GC KO mice). Since, of the various shape parameters obtained with the CNN, only circularity was included in the manuscript, in the following section, the additional morphological parameter area is show as well as the quantification of p-VASP and NO-GC obtained with western blots for human and murine platelets (Figure 11). The representative images of the western blots are shown in Figure 11, so only the quantification values will be presented below.

Riociguat and cinaciguat did not influence platelet area in human, murine wild-type, and platelet-specific NO-GC KO platelets. The lack of change in platelet circularity in murine platelet-specific NO-GC KO mouse after treatment with NO-GC activators or stimulator confirmed that platelet shape is influenced by the NO-GC/cGMP signaling pathway (Figure 12). Platelet shape can be correlated with different platelet adhesion and spreading stages, including platelet activation. The connection between platelet shape and the cytoskeleton is undeniable, because upon platelet activation lamellipodia and filopodia develop and consequently the overall platelet cytoskeleton structure is being modified.

To further quantify platelet morphology, platelet area was analyzed using deep learning platelet morphometry. Human and murine wild-type platelets had a similar median platelet area ranging between 15 μm^2 to 30 μm^2 without any significant difference after the drug treatments (Figure 14). cGMP-modulating drugs seem to have an influence only in platelet circularity but not in platelet area. Additionally, platelet area of platelet-specific NO-GC mice show smaller area values (10 μm^2 to 15 μm^2) in comparison with murine wild-type platelets (Figure 14c). The reason why platelets from the mice lacking NO-GC are smaller than WT is not clear; but the results suggest that NO-GC deletion affects platelet areas at baseline. Area is important in platelet spreading, so smaller platelets will take longer time to form a thrombus and block a hemorrhage in an injured blood vessel in comparison to functional murine WT platelets.

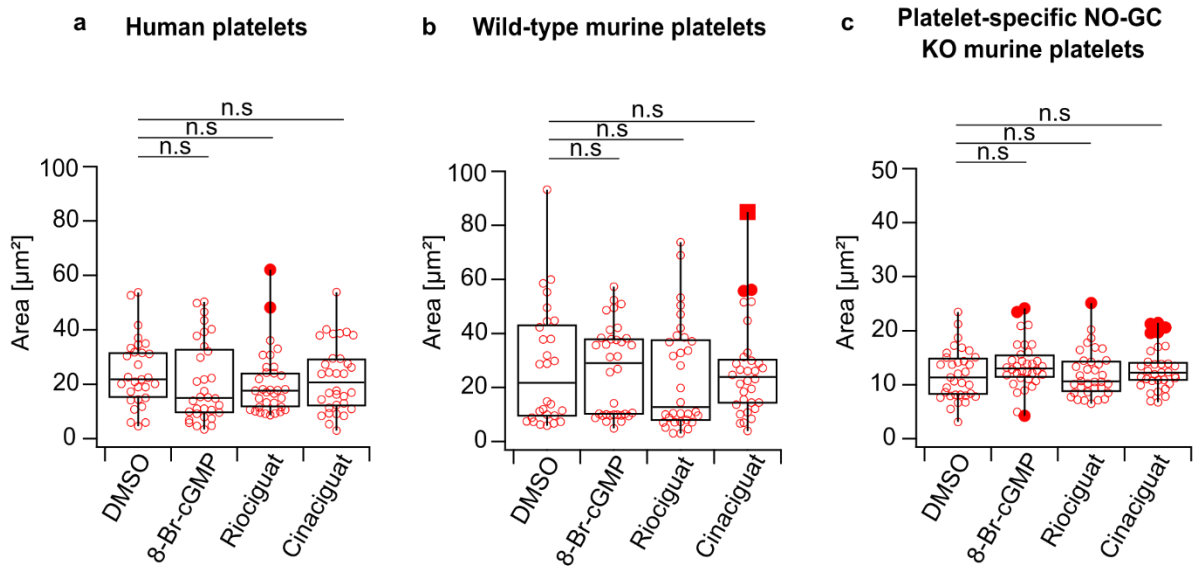

Figure 14. Platelet area is not altered in human platelets, wild-type (C57Bl6/J), and platelet-specific NO-GC KO murine platelets when treated with 8-Br-cGMP, riociguat, or cinaciguat. **(a,b,c)** Platelet area. DMSO (1:1000), 8-Br-cGMP (1 mM), riociguat (10 µM), cinaciguat (10 µM). The significance level of P-values is indicated by asterisks ($^{*}P < 0.05$; $^{**}P < 0.01$; $^{***}P < 0.001$; ns, not significant; Dunn's test). Experiments were performed with ≈15 platelets per donor from n=2 (human), n=2 (wild type mice), n=2 (NO-GC KO mice) donors.

Summarizing the key findings regarding the effect of cGMP-modulating drugs in platelet morphology. Circularity and area were investigated in platelets isolated from human, wild-type, and platelet-specific KO mice using deep learning morphometry. It was previously hypothesized (Figure 3) that a decrease in platelet circularity will occur upon stimulation of the NO-GC/cGMP signaling pathway because of the changes in platelet cytoskeleton. Interestingly, platelet area was not altered and only platelet circularity. Circularity (Equation 4) is a unitless parameter which defines a perfect circle with a value of 1.0.

$$C = \frac{4\pi A}{P^2} \tag{4}$$

where, C is the circularity, A is the area, and P is the perimeter.

Platelets can become circular in a resting state or when they are fully spread and activated. However, most of the platelets treated with cGMP-modulating drugs which showed increased circularity values were not fully spread and activated because according to Figure 10, release of P-selectin from the alpha granules was decreased upon cGMP-modulating drugs stimulation suggesting a lower degree of platelet activation. Consequently, platelets were less activated and in an intermediate state of platelet activation.

Deep learning morphometry has the enormous advantage that can screen images of thousands of platelets immediately and get several morphological parameters (64). The training of a CNN in imaging analysis facilitates automated analysis and removes the bias of manual analysis methods with commercial software. Previous studies with the same CNN, have shown similar area values to DMSO (vehicle control) (Figure 14a) in untreated human platelet area ranging from 10 μm^2 to 60 μm^2, indicating that the area values obtained are reproducible (64).

Additionally, other automated deep learning studies showed a circularity (circ=0.5) in untreated washed platelets (124). Mean area values (≈ 20 μm^2) in untreated human platelets (124) were comparable to the area values presented in Figure 14a. Semi-automated analysis of platelet spreading in untreated human platelets spread in collagen (area= 35 μm^2; circ=0.47) and in fibrinogen (area= 20 μm^2; circ=0.38) had circularity values close to the values presented in Figure 12a, 13a (125). However, it seems that collagen coating increases slightly platelet circularity in comparison with fibrinogen coating (126). It is important to mention that in this study, we only focused on fibrinogen coated surfaces.

Morphological parameters such as area and circularity help in the understanding of platelet spreading. Platelet circularity depends on the filopodia or lamellipodia formation and further cytoskeleton modifications (127). Platelet area is directly proportional to platelet spreading (127). Platelet area of a fully spread platelet is around 50 μm^2 (127). Mean area values from human and murine platelets treated with DMSO or cGMP-modulating drugs were ≈ 25μm^2 (Figure 14) suggesting that these platelets were partially spreaded. Taken together these results compared with other studies, platelet area (Figure 14) seems to agree with what was found in literature.

3.1.1.2.2 p-VASP and NO-GC quantification

Riociguat and cinaciguat did not significantly increase the relative amount of p-VASP and NO-GC in human and wild-type platelets in relation to 8-Br-cGMP. Representative western blot images were shown previously in Figure 11c, f, i. Western blot quantification from three donors per species were performed to determine whether riociguat or cinaciguat significantly upregulates p-VASP and NO-GC in human and wild-type platelets. The quantification results presented in Figure 15 were normalized to 8-Br-cGMP. Riociguat increased the relative amount of p-VASP present in human and wild-type platelets more than cinaciguat (Figure 15a, c), although the difference did not reach statistical significance. Riociguat has a dual mechanism of action, which could contribute to enhanced VASP phosphorylation in comparison with cinaciguat.

The amount of p-VASP from platelet-specific NO-GC KO murine platelets was significantly decreased when treated with riociguat (p-VASP = 0.09; $P = 1.594 \times 10^{-11}$) or cinaciguat (p-VASP = 0.04; $P = 7.693 \times 10^{-12}$) compared with 8-Br-cGMP (p-VASP = 1). These results suggest that in the absence of NO-GC in platelets, pVASP phosphorylation does not occur. The relative amount of NO-GC in human platelets treated with riociguat (NO-GC = 0.80; $P = 0.999$) or cinaciguat (NO-GC = 0.90; $P = 0.992$) did not show any significant decrease in comparison with 8-Br-cGMP (Figure 15a). Similarly, the relative amount of NO-GC in wild-type murine platelets treated with riociguat (NO-GC = 5.1; $P = 0.404$) or cinaciguat (NO-GC = 5.4; $P = 0.206$) did not show any significant increase in comparison with 8-Br-cGMP (Figure 15b). As expected, the relative amount of NO-GC in platelet-specific NO-GC KO murine platelets were undetected because of the genetic deletion in NO-GC.

In summary, and as shown in Figure 11c, f, i., riociguat and cinaciguat phosphorylates VASP in platelets, and there is no statistically significant difference in the level of phosphorylation between NO-GC stimulators or activators. The relative amount of NO-GC is also not significantly affected by riociguat or cinaciguat. Additionally, ADP-treated platelets (activated platelets) show phosphorylation levels similar to DMSO (vehicle control). Increase phosphorylation of p-VASP was associated with decreased platelet stiffness, as shown in Figure 11, and discussed in the manuscript.

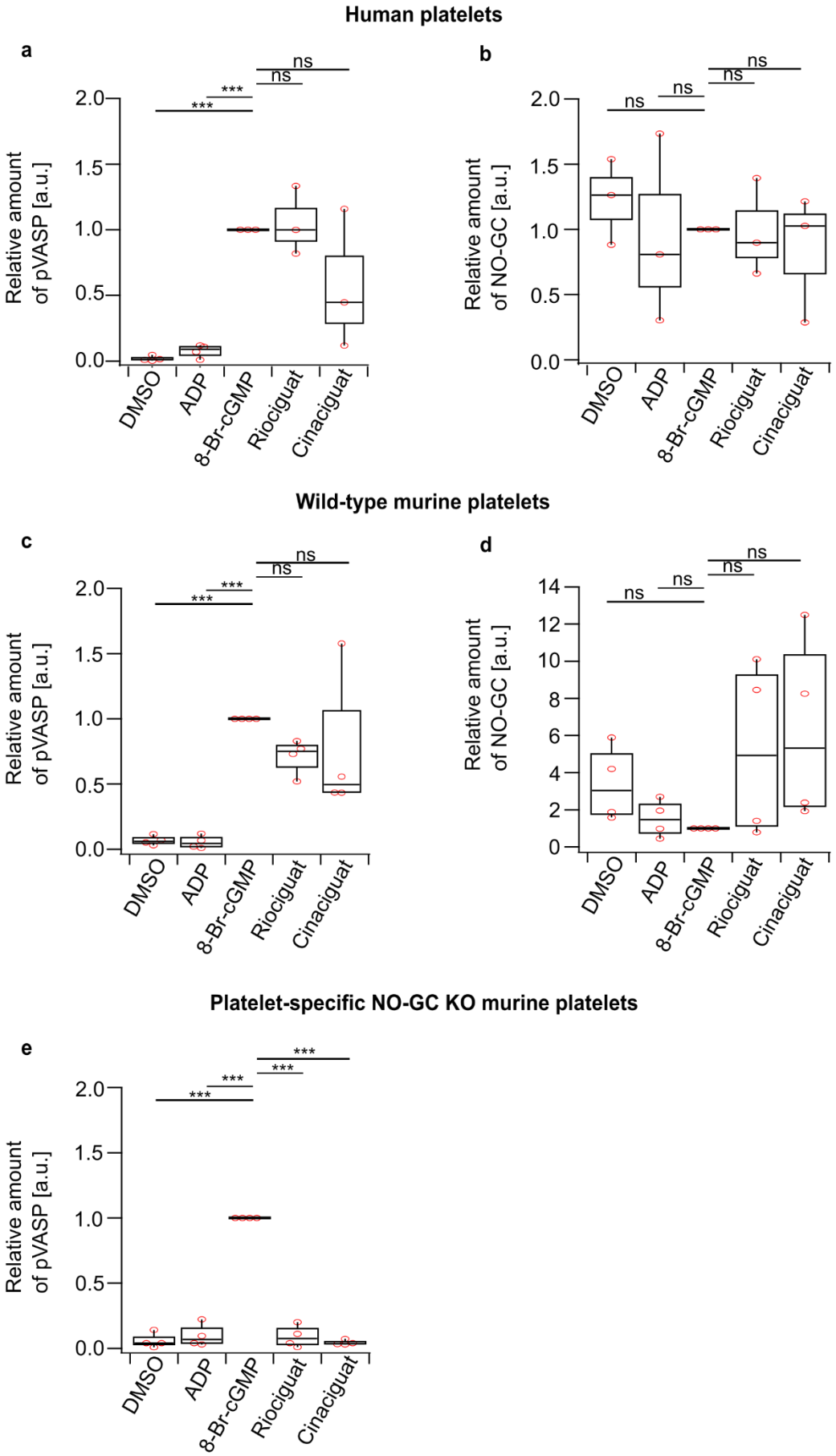
Human platelets
a
b
Relative amount of pVASP [a.u.]
Relative amount of NO-GC [a.u.]
ns
***
DMSO
ADP
8-Br-cGMP
Riociguat
Cinaciguat
Wild-type murine platelets
c
d
Platelet-specific NO-GC KO murine platelets
e

Figure 15. Platelet p-VASP is not altered in platelet-specific NO-GC KO murine platelets when treated with riociguat, or cinaciguat. **(a,c,e)** Relative amount of p-VASP. **(b,d)** Relative amount of NOGC. DMSO (1:1000), ADP (3 µM), 8-Br-cGMP (1 mM), riociguat (10 µM), cinaciguat (10 µM). The significance level of P-values is indicated by asterisks ($^{*}P < 0.05$; $^{**}P < 0.01$; $^{***}P < 0.001$; ns, not significant; Tukey´s test). Relative amount of p-VASP and NO-GC were normalized against 8-Br-cGMP. Experiments were performed with n=3 (human), n=4 (wild type mice), n=4 (NO-GC KO mice) donors. Western blots were done in collaboration with Daniel Pinto-Quintero. Representative western blots were shown in Figure 11.

Large variations of NO-GC levels were observed in human and wild-type platelets (Figure 15b, d). Most likely higher values came from donor-to-donor variation, which is one of the major limitations in this study. Figure 15d shows two outliers coming from two donors, which makes the overall median value increase for riociguat and cinaciguat treated wild-type murine platelets.

VASP is the major substrate of cGK in human platelets (51). Previous studies in VASP null mutants have proved the relevance of VASP in platelet recruitment, adhesion, and activation (52). The main phosphorylation sites of VASP are serine-157, serine-239, and threonince-278 (52). However, the phosphorylation at S239 and T278 are responsible for actin-fibers binding and filopodia growth in platelets (52). Figure 15a, c, e shows p-VASP at S239 to correlate with the stiffness values in Figure 11. This increased phosphorylation of p-VASP at S239 correlates with the cytoskeletal organization and downregulation of F-actin (Figure 10) which implicates a reduction in platelet stiffness (Figure 11).

Additionally, some studies have shown that phosphorylation of p-VASP at S239 is also involved in the inhibition of platelet activation by reducing P-selectin expression and GPIIb-IIa integrin-fibrinogen binding (52). This correlates with the P-selectin results obtained in Figure 10. Previous studies done in washed wild-type murine platelets treated with 10 µM of riociguat showed a 15-fold increase in cGMP compared to baseline, demonstrating a significant increase in cGMP release and an increased phosphorylation at p-VASP Ser^{239} (108). The results presented in Figure 15a, c, e agree with the literature, demonstrating that activating NO-GC leads to the formation of cGMP.

3.1.2. Conclusions and outlook

The effects of a NO-GC stimulator (riociguat), activator (cinaciguat), and a cGMP analog were investigated on platelet activation, morphology, and stiffness. Also, the study of a NO-GC stimulator (riociguat) was presented in platelets from HIV-positive patients taking ABC-containing regimens and HIV-negative patients. NO-GC/cGMP signaling pathway has been investigated extensively in platelets, but not to our knowledge the biomechanical properties of platelets. The current study shows novel results about platelet biology and the pharmacological effects of cGMP-modulating drugs in platelet biomechanics. Nevertheless, further studies will include the study of the mechanistic inside behind platelet stiffness like for example actin-myosin mediated contraction studies. Microtubules support actin-myosin interactions which maintain platelet structure and cause platelet centripetal forces during the spreading process.

It is important to recall the importance of platelet stiffness in this study. The platelet cytoskeleton plays an important role in platelet activation and supports platelet adhesion (35). Inherited platelet disorders (IPDs) are rare platelet diseases with mutations in the platelet cytoskeleton particularly integrins, which are characterized by spontaneous bleeding and a reduced platelet count (109). *MYH9*-related thrombocytopenia (109), Wiskott-Aldrich syndrome (WAS), and X-linked thrombocytopenia are examples of IPDs which have alterations in cytoskeletal components (35).

The impact in the biomechanical properties of platelet cytoskeleton in pathogenesis is still a field to explore. The implementation of a biomechanical assessment of platelet cytoskeleton in the diagnosis of IPDs will provide a more personalized treatment and prognosis. Therapeutic options that modulate platelet cytoskeleton are an alternative to treat IPDs (35). This study shows the possibility of pharmacologically targeting NO-GC/cGMP pathway in platelets and modulating platelet cytoskeleton, suggesting that low stiffness and high circularity values induced by high levels of cGMP are potential biomarkers.

Two morphological parameters were analyzed with deep-learning morphometry (circularity and area). The platelet area was unaffected, while circularity increased. Circular platelets can be resting platelets or fully spread platelets. Low circularity values show an early platelet spreading stage and activation followed by the formation of filopodia and lamellipodia. cGMP may induce an intermediate state of platelet activation in terms of platelet circularity, with a decreased P-selectin release from the α-granules. Riociguat, cinaciguat, and 8-Br-cGMP induced cGMP generation in pre-activated washed platelet, and inhibited platelet activation (Figure 10). Also, other studies have suggested that increased activity of cAMP-dependent kinase was related with inhibition of platelet activation and decreased thrombus formation (128). Considering the interaction and resemblance between cAMP and cGMP signaling, the inhibition of platelet activation observed in both pathways are congruent (128).

Platelet shape is a functional response to cytoskeletal changes and activation. ADP, TXA_2, integrins, and thrombin increases phosphorylation of myosin light chain (MLC) according to previous studies (63). Thrombin stimulates RhoA which leads to ROCK-mediated phosphorylation of MLCP (63). S-Nitrosoglutathione (GSNO) in an endogenous NO donor which blocks ROCK-mediated phosphorylation of MYPT1-thr^{853} in thrombin-activated platelets (63). This inhibition of the RhoA/ROCK pathway and MLC phosphorylation was mediated by NO-GC/cGMP signaling pathway (63). This study agrees with the results obtained with our circularity values (Figure 12) showed before, where platelets treated with cGMP modulating drugs do not have increased shape changes (increased circularity).

High-throughput screening of circularity in the past has been correlated with platelet anomalies in clinical samples (129). How stiffness and roundness tie into known roles of cGMP in controlling platelet adhesion and aggregation are the limitations of this study. Further experiments could include the manipulation of platelet stiffness with F-actin or stiffness enhancers, and then measure platelet aggregation and adhesion. Platelet agonists (ADP, thrombin, TXA_2) are not stiffness enhancers. Previously, it was demonstrated that thrombin-treated platelets induce platelet softening (130). Stiffness seems not to be directly linked to an increased platelet activation (130).

The platelet cytoskeleton undergoes dynamic changes during platelet spreading (131). Interestingly, actin-nodule like spots appear in early stages of adhesion and spreading, and just before lamellipodia formation (131). Actin-rich structures were unique for platelet-specific NO-GC KO murine platelets suggesting an early stage of adhesion and spreading (131). The presence of NO-GC in platelets suggests a pivotal role in the normal platelet spreading.

In summary, we studied the effect of pharmacological modulators of the NO-GC pathway on platelet cytoskeleton modulation, shape, and activation using NO-GC stimulators and activators. The lack of an effect of these drugs on stiffness, circularity, and CD62-P (P-selectin) in platelets from platelet-specific NO-GC KO murine platelets confirmed the importance of NO-GC/cGMP signaling pathway in platelet cytoskeleton modulation.

3.2 Role of NO-GC/cGMP pathway in platelets from PLHIV taking abacavir or tenofovir-containing regimens

The following chapter is not part of a manuscript, and it is not necessary to declare and disclose the detailed contributions.

3.2.1 Effect of NO-GC stimulators on platelet aggregation

The effect of riociguat and vericiguat (NO-GC stimulators), currently used in the clinics for the treatment of pulmonary hypertension, were investigated in platelets isolated from HIV-positive patients taking TFV- or ABC-containing regimens to study whether riociguat or vericiguat could reduce the risk of thrombogenicity and platelet reactivity. TFV- or ABC-containing regimes have been linked to an increased cardiotoxicity especially in ABC-containing regimes. However, the mechanism behind this cardiotoxicity has not been elucidated (78). There is also no clear evidence that withdrawal of ART improves cardiovascular risk in HIV-patients (78).

However, we cannot exclude that HIV patients with diabetes, lipidemia, hypertension will develop CVDs, independently of the ART (78). Platelet aggregation in response to ADP and collagen was measured. The thrombin receptor activator (TRAP-6), a PAR-1 agonist peptide, was also tested to test which platelet agonist was the most effective in activating platelets; however, in the preliminary tests TRAP-6 did not give the expected results, consequently only ADP and collagen were used to induce platelet aggregation and later platelet activation in HIV-negative and HIV-positive patients.

Microplate reader-based analysis of platelet aggregation showed decreased ADP-induced aggregation of isolated platelets from HIV-negative patients treated with riociguat (20% for riociguat, 45% for DMSO; P = 0.04) (Figure 16a). Additionally, collagen-induced aggregation also showed a decrease in platelets from HIV-positive patients taking TFV-containing regimens treated with vericiguat (50% for vericiguat, 90% for DMSO; P = 0.004) (Figure 16d). Although, platelets treated with riociguat or vericiguat did not show a significant decrease, in the case of HIV-negative and HIV-positive patients taking TFV-containing regimens a tendency to decrease platelet aggregation was observed in ADP- and collagen-induced platelet aggregation (Figure 16a, b, c, d). The reason why vericiguat was more effective in HIV-positive patients taking TFV-containing regimens is not clearly understood. When ODQ and riociguat or vericiguat were combined in the same sample preparation, the inhibition of the NO-GC enzyme by ODQ was reflected in the aggregation results observed ≈50% (Figure 16d).

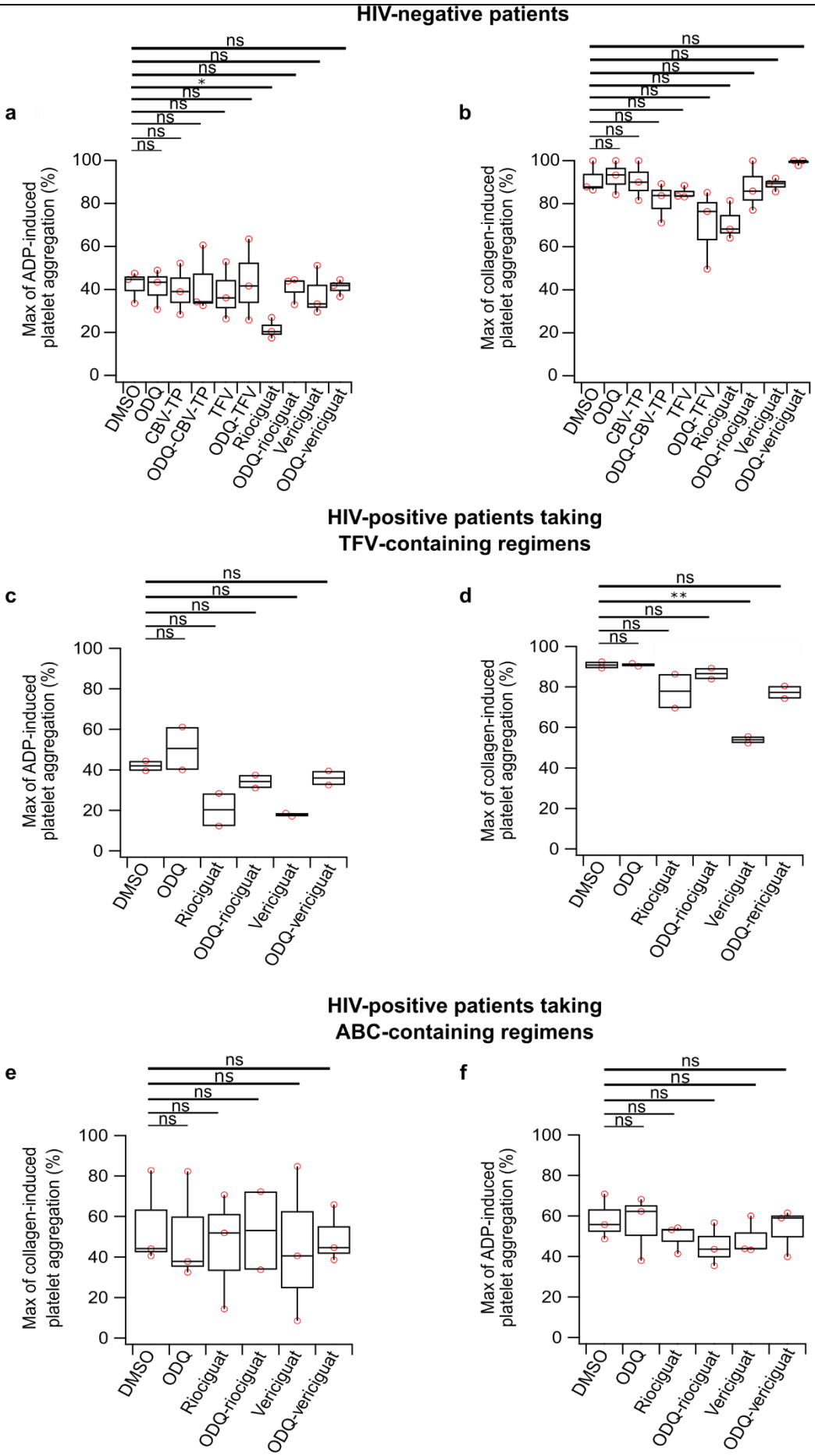
HIV-negative patients
a
b
Max of ADP-induced platelet aggregation (%)
Max of collagen-induced platelet aggregation (%)
DMSO
ODQ
CBV-TP
ODQ-CBV-TP
TFV
ODQ-TFV
Riociguat
ODQ-riociguat
Vericiguat
ODQ-vericiguat
HIV-positive patients taking TFV-containing regimens
c
d
HIV-positive patients taking ABC-containing regimens
e
f
ns
*
**

Figure 16. Riociguat decreases ADP-induced platelet aggregation in HIV-negative patients treated with riociguat and collagen-induced platelet aggregation in HIV-positive patients taking TFV-containing regimens treated with vericiguat. **(a, c, e)** Maximum of ADP-induced aggregation in response to indicated drug treatments. **(b, d, f)** Maximum of collage-induced aggregation in response to indicated drug treatments. ADP (3 µM), collagen (3 µM) DMSO (1:1000), CBV-TP (50 µM), TFV (50 µM), riociguat (10 µM), vericiguat (10 µM), ODQ (20 µM). The significance level of P-values is indicated by asterisks ($^{*}P < 0.05$; $^{**}P < 0.01$; $^{***}P < 0.001$; ns, not significant; Tukey's test). Donors: n=3 (HIV-negative patients, HIV-positive patients taking ABC-containing regimes), and n=2 (HIV-positive patients taking TFV-containing regimes).

Summarizing these results, riociguat decreased ADP-induced platelet aggregation only in HIV-negative volunteers but not in HIV-positive volunteers (Figure 16a). Riociguat or vericiguat inhibited platelet aggregation (Figure 16a, b) by increasing the release of cGMP, inhibiting the fibrinogen binding to the GPIIb/IIIa receptor, and decreasing intracellular calcium release (54). However, one of the limitations of this study is that we were not able to determine intracellular cGMP levels in the platelets from HIV-negative and positive patients. Previous studies done with inhaled NO have shown that inhibition of platelet aggregation, P-selectin expression, and consequently fibrinogen binding was inhibited in a dose-response manner (54). Higher doses of inhaled NO were required to achieve significant inhibition of platelet aggregation in platelet´s PRP (54). This could imply that perhaps higher doses of riociguat and vericiguat were required to see an effect, and this dose was also dependent on the type of agonist used to induce platelet aggregation (ADP or collagen). For that reason, riociguat only inhibited ADP-induced platelet aggregation and not collage-induced platelet aggregation (Figure 16a, b).

TFV-treated platelets showed a decrease in platelet aggregation in response to 3 µM ADP mediated by S-nitroso-N-acetyl-penicillamine (SNAP) in previous studies (65). However, NO-GC stimulators (riociguat or vericiguat) were not able to significantly inhibit ADP-induced platelet aggregation (Figure 16c). Additionally, other studies shown that a concentration above 50 µM of riociguat is required to inhibit ADP-induced platelet aggregation in whole blood and PRP (108). Based on that study, the concentration used in this study was too low (10 µM), and further studies with higher concentration must be undertaken. In summary, it is not conclusive that riociguat or vericiguat affect platelet aggregation in HIV-positive patients taking TFV-containing regiments and HIV-negative volunteers.

3.2.2 Effect of NO-GC stimulators on endothelial-platelet crosstalk

The vascular endothelium regulates vascular tone, VSM cell proliferation, and haemostasis. Endothelial microparticles (EMPs) are small vesicles which are released from endothelial cells upon inflammation, apoptosis, thrombosis, or vascular injury (132). The physiological mechanism by which EMPs are released from endothelial cells is called cell membrane blebbing and occurs mainly immediately after apoptosis (133). The exact mechanism of endothelial vesiculation is poorly understood, but increased release of EMPs has been correlated with severe cardiovascular diseases including hypertension (132). EMPs have receptors which target major coagulation pathways, immune regulation, angiogenesis, and fibrinolysis (133).

To produce EMPs, we incubated cultured HUVEC with the inflammatory cytokine tissue necrosis factor-α (95,133). Our goal was to study the interaction between isolated EMPs, previously treated with cGMP-modulating drugs, and platelets to investigate endothelial-platelet crosstalk. Maximum ADP- and collagen-induced PAC-1, CD62P, and CD63 activation were quantified in platelets from HIV-positive patients currently taking ABC or TFV-regimens.

Only platelets from HIV-positive patients were investigated to determine whether there is any difference in platelet activation solely based on the antiretroviral treatment (ABC or TFV). EMPs from HUVECs, previously incubated with DMSO (1:1000), riociguat (10 µM), vericiguat (10 µM), or ODQ (20 µM) for 48 hours, were isolated and quantified with FACS. The amount of EMPs per µL were different depending on the drug treatment (DMSO: ≈ 515; riociguat: ≈ 297; vericiguat: ≈ 297; ODQ: ≈ 539). EMPs production diminished under the stimulation of riociguat or vericiguat, suggesting a decrease in endothelial inflammation in comparison with DMSO (vehicle control). ODQ and DMSO had a similar EMPs release.

Platelets isolated from HIV-positive patients taking TFV- or ABC-containing regimens and pre-incubated with isolated EMPs from HUVEC previously treated with DMSO, riociguat, vericiguat, or ODQ did not show any change in their maximum of ADP- or collagen-induced PAC-1, CD62P, and CD63 activation markers in platelets (Figures 17, 18). EMPs did not exacerbate platelet activation, which is a positive outcome in HIV-patients. Similarly, we did not observe any effect of EMPs from vericiguat- or riociguat-treated HUVECs on the activation of platelets from HIV-patients taking TFV or ABC, measured by P-selectin. This lack of effect possibly reflects that integrin αIIbβ3 signaling pathway and P-selectin release from α-granules were not upregulated in platelets from HIV-positive patients taking TFV- or ABC-containing regimens (Figures 17, 18). Moreover, in the case of platelets isolated from HIV-positive patients currently taking ABC-containing regimes, the absence of a response in platelet activation is most likely related to the inhibition of the NO-GC/cGMP signaling pathway by ABC. Lastly, results were similar independently of whether ADP or collagen was used to induce platelet activation (Figure 17, 18).

Previous studies have shown that EMP alone were not able to induce platelet activation; however, ABC-EMP increased αIIbβ3 integrin activation by +1.9-fold in comparison to vehicle-EMP (95). The modulatory effect of ABC-EMP was only present in collagen-induced activation in previous studies (95) . However, figures 17 and 18 did not show any modulatory effect of DMSO-, riociguat-, vericiguat-, and ODQ-EMP upon platelet activation to ADP or collagen. Other studies have shown that ABC do not influence platelet activation, but influences platelet adhesion to endothelial cells via ATP-P_2X_7 receptors and further ICAM-1 and P-selectin interplay (134).

Platelet reactivity was studied with three different markers: αIIbβ3 (PAC-1) which is in the plasma membrane and α-granules´ membrane, CD62P (P-selectin) which is found in the α-granules´ membrane, and CD63 which is in the dense granule´s membrane (135). No significant response of all activation markers after stimulation of collagen and ADP is related to the diminished amount of α- and dense granules present in platelets from HIV-positive patients.

HUVECs were not explicitly tested whether they express NO-GC and respond to riociguat or vericiguat with an increase of cGMP, and perhaps this is one of the limitations of this study. Nevertheless, from literature is known that HUVECs migrate in response to DEA/NO and DETA/NO gradients enhancing cGMP signaling (136). Consequently, this study assumed that HUVECs express NO-GC enzyme. Previously, it was reported that 50µM of riociguat (108) decreased platelet aggregation using PRP. Probably, as further experiments a higher NO-GC stimulator concentration could be tested to confirm the current results found Figure 17 and 18.

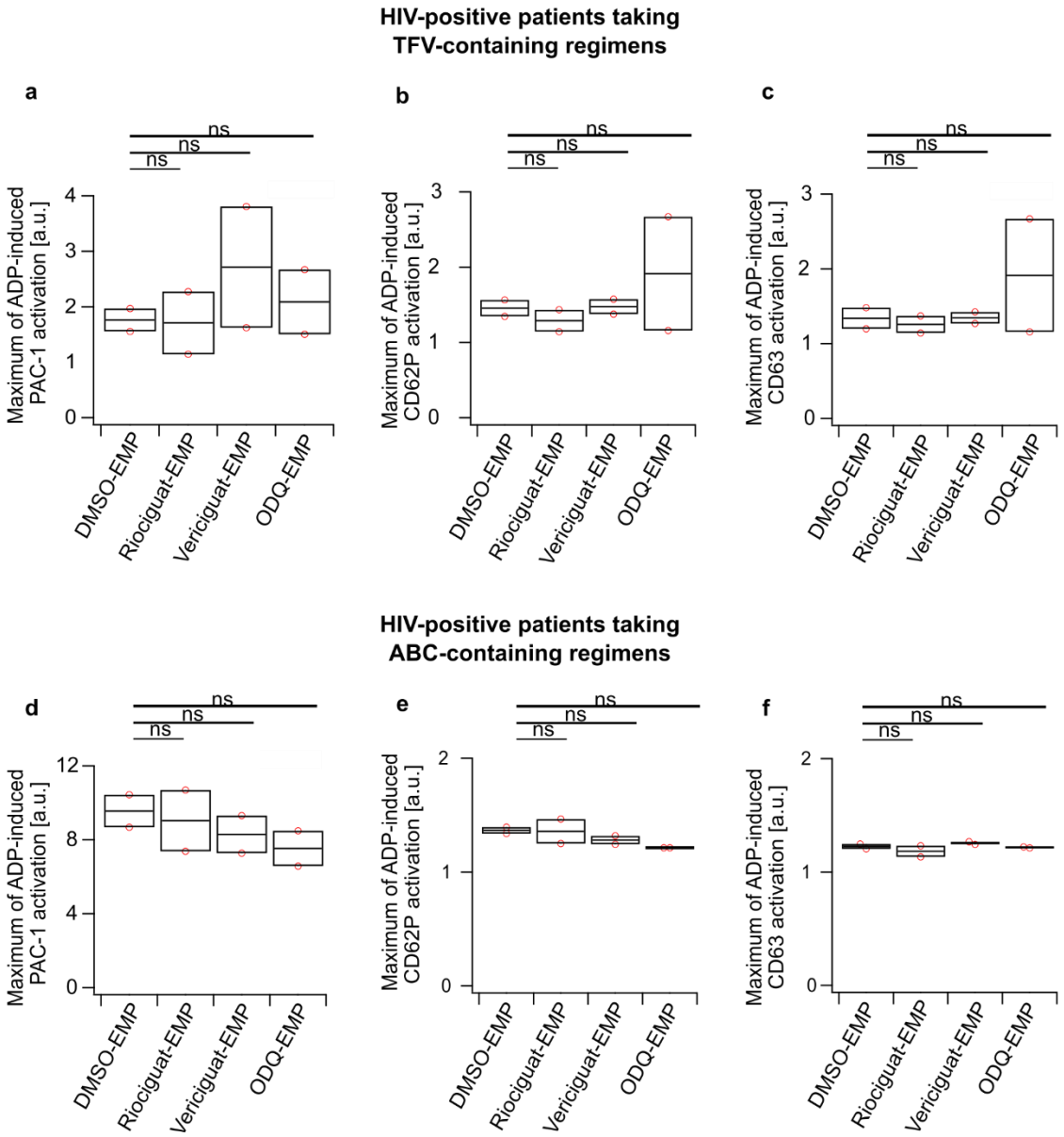

Figure 17. Riociguat-EMP or vericiguat-EMP does not alter maximum ADP-induced activation in HIV-positive patients taking TFV- or ABC-containing regimens. **(a, d)** PAC-1 activation. **(b, e)** CD62P activation. **(c, f)** CD63 activation. ADP (3 µM), collagen (3 µM) DMSO (1:1000), riociguat (10 µM), vericiguat (10 µM), ODQ (20 µM). The significance level of P-values is indicated by asterisks ($^{*}P < 0.05$; $^{**}P < 0.01$; $^{***}P < 0.001$; ns, not significant; Tukey's test). Donors: n=2 (HIV-positive patients taking TFV- or ABC-containing regimes).

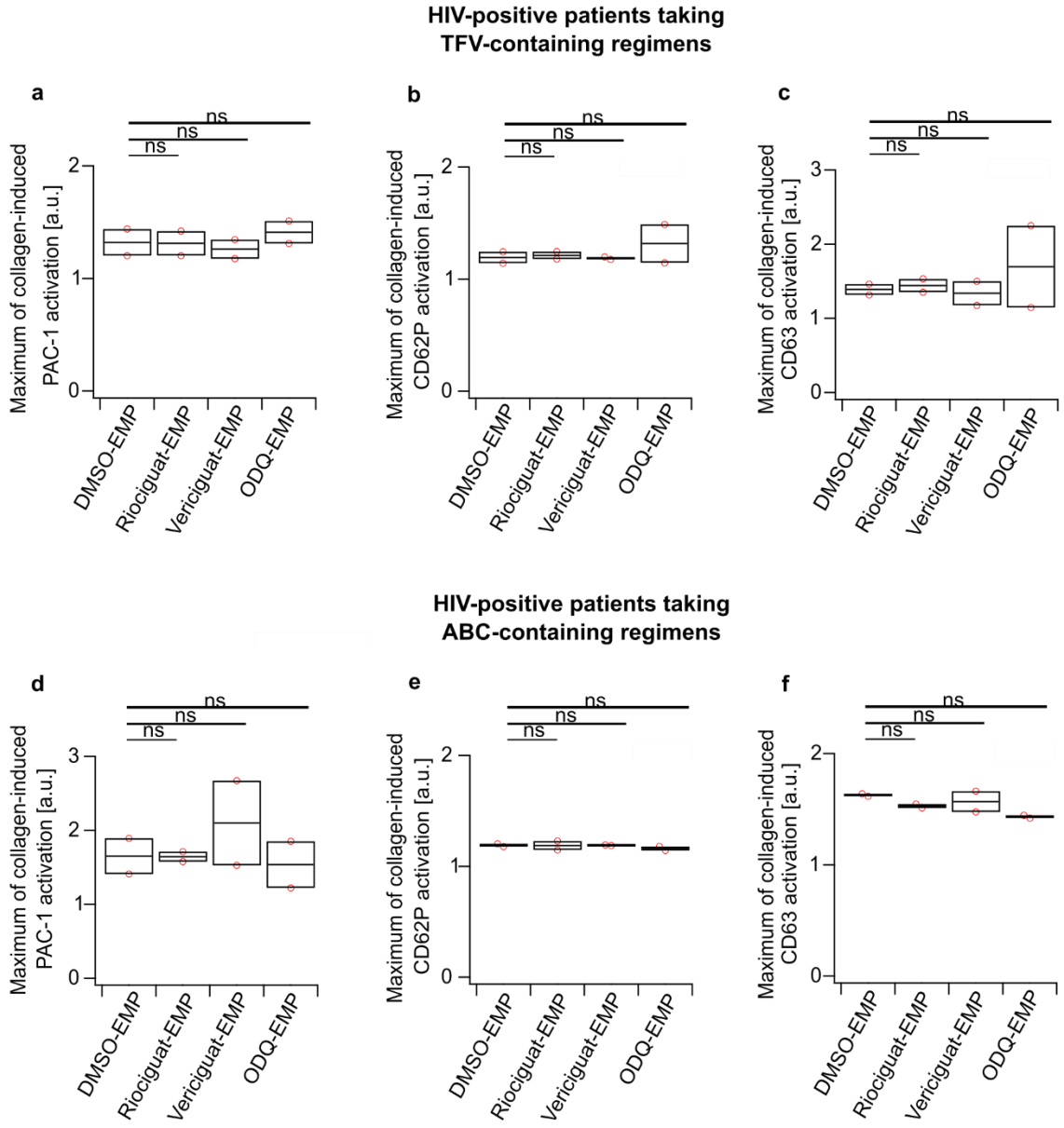

Figure 18. Riociguat-EMP or vericiguat-EMP does not alter maximum collagen-induced activation in HIV-positive patients taking TFV- or ABC-containing regimens. **(a, d)** PAC-1 activation. **(b, e)** CD62P activation. **(c, f)** CD63 activation. ADP (3 µM), collagen (3 µM) DMSO (1:1000), riociguat (10 µM), vericiguat (10 µM), ODQ (20 µM). The significance level of P-values is indicated by asterisks ($^{*}P < 0.05$; $^{**}P < 0.01$; $^{***}P < 0.001$; ns, not significant; Tukey's test). Donors: n=2 (HIV-positive patients taking TFV- or ABC-containing regimes).

3.2.3 Effect of NO-GC stimulators on platelet morphology

Circularity is increased in riociguat or vericiguat-treated platelets from HIV-negative and HIV-positive patients taking TFV-containing regimens, but not in platelets from HIV-positive patients taking ABC-containing regimens. The circularity of platelets from HIV-negative donors was significantly increased by ≈50% when treated with riociguat (circ = 0.55, *P* = 0.008) or vericiguat (circ = 0.58, *P*= 0.004) compared with DMSO (circ = 0.35) (Figure 19a). However, the circularity of platelets from HIV-negative donors did not change when treated with CBV-TP (circ = 0.31, *P* = 0.998) or TFV (circ = 0.40, *P* = 0.953) (Figure 19a).

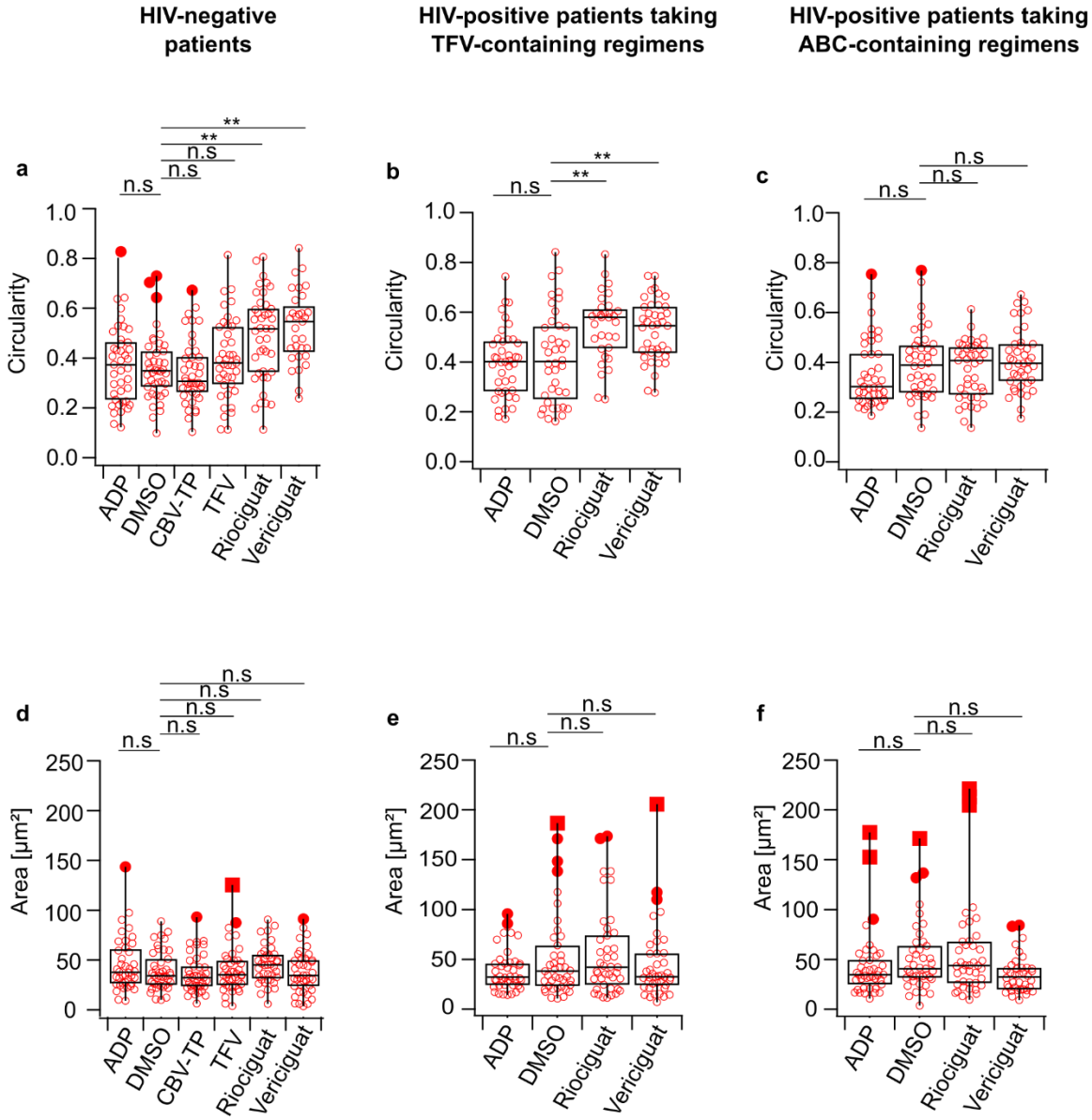

Figure 19. Platelet area is not altered in human platelets from HIV-negative patients and HIV-positive patients taking TFV-containing regimens when treated with riociguat or vericiguat. **(a)** Platelet circularity **(b)** Platelet area. ADP (3 µM), DMSO (1:1000), CBV-TP (50 µM), TFV (50 µM), riociguat (10 µM), vericiguat (10 µM). Platelet numbers for all conditions: n=45. The significance level of P-values is indicated by asterisks ($^{*}P < 0.05$; $^{**}P < 0.01$; $^{***}P < 0.001$; ns, not significant; Tukey's test). Experiments were performed with ≈15 platelets per donor from n=3 (HIV-negative patients, HIV-positive patients taking TFV- or ABC-containing regimes) donors.

Platelet circularity from HIV-positive patients taking TFV-containing regimens treated with riociguat (circ = 0.59, *P* = 0.005) or vericiguat (circ = 0.58, *P* = 0.014) significantly increased compared to DMSO (circ = 0.4) (Figure 19b). On the other hand, circularity of platelets from HIV-positive patients taking ABC-containing regimens did not change after treatment with riociguat (circ = 0.40, *P* = 0.941) or vericiguat (circ = 0.41, *P* = 0.172) in comparison to DMSO (circ = 0.38) (Figure 19c). These findings suggest that platelets previously exposed to CBV-TP, as observed in HIV-positive patients taking ABC-containing drugs, are not influenced by the NO-GC stimulators (riociguat or vericiguat) because NO-GC pathway is inhibited. The lack of change in circularity in HIV-positive patients taking ABC-containing drugs confirms the disruption of the NO-GC/cGMP signaling pathway and the loss of a thrombo/cardioprotective effect.

The median platelet area of HIV-negative patients and HIV-positive patients taking TFV- or ABC-containing regimens was similar independently of the treatments ≈40 μm^2 (Figure 19d, e, f). These results suggested that platelet area is not modified by NO-GC stimulators, CBV-TP, TFV, or ADP (Figure 19d, e, f). Additionally, the overall platelet area was not affected by HIV status (Figure 19 d, e, f). Previously, it was mentioned that an increased platelet circularity indicates a less activated platelet spreading stage with fewer formation of filopodia and lamellipodia. Furthermore, platelets from HIV-positive patients taking TFV-regimens treated with riociguat or vericiguat show a lower degree of platelet activation and are less prone to thrombogenicity. The opposite is observed in platelets from HIV-positive patients taking ABC-regimens treated with NO-GC stimulators. It is important to note that platelet adhesion during a vascular injury is mediated by platelet shape changes, disruption of the actin network, and increased surface tension (137).

Previous studies using high-throughput screening of platelet spreading analysis also used circularity as a parameter to identify different platelet phenotypes in different platelet-based disorders (129), so deep-learning morphological analysis is becoming a powerful technique in data analysis. This study focused on the morphological analysis of platelets from HIV-positive patients taking different drug regimens in comparison with HIV-negative patients. Circularity changes close to zero are mainly linked to the growth of filopodia and lamellipodia, suggesting activated platelets. On the other hand, circularity changes close to 1 are either unspread or fully spread platelets. However, based on the images most of the platelets are in an intermediate state of platelet activation explained before.

Normally, fully spreaded platelets are active but previously was demonstrated that cGMP-modulating drugs decrease release of P-selectin from α-granules. However, the limitation of this study is that P-selectin was not measured in HIV-patients. Taking that into consideration, an intermediate activation state was suggested for platelets treated with cGMP-modulating drugs. Normal circularity measurements from five representative controls in previous studies were ≈0.5, which are within the values in the platelet control group (129) (Figure 19 a, b, c). Platelet circularity could be a complementary study to determine how platelet spreading stages differ in patients and healthy volunteers.

3.2.4 Effect of NO-GC stimulators on F-actin

Platelet F-actin is not affected by riociguat and vericiguat in HIV-positive patients taking ABC-containing regimens. Previously, we have corroborated that NO-GC plays a role in the downregulation of F-actin polymerization and consequently in the modulation of platelet cytoskeleton. In platelets from HIV-negative patients, riociguat downregulated F-actin by ≈50% (Figure 10a, b); vericiguat (NO-GC stimulator) was not tested. Platelet F-actin CTCF values from HIV-positive patients taking TFV-containing regimens was significantly increased when treated with riociguat (P= 1.402×10^{-08}) and vericiguat (P= 4.907×10^{-11}), compared to DMSO (Figure 20a).

Additionally, platelets from HIV-positive patients taking TFV-containing regimens pre-incubated with ADP (*P*= 0.40) did not show any significant change in F-actin CTCF values (Figure 20a). ADP-activated platelets show a similar level of activation to DMSO (vehicle control) in HIV-positive patients taking TFV-containing regimens. It could be inferred from Figure 20a that platelets from HIV-positive patients taking TFV-containing regimes have a functional NO-GC/cGMP signaling pathway because of a F-actin upregulation in platelets treated with riociguat or vericiguat. This F-actin upregulation could be related to an increased platelet overactivation usually present in HIV-positive patients taking TFV-containing regimens.

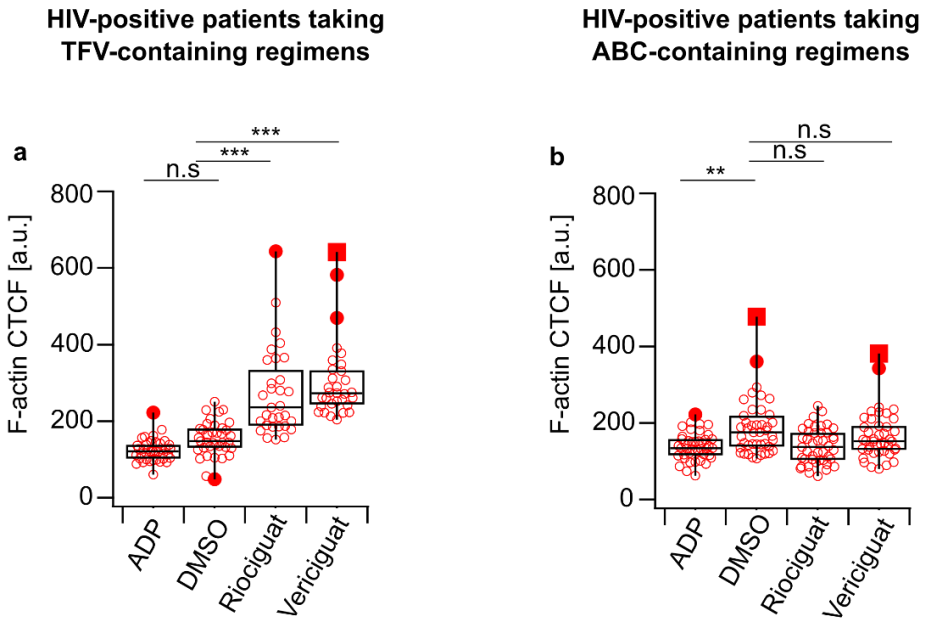

Figure 20. Platelet F-actin CTCF [a.u.] is not altered in HIV-positive patients taking ABC-containing regimens. **(a,b)** F-actin CTCF in HIV-positive patients taking TFV- or ABC-containing regimens. ADP (3 µM), DMSO (1:1000), riociguat (10 µM), vericiguat (10 µM). Platelet numbers for all conditions: n=45. The significance level of P-values is indicated by asterisks ($^{*}P < 0.05$; $^{**}P < 0.01$; $^{***}P < 0.001$; ns, not significant; Tukey's test). Experiments were performed with ≈15 platelets per donor from n=3 (HIV-positive patients taking TFV- or ABC-containing regimes) donors.

In platelets from HIV-positive patients taking ABC-containing regimens, F-actin was not altered by riociguat (*P*= 0.04) or vericiguat (*P*= 0.53) (Figure 20b). A significant difference between ADP and DMSO F-actin CTCF values (*P*= 0.004) was only observed in HIV-positive patients taking ABC-containing regimens. This finding could be related to the large spread on the platelet population observed in DMSO platelet F-actin CTCF values from HIV-positive patients taking ABC-containing regimens. Whether F-actin polymerization is affected in platelets from HIV-positive patients is unknown. However, platelets from HIV-positive patients tend to be in an activated state

and over-reactive in comparison with healthy volunteers, which could contribute to an increased risk of heart failure and cardiotoxicity in these patients. From our studies, it is not clear whether riociguat or vericiguat can downregulate F-actin in platelets from HIV-positive patients currently taking TVF. However, the absence of an alteration in F-actin in platelets from HIV-positive patients currently taking ABC could be related to the presence of CBV-TP in the blood of these patients and the inhibition of NO-GC/cGMP signaling pathway. Nevertheless, this cannot be confirmed because cGMP levels in platelets from HIV-positive patients were not measured.

Previous studies showed that a minimum of 20% actin polymerization is required to activate platelets and 55% of actin polymerization is needed to aggregate platelets. F-actin to G-actin ratio in platelets also contributes to understand the overall platelet cytoskeleton function, so this should be considered as an additional study. Actin polymerization induces further platelet shape changes, including lamellipodia and filopodia extension (35). Thrombocytopenia is a very common disease in HIV-positive patients, and around 40% percent will develop thrombocytopenia in late HIV-stages (138).

Impaired function in platelet cytoskeleton and alterations in the biomechanical properties have been observed in patients with thrombocytopenia and inherited platelet disorders (IPDs) (35). Suggesting, that most likely the biochemical properties (stiffness) in platelets from HIV-positive patients are different from HIV-negative patients´ platelets. Further, stiffness values from HIV-positive patients´ platelets are advisable to correlate with the current F-actin values obtained in Figure 20. Currently, there are no known up to date previous investigations regarding F-actin quantification and stiffness measurements in HIV-positive patients.

3.2.5 p-VASP quantification

Western blot quantification from three donors were performed to determine whether CBV-TP blocks the upregulation of p-VASP caused by 8-Br-cGMP or riociguat. The quantification results presented in Figure 21 were normalized to 8-Br-cGMP. Riociguat and 8-Br-cGMP increased the relative amount of p-VASP present in human platelets

likewise (Figure 15a). CBV-TP did not upregulate p-VASP in human platelets and the relative amount of p-VASP obtained was comparable to platelets incubated with DMSO or ADP (≈0.2) (Figure 21). Platelets pre-incubated with CBV-TP and then with riociguat or 8-Br-cGMP, did not show any significant difference in comparison with platelets incubated with riociguat or 8-Br-cGMP only. Suggesting, that CBV-TP do not intervene with the p-VASP phosphorylation increase mediated through NO-GC/cGMP signaling pathway in HIV-negative volunteers.

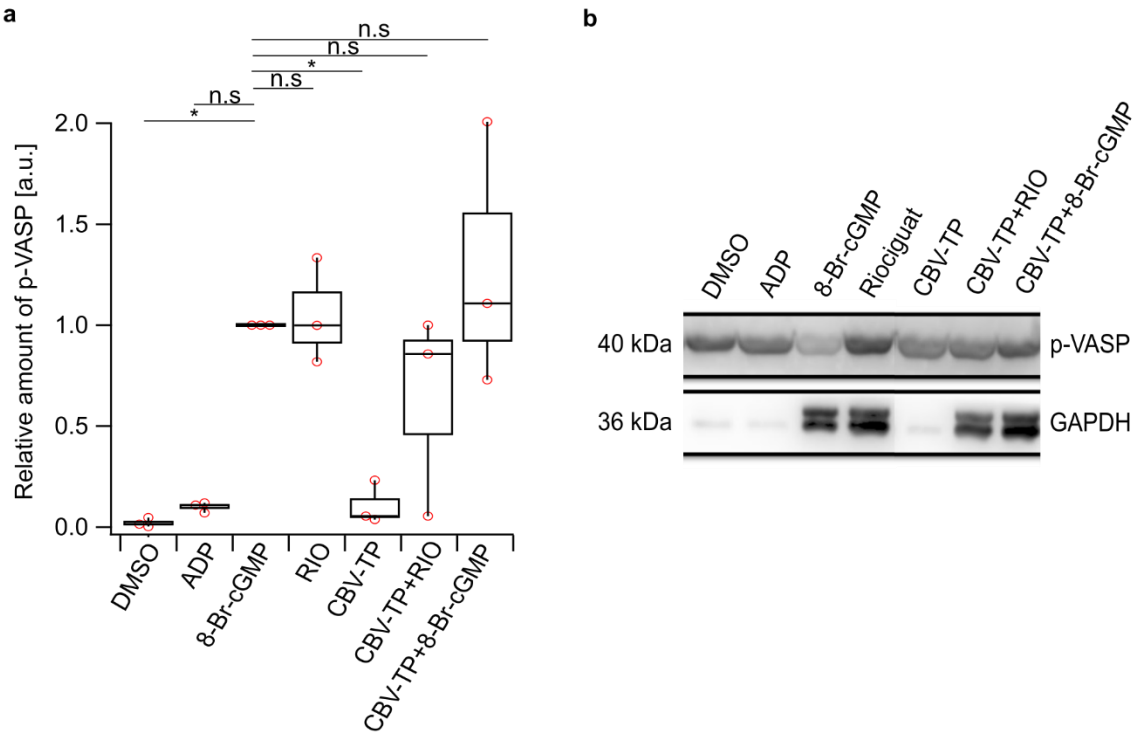

Figure 21. Carbovir does not affect p-VASP upregulation when incubated together with riociguat or 8-Br-cGMP. **(a)** Relative amount of p-VASP. **(b)** Western blot analysis of VASP phosphorylation (p-VASP) and NO-GC. GAPDH was used as loading control. DMSO (1:1000), ADP (3 µM), 8-Br-cGMP (1 mM), riociguat (10 µM), cinaciguat (10 µM). The significance level of P-values is indicated by asterisks ($^{*}P < 0.05$; $^{**}P < 0.01$; $^{***}P < 0.001$; ns, not significant; Tukey´s test). Relative amount of p-VASP were normalized against 8-Br-cGMP. Experiments were performed with n=3 (human). Western blots were done in collaboration with Daniel Pinto-Quintero.

Further, investigation of the relative amount of p-VASP in platelets from HIV-positive patients taking ABC- or TVF- is suggested. Additionally, quantification of cGMP levels with the platelet-specific cGi500 mice was planned. However, because of the results obtained with western blot (Figure 21) and time constraints, the FRET measurements were not done. Nevertheless, it is important to consider that previous studies showed

that flow-dependent FRET/cGMP signals correlate with phosphorylation of p-VASP and usually are three times higher in flow than in static conditions (33). For that reason, it could be interesting to corroborate the intracellular cGMP concentration in platelets treated with CBV-TP and riociguat under flow conditions. Taken together these results, CBV-TP do not affect p-VASP upregulation when incubated together with riociguat or 8-Br-cGMP.

3.2.6 Conclusions and outlook

The clinical applicability of riociguat and vericiguat (NO-GC stimulators) were studied in platelets from HIV-positive patients currently taking TFV- or ABC-containing regimens and HIV-negative patients. Previous studies suggested a potential link to an increased cardiovascular risk in patients taking ABC because of an inhibition of NO-GC/cGMP signaling pathway by the active anabolite of ABC (CBV-TP) (65). These preliminary platelet aggregation studies used nitric oxide derivatives like S-nitroso-N-acetyl-penicillamine (SNAP) (65) , but not NO-GC stimulators were not tested so far.

The goal was to investigate whether riociguat or vericiguat could decrease platelet thrombogenicity in HIV-positive patients taking TFV- or ABC-containing regimens. Caucasian HIV-positive patients between 51 to 62 years old currently taking ABC/ lamivudine (3TC)/dolutegravir (DTG) or nevirapine as their ART treatment for longer than 5 years were used in this study. DTG is a HIV integrase inhibitor which blocks DNA retroviral integration, while ABC/3TC incorporates their respective monophosphate form in the viral HIV DNA resulting in an inhibition of viral replication (139). The effects of the other two NRTIs (3TC or DTG) have not been investigated in this study, and this will be important to consider for further experiments.

The effect of riociguat and vericiguat on platelet aggregation, EMP-platelet crosstalk, morphology, and CTCF actin concentration were studied in platelets from HIV-negative patients and HIV-positive patients taking TFV- or ABC-containing regimens. Riociguat and vericiguat did not show any increase in platelet aggregation, EMP-induced platelet activation, circularity, area and CTCF actin concentration in HIV-positive patients taking ABC-containing regimens in comparison with HIV-positive patients taking TFV-containing regimens and HIV-negative volunteers. EMPs previously incubated with riociguat or vericiguat do not influence ADP- or collagen induced activation of PAC-1, CD62P, and CD63 in platelets from HIV-positive patients taking TDF- or ABC-containing regimens.

Platelet adhesion to HUVECs were studied in a flow chamber to determine platelet-endothelial interaction (134). The experimental design of this study was similar to what was performed in Figure 17 and 18, where the endothelial-platelet crosstalk was investigated. Incubation time of platelets were 30 min longer than in our study, and the concentrations used were clinically relevant (CBV-TP; 1- 25 µg/mL) and (TDF; 0.1 – 10 µg/mL) (134). The clinically relevant concentrations agreed with what we used for the experiments presented above. HUVECs and platelets were pre-treated with P_2-ATP receptor antagonists prior ABC or TFV treatment to check whether purine-signaling pathway and ATP-P_2X_7 receptors are involved in the increased thrombogenicity and vascular inflammation in HIV-positive patients currently taking ABC (134).

These studies showed that ABC-treated platelets do not induce a direct platelet activation, but the ABC-induced endothelial-platelet interaction induces further platelet aggregation and activation (134). Also, TDF had no effect on platelet-endothelial interaction and did not promote platelet adhesion to endothelial cells (134). According to this study, ATP-P_2X_7 receptors present on the endothelial cells induce vascular inflammation and then platelet hyperactivity (134). For further studies related to the endothelial-platelet cross talk will also be relevant to take in consideration the influence of purine-signaling pathway and ATP-P_2X_7 receptors present only in endothelial cells, but not in platelets.

Additionally, an increased phosphorylation of VASP in static platelet conditions observed in platelets treated with 8-Br-cGMP or riociguat are not affected by CBV-TP when incubated together with the cGMP-modulating drugs. It is important to recall that the NO generated by the vascular endothelium activates NO-GC in platelets in a shear-dependent manner, and p-VASP in flow conditions significantly different to static conditions.

PRPs from HIV-patients currently taking TFV- or ABC-containing regimens were used for platelet aggregation and activation experiments, while washed platelets for F-actin immunostaining, platelet morphology, and p-VASP quantification. Previously was discussed, that other studies observed only above 50 µM of riociguat a significant

decrease in platelet aggregation. However, 10 µM of riociguat was enough to observe an effect in washed platelets. Further, studies must include testing everything again with a concentration above 50 µM to compare with the current results obtained (Figure 16-21). Additionally, the average maximum drug concentration (Cmax) of CBV-TP in blood plasma from HIV-positive patients currently taking ABC-containing regimens is ≈4.3µg/mL (72). Although platelets from HIV-negative patients could be incubated for 30 min maximum, the amount of CBV-TP (≈4.3µg/mL) will never be the same as present in HIV-positive patients taking ABC-containing regimens. This also could be one of the reasons why p-VASP was unaffected when CBV-TP and riociguat or 8-Br-cGMP were incubated together. Consequently, p-VASP quantification is advisable in platelets from HIV-positive patients taking TFV- or ABC-containing regimens.

Previously, it was tested whether CBV-TP could inhibit NO-GC with an enzyme inhibition assay (72). cGMP production was assessed in whole blood or PRP with an ELISA assay (72). CBV-TP inhibited the activity of purified NO-GC from bovine and human enzymes (72). Other studies even suggested that ABC could induce vascular inflammation via ATP-P_2X_7 receptors (purine-signaling pathway) because of the close similarity between endogenous purines (ADP, AMP) and a guanosine analogue (81). The limitation of this study is the absence of a relative quantification of NO-GC levels after riociguat or vericiguat treatment in the platelets of HIV-positive patients currently taking ABC- or TFV-containing regimens and in HUVEC cells via western blot. This relative quantification levels of NO-GC would have helped to determine whether cGMP increased or not when platelets or HUVECs were exposed to cGMP-modulating drugs.

Taken together, these results suggest that NO-GC stimulators could have a potential clinical applicability and reduce thrombogenicity and hyperreactivity in platelets based on the circularity and aggregation readout obtained in Figures 16, 19. However, further studies need to be undertaken to corroborate that the cardiotoxicity present in HIV-positive patients taking ABC-containing regimens is mainly related with a dysfunctional NO-GC/cGMP pathway caused by CBV-TP

3.3 Effect of biochemical confinement on platelet morphology and mechanics

Authors of the related publication: Johanna G. Rodríguez, Carmela Rianna, Vincent Gidlund, Jan Seifert, Tilman E. Schäffer

Author position: 1

Title of paper: Effect of biochemical confinement on platelet morphology and mechanics

Status in publication process: Manuscript in preparation

Detailed contribution to the manuscript as part of this chapter

- Scientific ideas (45%)
  - Experimental design and detailed analysis were carried out.
  - Understanding the effect of biochemical confinement in platelet morphology and mechanics through the stimulation of platelet activation with soluble agonists.
- Data generation (50%)
  - Performance of sample preparation including isolation of human platelets.
  - Optimization of all the protocols for micro-contact printing (µCP) and biochemical confinement of platelets.
  - Performance of all the microscopy experiments for morphological analysis, including the images for the CNN deep-learning morphological analysis.
  - µCP patterned substrates were generated by Dr. Carmela Rianna.
  - Performance of all the AFM experiments by MSc. Vincent Gidlund (Fig. 24 and 25).
- Analysis & interpretation (50%)
  - Analysis of the data, composition, and interpretation in all figures.
  - CNN deep-learning morphological analysis was performed by Dr. Jan Seifert (Fig. 22). Further data analysis and interpretation was performed by Johanna Rodríguez.
- Paper writing (40%)

The methods section of this manuscript has been removed to avoid repetition, and everything was placed in the materials and methods section above.

Effect of biochemical confinement on platelet morphology and mechanics

Johanna G. Rodríguez[1], Carmela Rianna[1], Vincent Gidlund[1], Jan Seifert[1], and Tilman E. Schäffer[1]

[1] Institute of Applied Physics, University of Tübingen, Tübingen, Germany.

Abstract

An exacerbated release of platelet agonists induces platelet activation and consequently triggers the enhancement of cardiovascular pathologies like thrombosis. Furthermore, the study of platelet activation in an *in vitro* system similar to the size of blood capillaries is important to fully understand platelet function. The understanding of platelet stiffness and shape parameters in a more physiological environment created with micro-contact printing (µCP) provides a new understanding of platelet cytoskeleton modulation and spreading during agonist activation with ADP or thrombin. Two soluble platelet agonists (ADP and thrombin) were tested in human platelets to understand how biochemical confinement affects platelet morphology and mechanics in platelet activation. We used micro-contact printing (µCP) to create fluorescent fibrinogen lines (5 µm width, 15 µm periodicity) for confined platelets, and a flat area for unconfined platelets in the same pattern. We investigated the effect of confinement on platelet morphology and mechanics using optical microscopy and atomic force microscopy (AFM). Human platelet morphology and mechanics were strongly influenced by biochemical confinement. Confined ADP-activated platelets showed an increased volume and aspect ratio in comparison to untreated and thrombin-activated platelets. Further, the actin content and the stiffness for confined ADP-activated platelets were decreased in comparison with unconfined untreated and thrombin-activated platelets. Taken together, these results demonstrate that platelet mechanics and morphology are affected by confinement.

Introduction

Platelets play a critical role during vascular injury because of their function during clot formation and hemostasis (140). Platelets are immediately recruited when there is an endothelial injury or an inflammatory sign (141). After activation by released platelet agonists such as adenosine diphosphate (ADP) or thrombin, platelets adhere and spread to an underlying surface through the formation of filopodia and lamellipodia. This leads to multi-cellular aggregation and thrombus formation (116). Impaired platelet activation is associated with severe cardiovascular pathologies such as thrombosis, stroke, or myocardial infarction (142)(116). Additionally, clots can form on the surface of medical stents, leading to the development of thrombosis (143).

The understanding of cellular stiffness and its dependence on the extracellular environment is important for platelet research (34). The cytoskeleton generates contractile forces and essentially contributes to mechanotransducive and haptotactic mechanisms and platelet motility (43,141,144,145) Alterations in the cytoskeleton imply a change in cellular stiffness (146) and can potentially lead to increased bleeding tendencies (35).

In vitro mimicking of physiological conditions is important for the study and understanding of platelet behavior. Micro-contact printing (µCP) allows to investigate single platelet adhesion in a micro-environmental geometry space (143). For example, µCP has been used to study the migration of tumor and mesenchymal stem cells in confinement (147,148). µCP-3D collagen micro tracks were used to mimic physiological conditions for metastatic breast cancer cells to understand the effect of confinement on cancer cells (149). µCP aids in the development of versatile biologically relevant patterns (150). However, platelet activation under biochemical confinement has not yet been studied. In this study, we investigated how platelet morphology and mechanics are affected by biochemical confinement using optical microscopy and atomic force microscopy (AFM) on a single cell level. We used µCP to fabricate fluorescent fibrinogen lines with a width of 5 µm and a periodicity of 15 µm to provide a model system for platelet confinement in blood capillaries (151).

We found that platelets were strongly affected by confinement when they were activated with ADP. These platelets showed an increased aspect ratio, and volume in comparison to thrombin-activated and untreated platelets. Moreover, the confinement caused a drastic decrease in platelet stiffness and F-actin content for ADP-activated platelets. The influence of confinement on morphology and mechanics was weaker for thrombin-activated or untreated platelets. Taken together, these results suggest that biochemical confinement indeed affects the overall platelet morphology and biomechanics particularly when platelets are being activated with ADP.

Results

Morphology of platelets in confinement depends on activation agonist

We examined the morphology of platelets that were either untreated or activated with ADP or thrombin (Figure 22). Platelets on a substrate fully covered with fibrinogen showed a similar, spread-out morphology regardless of the activation agonist (Figure 22a). Platelets on a patterned fibrinogen substrate had an elongated morphology mostly aligned with the fibrinogen-covered areas when activated with ADP or thrombin (Figure 22b), whereas untreated platelets were mostly spread out regardless of the presence of fibrinogen. Accordingly, both ADP- and thrombin-activated platelets showed a significantly increased ($P = 1.179\times10^{-9}$ for ADP and $P = 3.572\times10^{-5}$ for thrombin) overlap with the fibrinogen-covered areas compared to untreated platelets (Figure 23a). Comparing both activation agonists, the platelet-fibrinogen overlap for ADP-activated platelets was significantly larger ($P = 0.002$) than for thrombin-activated platelets.

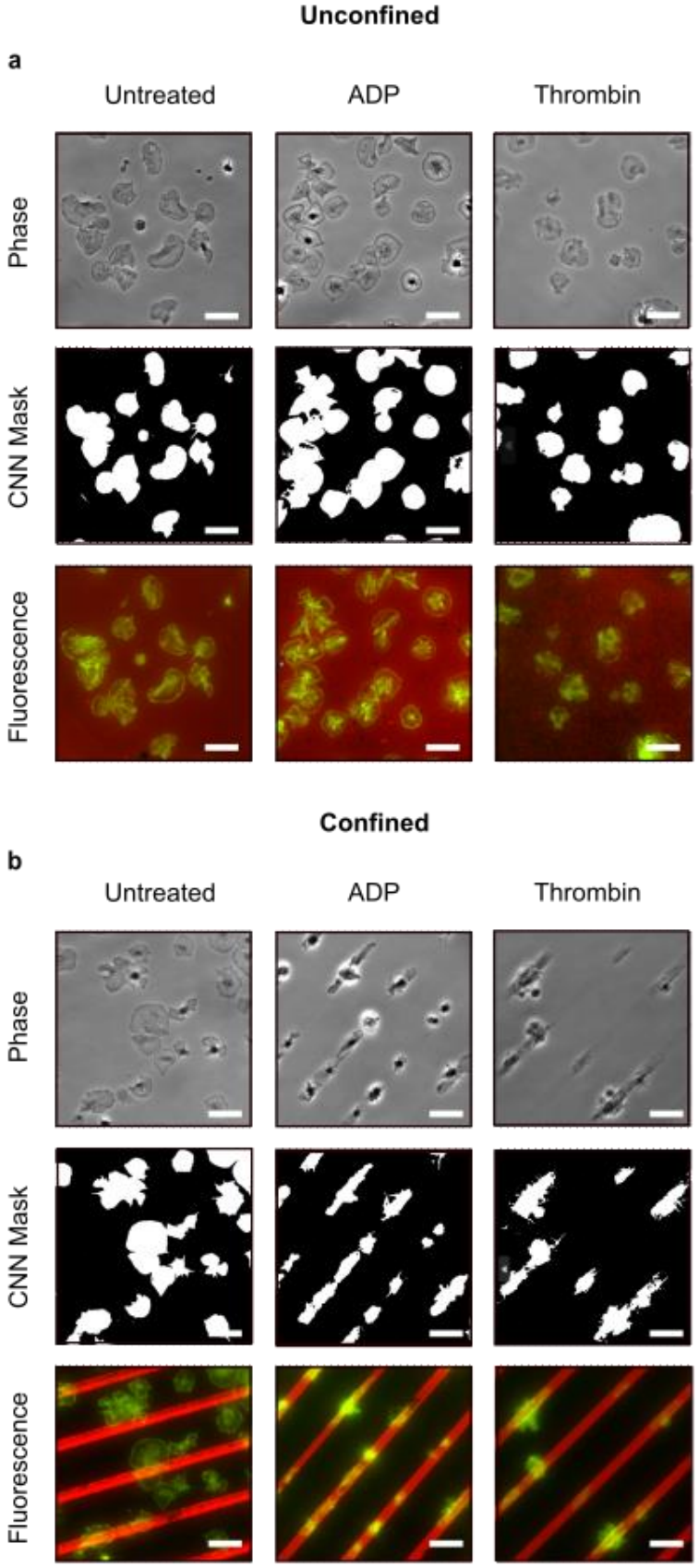
Unconfined
a
Untreated
ADP
Thrombin
Phase
CNN Mask
Fluorescence
Confined
b
Untreated
ADP
Thrombin
Phase
CNN Mask
Fluorescence

Figure 22. Biochemical confinement of platelets activated with different agonists. Phase contrast, CNN mask, and fluorescence images (green: F-actin, red: fibrinogen) of untreated platelets and platelets activated with ADP or thrombin on **(a)** a fully covered fibrinogen substrate and **(b)** on a line-patterned fibrinogen substrate. Scale bars: 10 µm.

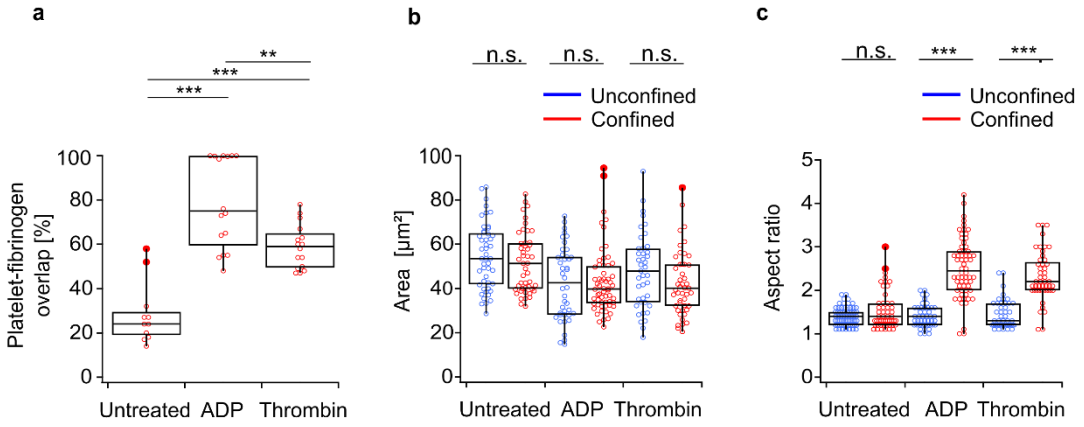

Figure 23. Morphological analysis of platelets in biochemical confinement. **(a)** Platelet-fibrinogen overlap on line-patterned fibrinogen substrates for untreated platelets and platelets activated with ADP or thrombin. Images analyzed: n = 15 containing approximately 750 platelets. **(b)** Area and **(c)** aspect ratio of platelets in unconfined and confined condition. Platelet numbers for each condition and treatment: n ≈ 15 platelets per donor from n=3. The significance level of P values is indicated by asterisks (* $P < 0.05$; ** $P < 0.01$; *** $P < 0.001$; n.s., not significant; Tukey's test).

To further quantify the platelet morphology, we analyzed platelet area and aspect ratio using deep learning platelet morphometry. Platelets on patterned substrates with a low platelet-fibrinogen overlap (<50%) were defined as unconfined and excluded from the analysis. Unconfined platelets had a similar platelet area (38 µm^2) and aspect ratio (0.1) for all activation treatments (P = 0.4 and P = 0.9, respectively). On the other hand, confined platelets showed an increased spreading aspect ratio regardless of the activation treatment (Figure 23b, c). Analogous to the platelet-fibrinogen overlap, the increase in platelet aspect ratio was highest for the ADP-activated platelets (P = 1.117×10^{-12}). This indicates that platelets were most affected by the confinement when they were activated with ADP. Thrombin-activated platelets also showed an increased aspect ratio (P = 3.493×10^{-12})

Biochemical confinement affects volume and mechanical properties of platelets

We investigated the three-dimensional morphology and the mechanics of platelets in confinement by AFM (Figure 24). Using force mapping, we recorded maps of topography and local stiffness (Figure 24a, b) of platelets. Unconfined platelets had a roundish morphology with flat regions at the lamellipodium and higher regions at the centrally located platelet body (Figure 24a, upper row). Stiffness maps of unconfined platelets show softer regions at the platelet body and stiffer regions at the lamellipodium. (Figure 24a, lower row). In contrast, confined platelets had an elongated morphology without a clearly distinguishable lamellipodium and platelet body (Figure 24b, upper row). Accordingly, stiffness maps of confined platelets showed local differences that could not be clearly correlated to a distinct part of the platelet (Figure 24b, lower row).

We analyzed the three-dimensional platelet morphology by calculating the platelet volume and height from the AFM topography images. The maximum height of ADP- and thrombin-activated platelets increased for confined vs. unconfined platelets (Figure 25a), with the largest increase for ADP (from 0.5 µm to 1.3 µm, $P = 1.131\times10^{-10}$). For untreated platelets, height (≈0.5 µm) and volume (≈9 pL) were unaffected by the confinement. Similarly, platelets activated with ADP and thrombin showed an increased volume in confinement (Figure 25b). Again, this increase was stronger for ADP than for thrombin (from ≈8 pL to ≈27 pL, $P = 1.480\times10^{-6}$).

The stiffness of biochemically confined platelets decreased in comparison with unconfined platelets (Figure 25c). The decrease in stiffness was strongest for ADP-activated platelets (from ≈20 kPa to ≈6 kPa, $P = 2.602\times10^{-7}$) and weakest for thrombin-activated platelets ($P = 0.993$). Similarly, the F-actin content (MFI) decreased in confined platelets (Figure 25d), with the strongest decrease for ADP-activated platelets (by approx. 50%, $P = 1.22578\times10^{-11}$). Biochemical confinement revealed an inverse correlation of platelet stiffness and volume for ADP-activated platelets (Figure 25e). For thrombin-activated platelets, the inverse correlation of platelet stiffness and volume was smaller (Figure 25e). For untreated platelets, only stiffness was affected by the confinement (Figure 25e).

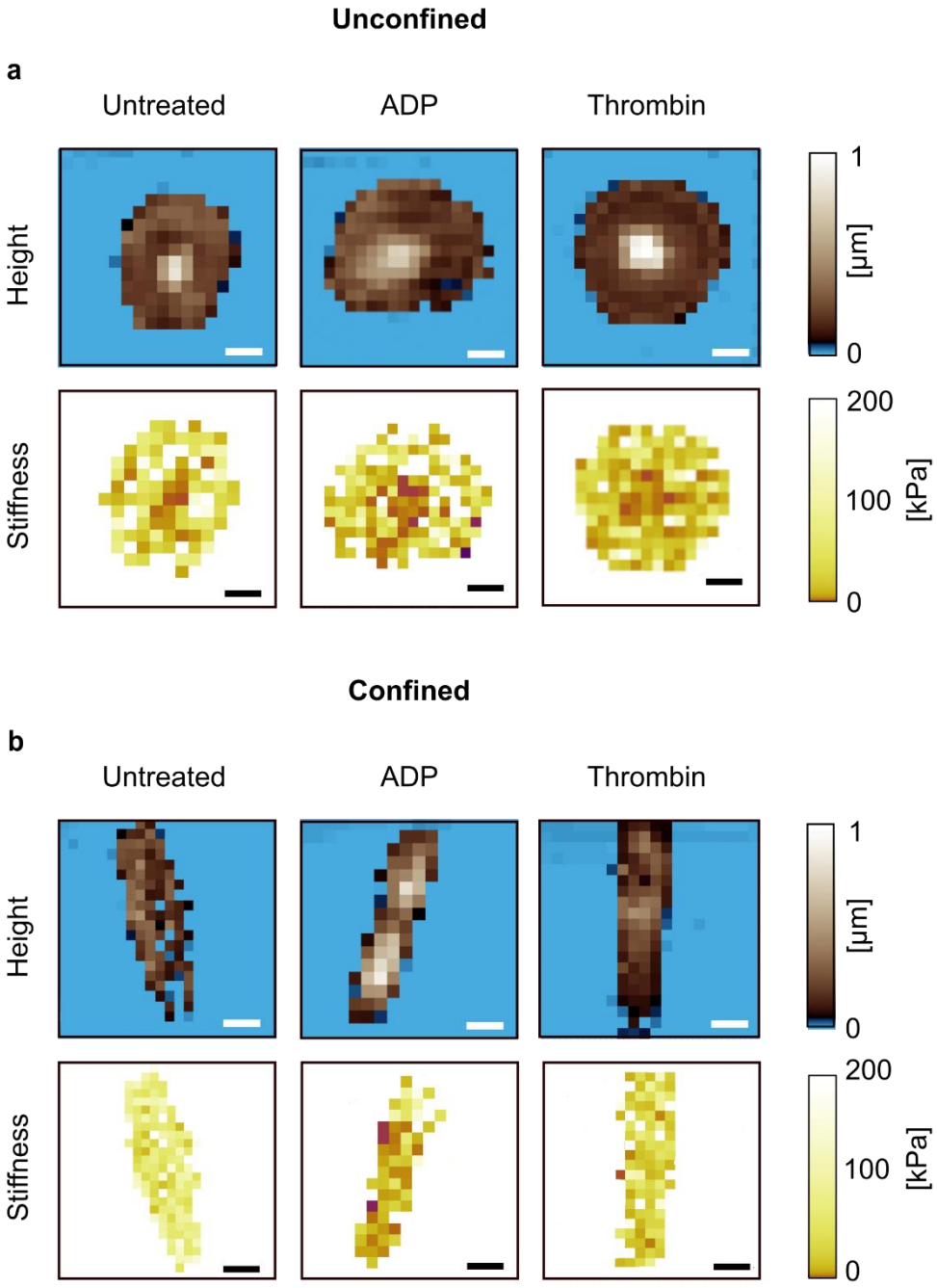

Figure 24. AFM force maps of unconfined and confined platelets. Topography (upper row) and stiffness (lower row) of untreated platelets and of platelets activated with ADP or thrombin **(a)** in unconfined and **(b)** in confined condition. Scale bars: 2 µm. Images were taken by Vincent Gidlund.

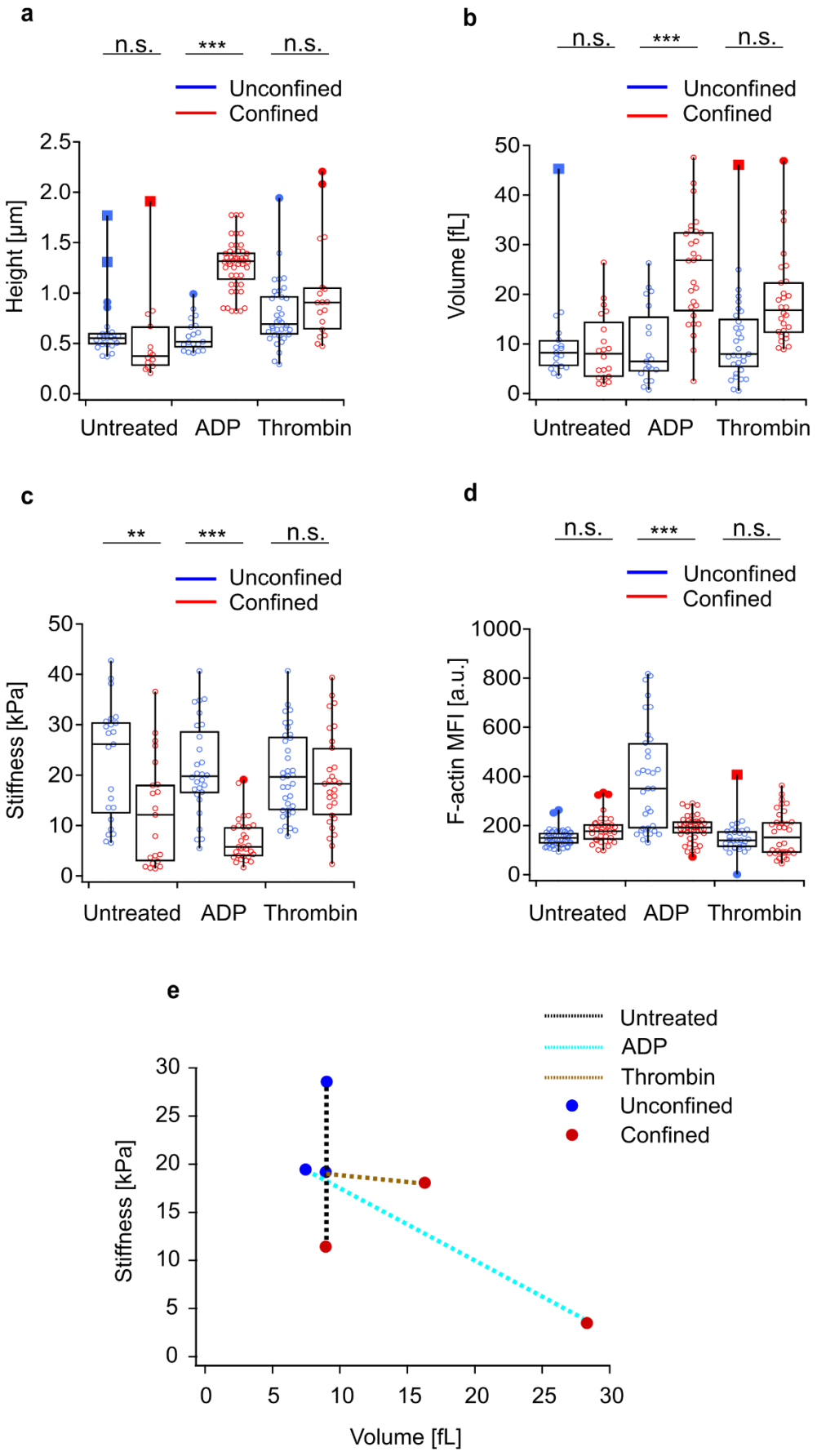
a
n.s.
***
n.s.
Unconfined
Confined
Height [µm]
2.5
2.0
1.5
1.0
0.5
0.0
Untreated
ADP
Thrombin
b
n.s.
***
n.s.
Unconfined
Confined
Volume [fL]
50
40
30
20
10
0
Untreated
ADP
Thrombin
c
**
***
n.s.
Unconfined
Confined
Stiffness [kPa]
50
40
30
20
10
0
Untreated
ADP
Thrombin
d
n.s.
***
n.s.
Unconfined
Confined
F-actin MFI [a.u.]
1000
800
600
400
200
0
Untreated
ADP
Thrombin
e
Untreated
ADP
Thrombin
Unconfined
Confined
Stiffness [kPa]
30
25
20
15
10
5
0
0
5
10
15
20
25
30
Volume [fL]

Figure 25. Platelet volume and mechanics in biochemical confinement. (a) Maximum height, (b) platelet volume, (c) average stiffness (in terms of Young's modulus), and (d) F-actin mean fluorescence intensity (MFI) of unconfined and confined platelets, untreated or activated with ADP or thrombin. (e) Median stiffness vs. median volume (red circles: unconfined; blue circles: confined). The significance level of P values is indicated by asterisks (* $P < 0.05$; ** $P < 0.01$; *** $P < 0.001$; n.s., not significant; Tukey's test). Platelet numbers for each condition and treatment: $n \approx 15$ platelets per donor from $n = 3$ donors. Height, volume, and stiffness data were recorded by Vincent Gidlund.

Discussion

We investigated different aspects of human platelet behavior in a biochemically confining environment. Micro-contact printed fibrinogen lines with a line width that resembles the diameter of blood capillaries provided a substrate for platelets (Figure 22). Previous studies have shown that micro-topography and biochemical confinement influence the spatial distribution of the platelet cytoskeleton (143), platelet spreading (152), and platelet adhesion (153). Using optical microscopy and AFM, we investigated the influence of biochemical confinement on platelet morphology and mechanics dependent on the type of activation agonist (152).

ADP and thrombin specifically activate platelets via P2Y1/P2Y12 and PAR-1/PAR-4 receptors, respectively, leading to platelet shape change and the activation of the fibrinogen-binding integrin $\alpha_{IIb}\beta_3$ (117)(5,144) Agonist-activated platelets had an elongated morphology largely overlapping with the fibrinogen pattern, showing a high platelet-ligand alignment (Figure 22, 23). Additionally, aspect ratio (Figure 23c) and platelet volume (Figure 25c) were significantly increased, and platelet stiffness was significantly decreased by the confinement for ADP-activated platelets. Here, an inverse correlation of volume and stiffness for platelets induced by biochemical confinement was found (Figure 25e). Similar results are known from nucleate cells, where increased cell volume and decreased cell stiffness can be induced by confinement with micropatterned collagen islands (154). In spatially unrestricted cell spreading, water efflux followed by molecular crowding leads to a decrease in cell volume (155)(156)(157). Further, changes in cell volume are associated with contractility in the cytoskeleton and changes in intracellular water content (158). This indicates that the morphological and mechanical alterations in platelets in confinement are caused by spatially limited incomplete spreading.

Biochemical confinement influences the overall spatial cytoskeletal organization in platelets, and actin filaments tend to get distributed on the cell borders (148). Previous studies in U2OS cells have shown that tumor cells are softer in confined spaces (97). Moreover, in renal carcinoma cells (A498) and renal cancer cells derived from a metastatic site at the pleural effusion (ACHN), cellular stiffness and topography were influenced by the cell microenvironment (159). Additionally, cells have been shown to behave more fluid-like after adaptation to a confined space (160) with a reduced F-actin content in the cell interior (160).

Untreated platelets showed a divergent response to biochemical confinement compared to agonist-treated platelets. Unspecific activation of platelets by surface contact and the consequently limited activation of integrins therefore potentially lowers the mechanosensitive capabilities of platelets and the ability to adapt to a ligand-defined pattern. In summary, our study indicates that an *in vitro* system based on µCP for platelets is feasible and allows the investigation of platelet morphology and biomechanics in a more biomimetic environment. Biochemical confinement affected both morphological and mechanical properties of platelets while the strength of the effect depended on the activation agonist. For untreated and thrombin-activated platelets, the effects on morphological and biomechanical parameters were not significant. Only in the presence of ADP a significant effect was observed. This therefore demonstrates that biochemical confinement by µCP can provide further understanding of platelet activation in a physiologically relevant environment.

Acknowledgments

This work was funded by the Deutsche Forschungsgemeinschaft (DFG, German Research Foundation) – Projektnummer 335549539/GRK2381 and Projektnummer 374031971 - TRR 240. Figure 1 was created with BioRender.com.

Informed Consent Statement

Informed consent from all donors was obtained before blood withdrawal.

Author Contribution

Conceptualization: J.R., C.R., T.E.S.; Investigation: J.R., C.R., V.G., J.S.; Resources: T.E.S.; Writing-original: J.R.; Writing – review and editing: J.R., J.S., C.R., V.G., T.E.S.; Visualization: J.R., C.R., J.S., T.E.S.; Supervision: C.R., J.S., T.E.S; Project administration: J.R., T.E.S.; Funding acquisition: T.E.S. All authors have read and agreed to the published version of the manuscript.

Conflict of Interest

The authors declare no conflict of interest.

3.3.1 Conclusions and outlook

The manuscript presented above summarizes the study of the effect of biochemical confinement in platelet activation and mechanics. This type of study with different platelet agonists such as ADP or thrombin, could be also transferred to the effect of confinement in platelets with cGMP-modulating drugs. This will improve the current understanding of platelet biology in confined physiological conditions. From the results obtained, we could conclude that physical space limitation has an impact on platelet morphology and mechanics.

Upon the exposure of activation agonists such as ADP or thrombin, platelet shape changes are induced by cytoskeletal re-organizations (117). Platelet shape changes facilitate platelet adhesion to sites of vascular injury and promote platelet aggregation (5). ADP and thrombin are the most relevant agonists interacting during thrombus formation (5)(99). ADP induces shape change through the activation of Gαi-coupled P2Y1 and P2Y12 receptors and amplifies the effect of thrombin release (161). Thrombin activates protease-activated receptor-1 and -4 (PAR-1 and PAR-4) in platelets, which leads to the release of dense granules, platelet activation, cytoskeleton, and further shape changes (161). Platelet-fibrinogen overlap occasionally reached 100% for ADP-activated platelets (Figure 23a). Glycoprotein GPIIb/IIIa or αIIbβ3 (CD41/CD61) is the main platelet integrin which binds to fibrinogen, fibrin, and von Willebrand factor (vWF) (162). The inside-out signaling of αIIbβ3 on platelets is initiated by ADP, thrombin, or other soluble agonists which triggers the binding of fibrinogen to αIIbβ3 integrin (162).

ADP and thrombin have similar kinetics and affinity to fibrinogen binding by the same class fibrinogen receptors (163). Previous studies suggest that high local concentrations of ADP can support fibrinogen binding and blockage of ADP release by apyrase in thrombin-stimulating platelets inhibits further fibrinogen binding (163). Thrombin induces the release of serotonin-containing dense granules which contain ADP, suggesting the synergistic role of ADP and thrombin in platelets (163). It is not clear the exact mechanistic role why ADP had more affinity for fibrinogen than thrombin in confinement; however, it could be related to the different receptors involved for each case and their expression. Targeting specifically with different antagonists P2Y1,

P2Y12, PAR-1 and PAR-4 are possible approaches to be considered in the future. Then, we know specifically which receptor influences shape change and adaptation to the µCP line shape. The platelet shape is different depending on the spreading stage, and influences platelet adhesion. The study of morphological parameters in platelets is essential to understand platelet function.

Platelet mechanics was one of the focus points in this dissertation. The understanding of cellular stiffness is important in platelet function, and the unique mechanical properties in the cytoskeleton could help in medical diagnosis (34). Inherited platelet disorders (IPDs) are rare diseases where there is an increased tendency to bleed because of alterations in platelet cytoskeleton (35). Previous studies have shown that stiffness is a novel biomarker which helps in the diagnosis of IPDs (35). Stiffness is a unique biomarker of the cytoskeleton which could help in the identification of new cell phenotypes based on their mechanical properties in the future (34). Additionally, as shown previously stiffness also influences platelet shape. When there is an alteration in platelet cytoskeleton, cellular stiffness is also affected (146).

This dissertation can be summarized in two main conclusions. First, the modulation of platelet cytoskeleton and shape through the pharmacological targeting of NO-GC/cGMP signaling pathway decreases platelet hyperreactivity and thrombogenicity. Second, biochemical confinement influences platelet morphology and biomechanics. However, the outcome is dependent on the platelet agonist. The physiological relevance of confinement should be taken in consideration for further experiments and drugs tests in platelets.

4 References

1. Franco AT, Corken A, Ware J. Platelets at the interface of thrombosis, inflammation, and cancer. Blood. 2015;126(5):582–528.
2. Mitchellson WB. *Platelets. 3th ed.* New York: Academic Press (Elsevier); 2014.
3. Thomas SG. The structure of resting and activated platelets. In: Michelson AD, editors. *Platelets. 4th ed.* Academic Press (Elsevier); 2019, p. 47-77.
4. Bearer EL. Cytoskeletal domains in the activated platelet. Cell Motil Cytoskeleton. 1995;30(1):50–66.
5. Koupenova M, Clancy L, Corkrey HA, Freedman JE. Circulating platelets as mediators of immunity, inflammation, and thrombosis. Circ Res. 2018;122(2):337–351.
6. Denis C V., Wagner DD. Platelet adhesion receptors and their ligands in mouse models of thrombosis. Arterioscler Thromb Vasc Biol. 2007;27:728–739.
7. Huo Y, Ley KF. Role of Platelets in the Development of Atherosclerosis. Trends Cardiovasc Med. 2004;14(1):18–22.
8. Smolenski A. Novel roles of cAMP/cGMP-dependent signaling in platelets. Journal of Thrombosis and Haemostasis. 2012;10(2):167–176.
9. Weber C. Platelets and chemokines in atherosclerosis: Partners in crime. Circ Res. 2005;96(6):612–616.
10. Nieswandt B, Varga-Szabo D, Elvers M. Integrins in platelet activation. J Thromb Haemost. 2009;7(Suppl. 1):206–209.
11. Yun SH, Sim EH, Goh RY, Park JI, Han JY. Platelet activation: The mechanisms and potential biomarkers. 2016, BioMed Research International. 2016;9060143.
12. Grüner S, Prostredna M, Schulte V, Krieg T, Eckes B, Brakebusch C, et al. Multiple integrin-ligand interactions synergize in shear-resistant platelet adhesion at sites of arterial injury in vivo. Blood. 2003;102(12):4021–4027.
13. Wen L, Feil S, Feil R. cGMP signaling in platelets. In: Zirlik A, Bode C, Gawaz M, editors. *Platelets, Haemostasis, and Inflammation.* Cham: Springer ; 2017.
14. Murugappan S, Kunapuli SP. The role of ADP receptors in platelet function. Frontiers in Bioscience. 2016;(11):1977-1986.

15. Daniel JL, Dangelmaier C, Jin J, Ashby B, Smith JB, Kunapuli SP. Molecular basis for ADP-induced platelet activation: I. Evidence for three distinct ADP receptors on human platelets. J Biol Chem. 1998;273(4):2024–2029.
16. Hechler B, Gachet C. P2 receptors and platelet function. Purinergic Signal. 2011;7(3):293–303.
17. Foster CJ, Prosser DM, Agans JM, Zhai Y, Smith MD, Zhang F, Gustafson E, Monsma J, Wiekowski M, Abbondanzo S, Cook S, Bayne M, Lira S, Chintala M. Molecular identification and characterization of the platelet ADP receptor targeted by thienopyridine antithrombotic drugs. J Clin Invest. 2001;107(12):1591–1598.
18. Offermanns S. Activation of platelet function through G protein-coupled receptors. Circ Res. 2006;99(12):1293–1304.
19. Jarvis GE, Atkinson BT, Frampton J, Watson SP. Thrombin-induced conversion of fibrinogen to fibrin results in rapid platelet trapping which is not dependent on platelet activation or GPIb. Br J Pharmacol. 2003;138(4):574–583.
20. Kahn ML, Zheng YW, Huang W, Bigornia V, Zeng D, Moff S, Farese RV, Tam C, Coughlin SR. Nature. 1998; 394: 690 – 695.
21. Francis SH, Busch JL, Corbin JD. cGMP-dependent protein kinases and cGMP phosphodiesterases in nitric oxide and cGMP action. Pharmacol Rev. 2010;62(3):525–563.
22. Feil R, Kemp-Harper B. cGMP signalling: From bench to bedside. EMBO Rep. 2006;7(2):149–153.
23. Hofmann F. The cGMP system: Components and function. Biol Chem. 2020;401(4):447–469.
24. Friebe A, Koesling D. Regulation of nitric oxide-sensitive guanylyl cyclase. Circulation Research. 2003;93(2):96–105.
25. Mellion BT, Ignarro LJ, Ohlstein EH, Pontecorvo EG, Hyman AL, Kadowitz PJ. Evidence for the Inhibitory Role of Guanosine 3’, 5’-Monophosphate in ADP-Induced Human Platelet Aggregation in the Presence of Nitric Oxide and Related Vasodilators, Blood. 1981;57(5):946-955.
26. Lincoln TM. Regulation of vascular smooth muscle cell phenotype by cyclic GMP and cyclic GMP-dependent protein kinase. Frontiers in Bioscience. 2006;11(1):356-367.

27. Vu Thao-Vi Dao, Elbatreek MH, FuchB T, Gradler U, Schmidt HHHW, Shah AM, Wallace A. Nitric Oxide Synthase Inhibitors into the Clinic at Last. In: Schnidt HHHW, Ghezzi P, Cuadrado A, editors. *Reactive Oxygen Species*. Cham: Springer ; 2021.
28. Sandner P, Follmann M, Becker-Pelster E, Hahn MG, Meier C, Freitas C, et al. Soluble GC stimulators and activators: Past, present and future. Br J Pharmacol. 2021;1-22
29. Frey R, Becker C, Saleh S, Unger S, van der Mey D, Mück W. Clinical Pharmacokinetic and Pharmacodynamic Profile of Riociguat. Clin Pharmacokinet. 2018;57(6):647–661.
30. Hahn MG, Lampe T, El Sheikh S, Griebenow N, Woltering E, Schlemmer KH, Dietz L, Gerish M, Wunder F, Becker-Pelster EM, Mondritzki T, Tinel H, Knorr A, Kern A, Lang D, Hueser J, Schomber T, Benardeu A, Eitner F, Truebel H, Mittendorf J, Kumar V, van den Akker F, Schaefer M, Geiss V, Sandner P, Stasch JP. Discovery of the Soluble Guanylate Cyclase Activator Runcaciguat (BAY 1101042). J Med Chem. 2021;64(9):5323–5344.
31. Bénardeau A, Kahnert A, Schomber T, Meyer J, Pavkovic M, Kretschmer A, Lawrenz B, Hartmann E, Mathar I, Hueser J, Kraehling JR, Eitner F, Hanh MG, Stasch JP, Sandner P. Runcaciguat, a novel soluble guanylate cyclase activator, shows renoprotection in hypertensive, diabetic, and metabolic preclinical models of chronic kidney disease. Naunyn Schmiedebergs Arch Pharmacol. 2021;394(12):2363–2379.
32. Németh BT, Mátyás C, Oláh A, Lux Á, Hidi L, Ruppert M, Kellermayer D, Kokeny G, Szabo G, Merkely B, Radovits T. Cinaciguat prevents the development of pathologic hypertrophy in a rat model of left ventricular pressure overload. Sci Rep. 2016;6:1–12.
33. Wen L, Feil S, Wolters M, Thunemann M, Regler F, Schmidt K, Friebe A, Olbrich M, Langer H, Gawaz M, de Wit C, Feil R. A shear-dependent NO-cGMP-cGKI cascade in platelets acts as an auto-regulatory brake of thrombosis. Nat Commun. 2018; 9(1): 1–11.

34. Mietke A, Otto O, Girardo S, Rosendahl P, Taubenberger A, Golfier S, Ulbricht E, Aland S, Guck J, Fischer-Friedrich E. Extracting Cell Stiffness from Real-Time Deformability Cytometry: Theory and Experiment. Biophys J. 2015;109(10):2023–2036.
35. Zaninetti C, Sachs L, Palankar R. Role of Platelet Cytoskeleton in Platelet Biomechanics: Current and Emerging Methodologies and Their Potential Relevance for the Investigation of Inherited Platelet Disorders. Hamostaseologie. 2020;40(3):337–347.
36. González-Bermúdez B, Guinea G V., Plaza GR. Advances in Micropipette Aspiration: Applications in Cell Biomechanics, Models, and Extended Studies. Biophys J. 2019;116(4):587–594.
37. Sachs L, Wesche J, Lenkeit L, Greinacher A, Bender M, Otto O, Palankar R. Ex vivo anticoagulants affect human blood platelet biomechanics with implications for high-throughput functional mechanophenotyping. Commun Biol. 2022;5(1):1-14.
38. Ando T. Directly watching biomolecules in action by high-speed atomic force microscopy. Biophys Rev. 2017;9(4):421–429.
39. Schäffer TE. Nanomechanics of molecules and living cells with scanning ion conductance microscopy. Anal Chem. 2013;85(15):6988–6994.
40. Seifert J, Rheinlaender J, Novak P, Korchev YE, Schäffer TE. Comparison of Atomic Force Microscopy and Scanning Ion Conductance Microscopy for Live Cell Imaging. Langmuir. 2015;31(24):6807–6813.
41. Rheinlaender J, Seifert J, Schächtele M, Schäffer TE, Vogel S, Borst O, et al. Imaging the elastic modulus of human platelets during thrombininduced activation using scanning ion conductance microscopy. Thromb Haemost. 2015;113(2):305–311.
42. Rheinlaender J, Schäffer TE. Mapping the mechanical stiffness of live cells with the scanning ion conductance microscope. Soft Matter. 2013;9(12):3230–3236.
43. Seifert J, Rheinlaender J, von Eysmondt H, Schäffer TE. Mechanics of migrating platelets investigated with scanning ion conductance microscopy. Nanoscale. 2022;14(22):8192–8199.

44. Qiu Y, Ciciliano J, Myers DR, Tran R, Lam WA. Platelets and physics: How platelets “feel” and respond to their mechanical microenvironment. Blood Rev.29(6):377–386.
45. Cerecedo D. Platelet cytoskeleton and its hemostatic role. Blood Coagulation and Fibrinolysis. 2013;24(8):798–808.
46. Reinhard M, Jarchau T, Walter U. Actin-based motility: Stop and go with Ena/VASP proteins. Trends Biochem Sci. 2001;26(4):243–249.
47. Aszódi A, Pfeifer A, Ahmad M, Glauner M, Zhou XH, Ny L, Anderson KE, Kehrel B, Offermanns S, Fassler R. The vasodilator-stimulated phosphoprotein (VASP) is involved in cGMP- and cAMP-mediated inhibition of agonist-induced platelet aggregation, but is dispensable for smooth muscle function. EMBO Journal. 1999;18(1):37–48.
48. Hauser W, Knobeloch KP, Eigenthaler M, Gambaryan S, Krenn V, Geiger JJ, Glazova M, Rohde E, Horak I, Walter U. Megakaryocyte hyperplasia and enhanced agonist-induced platelet activation in vasodilator-stimulated phosphoprotein knockout mice Proc Natl Acad Sci USA.1999;96:8120-8125.
49. Trichet L, Campàs O, Sykes C, Plastino J. VASP governs actin dynamics by modulating filament anchoring. Biophys J. 2007;92(3):1081–1089.
50. Bailly M, Ichetovkin I, Grant W, Zebda N, Machesky LM, Segall JE, Condeelis J. The F-actin side binding activity of the Arp2/3 complex is essential for actin nucleation and lamellipod extension. Brief Communication. 2001;11:620-625.
51. Butt E, Abel K, Krieger M, Palm D, Hoppe V, Hoppe J, Walter U. cAMP- and cGMP-dependent protein kinase phosphorylation sites of the focal adhesion vasodilator-stimulated phosphoprotein (VASP) in vitro and in intact human platelets. J Biol Chem;269(20):14509–14517.
52. Massberg S, Sausbier M, Klatt P, Bauer M, Pfeifer A, Siess W, Fassler R, Ruth P, Krombach F, Hofmann F. Increased adhesion and aggregation of platelets lacking cyclic guanosine 3’,5’-monophosphate kinase I. J Exp Med. 1999;189(8):1255–1263.
53. Bachmann C, Fischer L, Walter U, Reinhard M. The EVH2 domain of the vasodilator-stimulated phosphoprotein mediates tetramerization, F-actin binding, and actin bundle formation. J Biol Chem. 1999;274(33):23549–23557.

54. Gries A, Bode C, Peter K, Herr A, Böhrer H, Motsch J, Martin E. Inhaled Nitric Oxide Inhibits Human Platelet Aggregation, P-Selectin Expression, and Fibrinogen Binding In Vitro and In Vivo. Circulation.1998;97:1481-1487.
55. Antl M, von Brü hl ML, Eiglsperger C, Werner M, Konrad I, Kocher T, Kocher T, Wilm M, Hoffman F, Massberg S, Scholossmann J. IRAG mediates NO/cGMP-dependent inhibition of platelet aggregation and thrombus formation. Blood. 2007; 109(2): 552-559.
56. Verderame M, Alcorta D, Egnor M, Smith K, Pollack R. Cytoskeletal F-actin patterns quantitated with fluorescein isothiocyanate-phalloidin in normal and transformed cells. Proc Natl Acad Sci USA. 1980;77(11):6624-6628.
57. Gambaryan S. The Role of NO/sGC/cGMP/PKG Signaling Pathway in Regulation of Platelet Function. Cells. 2022;11(22),3704.
58. Li Z, Xi X, Gu M, Feil R, Ye RD, Eigenthaler M, Hoffmann F, Du X. A Stimulatory Role for cGMP-Dependent Protein Kinase in Platelet Activation brand disease in which a genetic deficiency in GPIb-IX or vWF, respectively, causes defects in platelet adhe-sion and activation and results in bleeding disord. Cell. 2003;112,77-86.
59. Bender M, Palankar R. Platelet Shape Changes during Thrombus Formation: Role of Actin-Based Protrusions. Hamostaseologie. 2021;41(1):14–21.
60. Ahrens I, Bode · C, Peter · K. Inhibition of Platelet Activation and Aggregation. HEP. Springer-Verlag. 2005;170:443-462.
61. Schwarz UR, Walter U, Eigenthaler M. Taming platelets with cyclic nucleotides. Biochem Pharm. 2001;62:1153-1161.
62. Moskalensky AE, Litvinenko AL. The platelet shape change: biophysical basis and physiological consequences. Platelets. 2019;30(5):543-548.
63. Aburima A, Walladbegi K, Wake JD, Naseem KM. cGMP signaling inhibits platelet shape change through regulation of the RhoA-Rho Kinase-MLC phosphatase signaling pathway. Journal of Thrombosis and Haemostasis. 2017;15(8):1668–1678.
64. Seifert J, von Eysmondt H, Chatterjee M, Gawaz M, Schäffer TE. Effect of oxidized LDL on platelet shape, spreading, and migration investigated with deep learning platelet morphometry. Cells. 2021;10(11):2932.

65. Taylor KA, Smyth E, Rauzi F, Cerrone M, Khawaja AA, Gazzard B, Nelson M, Boffito M, Emerson M. Pharmacological impact of antiretroviral therapy on platelet function to investigate human immunodeficiency virus-associated cardiovascular risk. Br J Pharmacol. 2019;176(7):879–889.
66. Mcgowan JP, Fine SM, Vail R, Merrick ST, Radix A, Hoffmann CJ, et al. Selecting an Initial ART Regimen Guideline Information. 2022.
67. Tien P, Lazar J. Antiretroviral Drugs and the Risk of Myocardial Infarction. N Engl J Med. 2022;357(7):715-717.
68. Sabin CA, Worm SW, Weber R, Reiss P, El-Sadr W, Dabis F, et al. Use of nucleoside reverse transcriptase inhibitors and risk of myocardial infarction in HIV-infected patients enrolled in the D:A:D study: A multi-cohort collaboration. The Lancet. 2008;371(9622):1417–1426.
69. de Wit S, Sabin CA, Weber R, Worm SW, Reiss P, Cazanave C, El-Sadr W, Monforte A, Fontas E, Law MG, Moller NF, Phillips A. Incidence and risk factors for new-onset diabetes in HIV-infected patients. Diabetes Care. 2008;31(6):1224–1229.
70. Sax PE, Wohl D, Yin MT, Post F, DeJesus E, Saag M, et al. Tenofovir alafenamide versus tenofovir disoproxil fumarate, coformulated with elvitegravir, cobicistat, and emtricitabine, for initial treatment of HIV-1 infection: Two randomised, double-blind, phase 3, non-inferiority trials. The Lancet. 2015;385(9987):2606–2615.
71. Yager JL, Anderson PL. Pharmacology and drug interactions with HIV PrEP in transgender persons receiving gender affirming hormone therapy. Expert Opinion on Drug Metabolism and Toxicology. 2020;16(6):463-474.
72. Baum PD, Sullam PM, Stoddart CA, McCune JM. Abacavir increases platelet reactivity via competitive inhibition of soluble guanylyl cyclase. AIDS. 2011;25(18):2243–2248.
73. Choi AI, Vittinghoff E, Deeks SG, Weekley CC, Li Y, Shlipak MG. Cardiovascular risks associated with abacavir and tenofovir exposure in HIV-infected persons. AIDS. 2011;25(10):1289–1298.

74. Collado-Díaz V, Martinez-Cuesta MÁ, Blanch-Ruiz MA, Sánchez-López A, García-Martínez P, Peris JE, et al. Abacavir Increases Purinergic P2X7 Receptor Activation by ATP: Does a Pro-inflammatory Synergism Underlie Its Cardiovascular Toxicity? Front Pharmacol. 2021;12:613449.
75. Satchell CS, Cotter AG, O'Connor EF, Peace AJ, Tedesco AF, Clare A, et al. Platelet function and HIV: A case-control study. AIDS. 2010;24(5):649–657.
76. Moore C, Sanz-Rosa D, Emerson M. Distinct role and location of the endothelial isoform of nitric oxide synthase in regulating platelet aggregation in males and females in vivo. Eur J Pharmacol. 2011;651(1–3):152–158.
77. Apostoli GL, Solomon A, Smallwood MJ, Winyard PG, Emerson M. Role of inorganic nitrate and nitrite in driving nitric oxide-cGMP-mediated inhibition of platelet aggregation in vitro and in vivo. Journal of Thrombosis and Haemostasis. 2014;12(11):1880–1889.
78. Alvarez A, Orden S, Andújar I, Collado-Diaz V, Núñez-Delgado S, Galindo MJ, Estrada V, Apostolova N, Esplugues JV. Cardiovascular toxicity of abacavir: A clinical controversy in need of a pharmacological explanation. AIDS. 2017;31(13):1781–1795.
79. Wang X, Chai H, Lin PH, Yao Q, Chen C. Roles and mechanisms of human immunodeficiency virus protease inhibitor ritonavir and other anti-human immunodeficiency virus drugs in endothelial dysfunction of porcine pulmonary arteries and human pulmonary artery endothelial cells. American J Path. 2009;174(3):771–781.
80. Muñoz RP, González-Correa JA, Ruiz J, Nuño E, Márquez M, de la Cruz JP, Santos Jesus. Whole blood platelet aggregometry in HIV-infected patients on treatment with abacavir. Open J Intern Med. 2012;02(02):62–66.
81. Esplugues JV, De Pablo C, Collado-Diaz V, Hernandez C, Orden S, Alvarez A. Interference with purinergic signallig: an explanation for the cardiovascular effect of abacavir? AIDS. 2016;30:1341-1351.
82. Kilkenny C, Browne WJ, Cuthill IC, Emerson M, Altman DG. Improving bioscience research reporting: The arrive guidelines for reporting animal research. PLoS Biol. 2010;8(6).e1000412.

83. Rukoyatkina N, Walter U, Friebe A, Gambaryan S. Differentiation of cGMP-dependent and -independent nitric oxide effects on platelet apoptosis and reactive oxygen species production using platelets lacking soluble guanylyl cyclase. Thromb Haemost. 2011; 106(5): 922–933.
84. Tiedt R, Schomber T, Hao-Shen H, Skoda RC. Pf4-Cre transgenic mice allow the generation of lineage-restricted gene knockouts for studying megakaryocyte and platelet function in vivo. Blood. 2007; 109(4): 1503–1506.
85. Friebe A, Mergia E, Dangel O, Lange A, Koesling D, Beavo JA. Fatal gastrointestinal obstruction and hypertension in mice lacking nitric oxide-sensitive guanylyl cyclase. PNAS. 2007; 104(18): 7699–7704.
86. Shakes DC, Miller DM, Nonet ML. Immunofluorescence Microscopy. In: Methods in Cell Biology. Academic Press Inc.; 2012. p. 35–66.
87. Rheinlaender J, Geisse NA, Proksch R, Schäffer TE. Comparison of scanning ion conductance microscopy with atomic force microscopy for cell imaging. Langmuir. 2011;27(2):697–704.
88. Rheinlaender J, Schäffer TE. Mapping the mechanical stiffness of live cell with the scanning ion conductance microscopy. Soft Matter. 2013; 9(12): 561–574.
89. Rheinlaender J, Schäffer TE. The effect of finite sample thickness in scanning ion conductance microscopy stiffness measurements. Appl Phys Lett. 2020;117(11):113701-113711.
90. von Eysmondt H, Schäffer TE. Scanning Ion Conductance Microscopy and Atomic Force Microscopy: A Comparison of Strengths and Limitations for Biological Investigations. In: *Bioanalytical Reviews.* Springer Science and Business Media Deutschland GmbH; 2022. p. 23–71.
91. Alessandrini A, Facci P. AFM: A versatile tool in biophysics. Meas Sci Technol. 2005;16(6):65–92.
92. Cook SM, Schäffer TE, Chynoweth KM, Wigton M, Simmonds RW, Lang KM. Practical implementation of dynamic methods for measuring atomic force microscope cantilever spring constants. Nanotechnology. 2006;17(9):2135–2145.
93. Hertz H (1882) Uber die Beruhrung fester elastischer Korper. J Reine Angew Math 92:156-171.

94. Gwozdz T, Dorey K. Western Blot. In: *Basic Science Methods for Clinical Researchers.* Elsevier Inc, Cham.; 2017. p. 99–117.
95. Khawaja AA, Taylor KA, Lovell AO, Nelson M, Gazzard B, Boffito M, et al. HIV Antivirals Affect Endothelial Activation and Endothelial-Platelet Crosstalk. Circ Res. 2020 Nov 6;127(11):1365–1380.
96. Frontroth JP. Light transmission aggregometry. Met Mol Biol. 2013;992:227–240.
97. Rianna C, Radmacher M, Kumar S. Direct evidence that tumor cells soften when navigating confined spaces. Mol Biol Cell. 2020;31(16):1726–1734.
98. Cooper JN, Evans RW, Mori Brooks M, Fried L, Holmes C, Barinas-Mitchell E, Sutton-Tyrrel,K. Associations between arterial stiffness and platelet activation in normotensive overweight and obese young adults. Clin Exp Hypertens. 2014;36(3):115–122.
99. Aslan JE. Platelet Proteomes, Pathways, and Phenotypes as Informants of Vascular Wellness and Disease. Arterioscler Thromb Vasc Biol. 2021;41:999–1011.
100. Sachs L, Wesche J, Lenkeit L, Greinacher A, Bender M, Otto O, Palankar RI. Ex-vivo anticoagulants affect the mechanical properties of human blood platelets with implications for in vitro functional mechanophenotyping. Commun Biol. 2022; 5(86):1-20.
101. Qiu Y, Brown AC, Myers DR, Sakurai Y, Mannino RG, Tran R, Ahn B, Hardy ET, Kee MF, Kumar S, Bao G, Barker TH, Lam WA. Platelet mechanosensing of substrate stiffness during clot formation mediates adhesion, spreading, and activation. Proc Natl Acad Sci USA. 2014; 111(40): 14430–14435.
102. Pan J, Zhong F, Tan X. Soluble guanylate cyclase in NO signaling transduction. Rev Inorg Chem. 2013; 33(4): 193–206.
103. Dangel O, Mergia E, Karlisch K, Groneberg D, Koesling D, Friebe A. Nitric oxide-sensitive guanylyl cyclase is the only nitric oxide receptor mediating platelet inhibition. J Thromb Haemost. 2010; 8: 1343–1352.
104. Denninger JW, Marletta MA. Guanylate cyclase and the .NO/cGMP signaling pathway. Biochim Biophys Acta Bioenerg. 1999;1411(2–3):334–350.

105. Emerson M, Momi S, Paul W, Alberti F. Endogenous nitric oxide acts as a natural antithrombotic agent in vivo by inhibiting platelet aggregation in the pulmonary vasculature. Thromb Haemost. 1999; 81(6): 961-966.
106. Schmidt H, Schmidt PM, Stasch JP. NO- and haem-independent soluble guanylate cyclase activators. In: Schmidt H, Hofmann F, Stasch JP, editors. *cGMP: Generators, Effectors and Therapeutic Implications.* Springer; 2009, p. 309–339.
107. Stasch JP, Schlossmann J, Hocher B. Renal effects of soluble guanylate cyclase stimulators and activators: A review of the preclinical evidence. Curr Opin Pharmacol. 2015; 21: 95–104.
108. Reiss C, Mindukshev I, Bischoff V, Subramanian H, Kehrer L, Friebe A, Stasch JP, Gambaryan S, Walter U. The sGC stimulator riociguat inhibits platelet function in washed platelets but not in whole blood. Br J Pharmacol. 2015; 172(21): 5199–5210.
109. Baumann J, Sachs L, Otto O, Schoen I, Nestler P, Zaninetti C, Kenny M, Kranz R, von Eysmondt H, Rodriguez J, Schäffer TE, Nagy Z, Greinacher A, Palankar R, Bender M. Reduced platelet forces underlie impaired hemostasis in mouse models of MYH9-related disease. Sci Adv. 2022; 8(20): eabn2627.
110. Taylor KA, Smyth E, Rauzi F, Cerrone M, Khawaja AA, Gazzard B, Nelson M, Boffito M, Emerson M. Pharmacological impact of antiretroviral therapy on platelet function to investigate human immunodeficiency virus-associated cardiovascular risk. Br J Pharmacol. 2019; 176(7): 879–889.
111. Li Z, Zhang G, Marjanovic JA, Ruan C, Du X. A platelet secretion pathway mediated by cGMP-dependent protein kinase. J Biol Chem. 2004; 279(41): 42469 – 42475.
112. Libersan D, Rousseau G, Merhi Y. Differential regulation of P-selectin expression by protein kinase A and protein kinase G in thrombin-stimulated human platelets. Thromb Haemost. 2003; 89(2): 310–317.
113. Oelze M, Mollnau H, Hoffmann N, Warnholtz A, Bodenschatz M, Smolenski A, Walter U, Skatchkov M, Meinertz T, Münzel T. Vasodilator-stimulated phosphoprotein serine 239 phosphorylation as a sensitive monitor of defective nitric oxide/cGMP signaling and endothelial dysfunction. Circ Res. 2000; 87(11): 999–1005.

114. Bearer EL, Prakash JM, Li Z. Actin dynamics in platelets. Int Rev Cytol 2002; 217: 137–182.
115. Horstrup K, Jablonka B, Hönig-Liedl P, Just M, Kochsiek K, Walter U. Phosphorylation of Focal Adhesion Vasodilator-Stimulated Phosphoprotein at Ser157 in Intact Human Platelets Correlates with Fibrinogen Receptor Inhibition. Eur J Biochem. 1994; 225(1): 21–27.
116. Yun SH, Sim EH, Goh RY, Park JI, Han JY. Platelet activation: The mechanisms and potential biomarkers. Biomed Res Int. 2016; 2016: 906143.
117. Shin EK, Park H, Noh JY, Lim KM, Chung JH. Platelet shape changes and cytoskeleton dynamics as novel therapeutic targets for anti-thrombotic drugs. Biomol Ther. 2017; 25(3): 223–230.
118. Pike JA, Simms VA, Smith CW, Morgan N V., Khan AO, Poulter NS, Styles IB, Thomas SG. An adaptable analysis workflow for characterization of platelet spreading and morphology. Platelets. 2021; 32(1): 54–58.
119. Feil R, Lohmann SM, de Jonge H, Walter U, Hofmann F. Cyclic GMP-Dependent Protein Kinases and the Cardiovascular System. Circ Res. 2003; 93(10): 907–916.
120. Smolenski A. Novel roles of cAMP/cGMP-dependent signaling in platelets. J Thromb Haemost. 2012; 10(2): 167–176.
121. Gresele P, Momi S, Falcinelli E. Anti-platelet therapy: Phosphodiesterase inhibitors. Br J Clin Pharmacol. 2011; 72(4): 634–646.
122. Yamasaki F, Furuno T, Sato K, Zhang D, Nishinaga M, Sato T, Doi Y, Sugiura T. Association between arterial stiffness and platelet activation. J Hum Hypertens. 2005; 19(7): 527–533.
123. Lyle AN, Raaz U. Killing me un-softly: Causes and mechanisms of arterial stiffness Recent Highlights of ATVB: Early Career Committee Contribution. Arterioscler Thromb Vasc Biol. 2018; 37(2): e1-e11.
124. Kempster C, Butler G, Kuznecova E, Taylor KA, Kriek N, Little G, Sowa MA, Sage T, Johnson LJ, Gibbins JM, Pollit AY Fully automated platelet differential interference contrast image analysis via deep learning. Sci Rep. 2022;12(1):4614.

125. Pike JA, Simms VA, Smith CW, Morgan N V., Khan AO, Poulter NS, Styles IB, Thomas SG. An adaptable analysis workflow for characterization of platelet spreading and morphology. Platelets. 2021;32(1):54–58.
126. Khan AO, Maclachlan A, Lowe GC, Nicolson PL, Ghaithi AI, Thomas SG, Watson SP, Pike JA, Morgan NV, Group UGS. High-throughput platelet spreading analisis: a tool for the diagnosis of platelet-based bleeding disorders. Haematologica. 2020;105(3):e124-e128.
127. Park IL, H&o FW, Park H. Morphological characterization of surface-induced platelet activation. Biomaterials. 1990;11:24-31
128. Hiratsuka T, Sano T, Kato H, Komatsu N, Imajo M, Kamioka Y, et al. Live imaging of extracellular signal-regulated kinase and protein kinase A activities during thrombus formation in mice expressing biosensors based on Förster resonance energy transfer. Journal of Thrombosis and Haemostasis. 2017;15(7):1487–1499.
129. Morgan N High-throughput platelet spreading analysis: a tool for the diagnosis of platelet-based bleeding disorders. Haematologica. 2020;105:e127.
130. Seifert J, Rheinlaender J, Lang F, Gawaz M, Schäffer TE. Thrombin-induced cytoskeleton dynamics in spread human platelets observed with fast scanning ion conductance microscopy. Sci Rep. 2017;7(1):1–11.
131. Calaminus SDJ, Thomas S, McCarty OJT, Machesky LM, Watson SP. Identification of a novel, actin-rich structure, the actin nodule, in the early stages of platelet spreading. J Thromb Haemost. 2008;6(11):1944–1952.
132. Preston RA, Jy W, Jimenez JJ, Mauro LM, Horstman LL, Valle M, Aime G, Ahn YS. Effects of severe hypertension on endothelial and platelet microparticles. Hypertension. 2003;41(2):211–217.
133. Leroyer AS, Anfosso F, Lacroix R, Sabatier F, Simoncini S, Njock SM, Jourde N, Brunet P, Camoin-Jau L, Sampol J, Dignat-George F. Endothelial-derived microparticles: Biological conveyors at the crossroad of inflammation, thrombosis and angiogenesis. Throm Haemost. 2010;104(3):456-463.
134. Alvarez A, Rios-Navarro C, Blanch-Ruiz MA, Collado-Diaz V, Andujar I, Martinez-Cuesta MA, Orden S, Esplugues JV. Abacavir induces platelet-endothelium interactions by interfering with purinergic signalling: A step from inflammation to thrombosis. Antiviral Res. 2017;141:179–185.

135. Van Velzen JF, Laros-Van Gorkom BAP, Pop GAM, Van Heerde WL. Multicolor flow cytometry for evaluation of platelet surface antigens and activation markers. Thromb Res. 2012;130(1):92–98.
136. Isenberg JS, Ridnour LA, Thomas DD, Wink DA, Roberts DD, Espey MG. Guanylyl cyclase-dependent chemotaxis of endothelial cells in response to nitric oxide gradients. Free Radic Biol Med. 2006;40(6):1028–1033.
137. Moskalensky AE, Litvinenko AL. The platelet shape change: biophysical basis and physiological consequences. Platelets. 2019;30(5):543-548.
138. Nascimento FG, Tanaka PY. Thrombocytopenia in HIV-infected patients. Indian Journal of Hematology and Blood Transfusion. 2012;28(2):109–111.
139. Comi L, Maggiolo F. Abacavir + dolutegravir + lamivudine for the treatment of HIV. Expert Opin Pharmacother. 2016;17(15):2097–2106.
140. Woolley R, Prendergast Ú, Jose B, Kenny D, McDonagh C. A rapid, topographical platelet activation assay. Analyst. 2013;138(16):4512–4518.
141. Gaertner F, Ahmad Z, Rosenberger G, Fan S, Nicolai L, Busch B, Yavuz G, Luckner M, Ishikawa-Ankerhold H, Hennel R, Benechet A, Lorenz M, Chandraratne S, Schubert I, Helmer S, Striednig B, Stark K, Janko M, Bottcher RT, Verschoor A, Leon C, Gudermann T, Mederos y Schnitzler M, Pincus Z, Iaannacone M, Hass R, Wanner G, Lauber K, Sixt M, Massberg S. Migrating Platelets Are Mechano-scavengers that Collect and Bundle Bacteria. Cell. 2017;171(6):1368-1382.
142. Gibbins JM. Platelet adhesion signalling and the regulation of thrombus formation. J Cell Sci. 2004;117(16):3415–3425.
143. Kita A, Sakurai Y, Myers DR, Rounsevell R, Huang JN, Seok TJ, Yu K, Wu MC, Fletcher D, Lam WA. Microenvironmental geometry guides platelet adhesion and spreading: A quantitative analysis at the single cell level. PLoS One. 2011;6(10):e26437.
144. Bender M, Palankar R. Platelet Shape Changes during Thrombus Formation: Role of Actin-Based Protrusions. Hamostaseologie. 2021;41(1):14–21.
145. Kaiser R, Anjun A, Kammerer LM, Akhalkatsi A, Rossaro D, Escaig R, Droste Zu Senden A, Raude B, Lorenz M, Gold C, Pekayvaz K, Brocker T, Kranich J, Holch JW, Spiekermann K, Massberg S, Gaertner F, Nicolai L. Mechanosensing via a GpIIb/Src/14-3-3ζ axis critically regulates platelet migration in vascular inflammation. Blood. 2023;blood.2022019210.

146. Sachs L, Denker C, Greinacher A, Palankar R. Quantifying single-platelet biomechanics: An outsider's guide to biophysical methods and recent advances. Res Pract Thromb Haemost. 2020;4:386-401.
147. Pathak A, Kumar S, Discher DE. Independent regulation of tumor cell migration by matrix stiffness and confinement. PNAS. 2012;109(26):10334-10339.
148. Doolin MT, Moriarty RA, Stroka KM. Mechanosensing of Mechanical Confinement by Mesenchymal-Like Cells. Front Physiol. 2020;11:1–19.
149. Mosier JA, Rahman-Zaman A, Zanotelli MR, VanderBurgh JA, Bordeleau F, Hoffman BD, et al. Extent of Cell Confinement in Microtracks Affects Speed and Results in Differential Matrix Strains. Biophys J. 2019;117(9):1692–1701.
150. Chiu DT, Li Jeon N, Huang S, Kane RS, Wargo CJ, Choi IS, et al. Patterned deposition of cells and proteins onto surfaces by using three-dimensional microfluidic systems PNAS. 2000;97(6):2408-2413
151. Wiedeman MP. Dimensions of Blood Vessels from Distributing Artery to Collecting Vein. Circulation Research. 1962;7:375-378.
152. Sandmann R, Henriques SSG, Rehfeldt F, Köster S. Micro-topography influences blood platelet spreading. Soft Matter. 2014;10(14):2365–2371.
153. Koh LB, Rodriguez I, Venkatraman SS. The effect of topography of polymer surfaces on platelet adhesion. Biomaterials. 2010;31(7):1533–1545
154. Guo M, Pegoraro AF, Mao A, Zhou EH, Arany PR, Han Y, et al. Cell volume change through water efflux impacts cell stiffness and stem cell fate. Proc Natl Acad Sci U S A. 2017;114(41):E8618–27.
155. Minton AP. The Influence of Macromolecular Crowding and Macromolecular Confinement on Biochemical Reactions in Physiological Media. J Biol Chem. 2001;276(14):10577–10580.
156. Watkins S, Sontheimer H. Hydrodynamic cellular volume changes enable glioma cell invasion. Journal of Neuroscience. 2011;31(47):17250–17259.
157. Habela CW, Ernest NJ, Swindall AF, Sontheimer H. Chloride accumulation drives volume dynamics underlying cell proliferation and migration. J Neurophysiol. 2009;101(2):750–757.
158. Wiggins P, Phillips R. Membrane-protein interactions in mechanosensitive channels. Biophys J. 2005;88(2):880–902.

159. Rianna C, Radmacher M. Influence of microenvironment topography and stiffness on the mechanics and motility of normal and cancer renal cells. Nanoscale. 2017;9(31):11222–11230.
160. Balzer EM, Tong Z, Paul CD, Hung WC, Stroka KM, Boggs AE, et al. Physical confinement alters tumor cell adhesion and migration phenotypes. FASEB J. 2012;26(10):4045–4056.
161. Jiang L, Xu C, Yu S, Liu P, Luo D, Zhou Q, Gao C, Hu H. critical role of thrombin/PAR-1 in ADP-induced platelet secretion and the second wave of aggregation. J Thromb Haemost. 2013;11(5):930–940.
162. Huang J, Li X, Shi X, Zhu M, Wang J, Huang S, Huang X, Wang H, Li L, Deng H, Zhou Y, Mao J, Long Z, Ma Z, Ye W, Pan J, Xi X, Jin J. Platelet integrin αIIbβ3: Signal transduction, regulation, and its therapeutic targeting. J Hematol Oncol. 2019;12(1):26.
163. Plow EF, Marguerie GA. Participation of ADP in the Binding of Fibrinogen to Thrombin-Stimulated Platelets. Blood. 1980;56(3):553-555.

5 Acknowledgements

I would like to thank Prof. Dr. Tilman Schäffer, Prof. Dr. Robert Feil, Prof. Dr. Robert Lukowski, and Prof. Dr. Francesca Seta for being my supervisors and always providing a helpful guidance during my research stay in Germany. Thanks also to Dr. Susanne Feil for her fruitful advices and discussions about cGMP and platelets. But overall, to all the members of the RTG2381 (PIs, students from first and second cohort, and our secretary Petya Georgieva) for a great time together.

Thanks to all my co-workers from the AG Schäffer, principally to Jan Seifert for his patience and input with experimental design, data analysis, microscope training, and more. I am thankful to have collaborated and achieved great results with Aylin Balmes, Vincent Gidlund, and Carmela Rianna (although she is no longer there). Also, a big vielen Dank für alles (especially for the singing in the office) to my lovely betrüger y queridos amigos Paul Kalwa and Konstantin Krutzke. Thanks, also should go to Johannes Rheinlaender for all his help and guidance during the last years. To all my collaborators and friends from the AG Feil: Daniel Pinto-Quintero, Moritz Lehners, Maria-Giovanna Barresi, Frank Regler, and Liubov Unger, who taught me a lot about cGMP signaling and more.

Many thanks to Dr. Mike Emerson for giving me the opportunity to be part of his platelet biology team at Imperial College London, to Dr. Akif Khawaja for his assistance during experiments, to the FILM facility (Dr. Andreas Bruckbauer & Dr. David Gaboriau), and to Dr. Marta Boffito for her help finding the patients we needed to recruit. My gratefulness to my ex-labmate and now very good friend Renos Keniyopoullos. I have invaluable memories from London that I will always cherish.

I do not have enough words to express my gratitude for the support, encouragement, and patience during this time to my parents and all my family. Also, to my LEVTUMs in Canada and Ecuador (Soraya Cushicóndor, Liseth Fierro and Paola Rodríguez), and my dearest friends from Manchester, the NANOMED master, and Tübingen which are my family outside Ecuador (Vicente Costalago, Refaya Rezwan, Hien Phan, Reema Chowdhury, Khaled Elhady, Krithika Rajeeth, Sydney Rüger, and Dila Calis just to name a few). I love you all so much.